THE VARIATIONAL SOLUTION OF THE PROBLEM OF PLANE POISEUILLE FLOW WITH FLEXIBLE WALLS.

by

Christopher Harry Green

Mathematics Department

Imperial College of Science and Technology

September 1970

Abstract.

The problem of plane Poiseuille flow with flexible walls is set up as an eigenvalue problem for the wave speed of infinitesimal disturbances and solved by use of a new variational method. This novel variational technique, developed in the present work, overcomes the difficulty in the present problem that the eigenvalue is contained in the boundary conditions. It also allows a completely general series of functions to be used to approximate the stream function of the problem. The eigenvalues obtained from the method are used to give stability curves, and the eigenvectors obtained are used to give stream function and Reynolds stress distributions. The computer program, developed from the variational method, is used to obtain stability results for the flexible wall problem, and, by taking a limiting case of this problem, to obtain results for the rigid wall problem. Convergence tests and comparisons with previous work, for both the flexible wall and rigid wall problems, give great confidence in the accuracy of the present method. Stability results are obtained for two flexible wall models: firstly, membrane walls, where the effects of variations in the damping and free wave speed in the wall are examined, and secondly, thin plates, where the effects of flexural rigidity are examined.

Acknowledgements.

It is with great pleasure that I acknowledge my indebtedness to Dr. C. H. Ellen for his continued guidance and encouragement throughout the past three years.

The present work was financially supported by the Science Research Council.

Table of contents.

List of symbols.

Symbols are not repeated which have merely the addition of a tilde, bar or star (denoting dimensional, complex conjugate or adjoint terms, respectively).

x, y	coordinates of the flow
y_c	the critical point
h	half the width of the pipe
η	displacement of a wall from its unperturbed state
t	time
$\tilde{\underline{v}}$	dimensional velocity
u,v	velocity components
u', v'	perturbation velocity components
U	steady state velocity
U_0	velocity of the steady state flow at $y = 0$
p	pressure
P	steady state pressure
p'	pressure perturbation
ψ	stream function
$\phi = \phi_r + i\phi_i$	the "y" dependence of the stream function
a	wave number
$c = c_r + ic_i$	wave speed
$c_p = c_{pr} + ic_{pi}$	physical wave speed

c^o, c^1, c_1^1, c_2^1, c^2, c^3	values of the wave speed used in the iterative scheme
λ_o	eigenvalue pivot
R	Reynolds number
R_o	critical Reynolds number
ν	kinematic viscosity
ρ	density
μ	viscosity
T_j, m_j, e_j, d_j, s_j, c_{oj}, D_j $(j=1,2)$	flexible wall parameters
$\tilde{\tilde{I}}_{yy}$	component of the stress tensor normal to the wall
E_j $(j=1,2)$	boundary condition parameters
e, e^o, e_1^o, e_2^o, e_1^1, e_2^1, e^2, e^3	values of the boundary condition parameters used in the iterative scheme
L	differential operator
B	boundary condition operator
$\underline{H}$	vector operator of the variational method
$\underline{u}$	vector function of the variational method
I	functional of the variational method
a_m $(m=1, \ldots, N)$	components of the approximating series

B_{nm}, D_{nm}, B_{11}, B_{12}, B_{21}, B_{22}, D_{11}, D_{12}, D_{21}, D_{22}	matrices of the variational method
I_j $(j=1, \ldots, 8)$, T_j $(j= 1,2,3,4,)$	integrals in the expressions for the entries of the matrices of the variational method

Chapter 1. Introduction.

1.1. General introduction.

Calculations of skin friction drag on stream-lined bodies are necessarily based on the correct location of the transition region. The transition region is characterised by a basic instability of the laminar boundary layer resulting in a turbulent state downstream of this region. Although recent work on non-linear stability has shown that subcritical and supercritical instabilities are important in considering transition to turbulence, there is still value in studying the classical linear problem. This is especially so when the added complication of flexible walls is included.

The problem of plane Poiseuille flow with flexible walls, considered in the present work, is a linearised stability problem in which the steady flow is purely parallel and there is an interaction between the wall waves and the fluid waves. In the boundary layer stability problem the steady flow is only approximately parallel, the boundary layer thickness increasing in the stream-wise direction. The boundary layer problem therefore presents difficulties when considering the change in the nature of the problem at very low Reynolds numbers. It is advantageous to consider a purely parallel steady flow problem where the

formulation of the problem is valid for all Reynolds numbers since the modification of stable boundary layers by flexible walls may be significant and introduce instabilities in regions where, strictly speaking, the mathematical formulation of the problem is invalid (see Landahl (1962)).

Although Benjamin (1960) has presented excellent qualitative arguments for the beneficial design of flexible walls, it should be remembered that he considers walls which are nearly rigid or fluids which produce only a small effect on the walls, and these are probably exceptional cases. Landahl and Kaplan (1965) and Hains and Price (1962) have obtained numerical results for some intermediate cases by integrating across the flow. The method adopted herein to solve the problem is a novel variational method which is adapted to the requirements of the present problem but which is generally applicable to other boundary value problems.

1.2. Statement of the problem.

The problem considered herein is of an incompressible, viscous fluid flowing down a two-dimensional pipe (see Figure 1). The basic direction of flow is taken in the $\tilde{x}$ direction, parallel to the flexible side walls situated at $\tilde{y} = \pm h$ (the tilde, ~, denotes dimensional quantities). The basic flow is plane Poiseuille flow (which is taken as $\tilde{U} = U_0(1-\tilde{y}^2/h^2)$). The fluid is

incompressible, two-dimensional and only infinitesimal disturbances from the basic flow are considered. Hence a stream function for the dimensionless disturbance velocity of the form $\phi(y)\exp\{-ia(x-ct)\}$ may be chosen where t is the time, a is the wave number (considered as real) and c is the wave speed (considered as complex). The Reynolds number, R, of the problem is defined by

$$R = \frac{\text{(maximum stream velocity)x(half the width of the pipe)}}{\text{(the kinematic viscosity)}}$$

$$= \frac{U_0 x h}{\nu} \quad .$$

The mathematical problem consists in solving the differential equation associated with the fluid flow (the Orr-Sommerfeld equation), coupled with the boundary conditions associated with the flexible walls. We wish to examine the spectrum of c which is obtained for given values of a and R. If the imaginary part of c is less than zero we have amplification, if greater than zero we have decay. Neutral stability is found where c is purely real. We may plot curves of neutral stability in the (a,R) plane, as is customary (see Figure 2), and neutral stability curves will be presented for inextensible walls with various characteristics. We will mainly be considering stability in a temporal sense but

curves of neutral stability in the spatial sense are obtained with temporal stability results and will be presented.

1.3. Plane Poiseuille flow with rigid walls.

The problem of plane Poiseuille flow with flexible walls is, in several respects, a continuation of the problem of plane Poiseuille flow with rigid walls. Hence, consideration of the rigid wall problem is important in the present problem. Also, a limiting case of the flexible wall problem may be taken and numerical results for the rigid wall problem obtained. Previous results for the rigid wall problem will provide a good check on the accuracy of our computations.

Heisenberg (1924) was the first to consider the stability of plane Poiseuille flow with rigid walls. He did not calculate a critical Reynolds number but did conclude that the flow was unstable for large enough Reynolds numbers. (The critical Reynolds number is the smallest Reynolds number at which infinitesimal disturbances may be unstable.) Lin (1944) calculated the neutral stability curve using an asymptotic expansion and Shen (1954) calculated the curves of constant amplification by a perturbation from Lin's neutral curve. In these last results the critical Reynolds number was found to be 5300.

The first numerical calculations were made by Thomas (1953).

His results confirmed those of Lin, except at large values of the wave number where the asymptotic expansions would be expected to be inaccurate, and he found a critical Reynolds number of 5780. Other work has been done in this field, but of particular interest here are the papers by Lee and Reynolds (1967) and Grosch and Salwen (1968). Lee and Reynolds adopted a variational approach to the rigid wall problem. Grosch and Salwen obtained numerical results for the rigid wall problem using a basically similar technique in their study of time dependent plane Poiseuille flow with rigid walls. These variational, Rayleigh Ritz or Galerkin approaches, which have been widely used in structural mechanics, have only recently been applied to problems in fluid mechanics. In the normal course of calculations, these methods find a particular eigenvalue accurately and values of the other eigenvalues to varying degrees of approximation. Grosch and Salwen obtained higher eigenvalues (i.e. eigenvalues other than the most unstable in the spectrum of c). Previously, the only person to consider this problem for the rigid wall problem was Grohne (1954). Although there was disagreement in the exact results of Grohne and Grosch and Salwen, both concluded that at most one eigenvalue in the spectrum becomes unstable.

1.4. Plane Poiseuille flow with flexible walls.

Present interest in this problem stems from the experimental work of Kramer (1957, 1960). Kramer's first experiments (1957) suggested that the transition of boundary layers from laminar to turbulent flow may be delayed by introduction of artificial damping (the artificial damping being introduced by use of a flexible wall). His later experiments (1960) suggested that the addition of a flexible coating to a stream-lined body may reduce its drag.

These findings stimulated several theoretical studies examining the possibilities of stabilisation of fluid flows by flexible walls, but these all tend to refute Kramer's ideas, although suggesting other possible ways of improving stability. The main insight into the problem came from Benjamin's (1960) investigation of the two-dimensional, incompressible, viscous boundary layer over a plane flexible wall when the wall was made slightly flexible or when the fluid produced a small loading on the wall. His model for the flexible wall was an inextensible membrane and he recognised three types of wave disturbance which he denoted by classes A, B and C.

Class A waves may be considered as the Tollmien-Schlichting waves which occur in the rigid wall problem but now being modified

by the effects of the flexible wall. Benjamin found that this class of waves is stabilised by a stiffness controlled wall (i.e. one with an "elastic response" as described by Benjamin), the greatest stabilisation being, in the absence of other factors, when c is near but less than the free wave speed in the flexible wall. This class he found to be destabilised by damping in the wall. (Stability here is considered in terms of the critical Reynolds number. A stabilising effect is denoted by an increase in critical Reynolds number and vice versa.) Another important effect is that under suitable conditions the unstable region in the (a, R) plane may be shifted to smaller wave numbers.

Class B waves are associated with the waves which can propagate on the free flexible wall in the absence of any fluid. This class is only excited when the fluid velocity exceeds the free wave speed and it is found that damping in the wall is stabilising. Thus the damping requirements of class A and class B waves are in conflict.

Class C instability may be considered as Kelvin-Helmholtz instability in that it propagates along the interface between the fluid and the flexible wall, is dependent on the presence of both the fluid and the flexible wall and is largely independent of viscosity. It occurs when the wall becomes too flexible.

The previous provides a convenient classification when

discussing the problem. However, in general, the interaction produces a wave spectrum whose precise origins may be difficult to recognise. Indeed, where wall and fluid are of equal importance, the various classes may appear to be merged on a single stability curve as may be seen in results presented later.

Landahl (1962) investigated the same problem and gave further physical insight into the principles behind the classification of the disturbances. His explanations were further amplified by Benjamin (1963). Landahl explains that the excitation of disturbances depends on energy transfers within the complete system. For class C waves the total energy level remains virtually unchanged and instability occurs with a unidirectional transfer of energy to the flexible wall, Landahl found that the amplitude of class A waves increases with a decrease in the energy of the system. This explains the destabilising effect of wall damping on class A waves since this damping absorbs energy. Amplification of class B waves involves an increase in energy level. Hence the stabilising effect of damping in the wall.

These ideas still hold for an inviscid fluid and are generally applicable to coupled fluid solid systems.

Kaplan (1964) and Landahl and Kaplan (1965) have carried out numerical calculations for the boundary layer problem. These calculations, based on a Runge-Kutta numerical integration across

the boundary layer, were mainly calculations for class A disturbances. There has been little interest in wall instability caused by the flow apart from Landahl (1962) who gave a few tentative class B curves. These were at very low Reynolds number, however, where the Orr-Sommerfeld equation is not, strictly speaking, applicable to the boundary layer stability problem. Kaplan (1964) gives a few class B curves which are, however, incorrect (see Landahl and Kaplan (1965)). For the class A waves, Benjamin (1964) gave three possibilities for the favourable use of a flexible wall. Firstly, an increase in critical Reynolds number. Increases in critical Reynolds number have generally been found to be small for practical walls. Secondly, a reduction in the amplification rate of unstable disturbances. Thirdly, an increase in the group velocity of the unstable disturbances. In both of the last two cases Kaplan has found strong effects for certain cases. The numerical results of Kaplan and Landahl and Kaplan agree with the qualitative results found theoretically by Benjamin and Landahl.

Hains and Price (1961a and b, 1962a and b) and Hains (1964) have carried out numerical calculations for the problem of plane Poiseuille flow over flexible walls using a similar numerical integration to that of Kaplan, and Landahl and Kaplan. They considered the two-dimensional problem of a viscous, incompressible fluid flowing between membrane walls. Considering walls with tension only, where the only possibility is class A disturbances,

they found that as they reduced the tension from its rigid wall value of infinity, the curve first closed and then reduced to a point. For lower values of the tension the flow was completely stable. This is however an unrealistic situation since the wall would have to be so light and under such a small tension that other stiffness criteria would dominate the design.

Other work in this field has been done by Miles (1957, 1959a and b, 1962) where the emphasis was on water wave generation by wind, Linebarger (1961) who considered the effects of compressibility, Nonweiler (1963) who obtained qualitative results for an elastic layer model of the wall, Boggs and Tokita (1962) who determined free wave speeds for various elastic layer models of the wall without considering the fluid interaction and Korotkin (1965, 1966) who considered a flexible wall pliant in the tangential direction.

Chapter 2. The boundary value problem.

2.1. Governing equations.

The Navier-Stokes equations for a viscous, incompressible, two-dimensional fluid are

$$\frac{\partial \tilde{\underline{v}}}{\partial \tilde{t}} + (\tilde{\underline{v}}.\tilde{\underline{grad}})\tilde{\underline{v}} = -\frac{\tilde{\underline{grad}}\,\tilde{p}}{\rho} + \nu\,\tilde{\underline{grad}}^2\,\tilde{\underline{v}} \quad , \qquad 2.1.1$$

where $\tilde{\underline{v}} = (\tilde{u},\tilde{v})$ is the velocity,

$$\tilde{\underline{grad}} = \left\{ \frac{\partial}{\partial \tilde{x}}, \frac{\partial}{\partial \tilde{y}} \right\},$$

$$\tilde{\underline{grad}}^2 = \frac{\partial^2}{\partial \tilde{x}^2} + \frac{\partial^2}{\partial \tilde{y}^2} \quad ,$$

$\tilde{p}$ = the pressure,

ρ = the density,

ν = the kinematic viscosity

and the coordinates are as previously defined in Section 1.2 and Figure 1. (N.B. The tilde, ~, denotes dimensional quantities.) The continuity equation is

$$\tilde{\underline{grad}}.\tilde{\underline{v}} = 0 \quad . \qquad 2.1.2$$

The equations are made dimensionless with respect to U_o, the velocity of the steady state flow at $\tilde{y} = 0$, h, half the width of the pipe, and ρ, the density of the fluid. We take the dimensionless variables

$$u = \frac{\tilde{u}}{U_o} \quad , \quad v = \frac{\tilde{v}}{U_o} \quad , \quad x = \frac{\tilde{x}}{h} \quad , \quad y = \frac{\tilde{y}}{h} \quad , \quad t = \frac{\tilde{t}\, U_o}{h} \quad \text{and} \quad p = \frac{\tilde{p}}{\rho\, U_o^2} \quad , \text{ and,}$$

substituting in Equations 2.1.1 and 2.1.2, derive the equations

$$\frac{\partial u}{\partial t} + u \frac{\partial u}{\partial x} + v \frac{\partial u}{\partial y} = - \frac{\partial p}{\partial x} + \frac{1}{R} \operatorname{grad}^2 u \quad , \qquad 2.1.3$$

$$\frac{\partial v}{\partial t} + u \frac{\partial v}{\partial x} + v \frac{\partial v}{\partial y} = - \frac{\partial p}{\partial x} + \frac{1}{R} \operatorname{grad}^2 v \qquad 2.1.4$$

and

$$\frac{\partial u}{\partial x} + \frac{\partial v}{\partial y} = 0 \, . \qquad 2.1.5$$

We now take $(u,v) = (U+u',v')$ and $p = P + p'$, where $U = (1-y^2)$ is the steady state velocity, P is the steady state pressure and u', v' and p' are small disturbances from the steady state. We take a stream function, $\psi = \phi(y)\exp\{-ia(x-ct)\}$,† for the disturbance velocities, u' and v', which automatically satisfies Equation 2.1.5. Hence we obtain

$$(u',v') = \left\{ \frac{d\phi(y)}{dy} \exp\{-ia(x-ct)\}, \; ia\phi(y)\exp\{-ia(x-ct)\} \right\} .$$

Substituting into Equations 2.1.3 and 2.1.4 and eliminating pressure, we obtain the Orr-Sommerfeld equation

$$\frac{d^4\phi}{dy^4} - 2a^2 \frac{d^2\phi}{dy^2} + a^4\phi + iaR \left\{ (U-c) \left\{ \frac{d^2\phi}{dy^2} - a^2\phi \right\} - \frac{d^2U}{dy^2}\phi \right\} = 0 \, , \qquad 2.1.6$$

† We make $\tilde{a}$ and $\tilde{c}$ dimensionless by $a = \tilde{a}\, h$ and $c = \frac{\tilde{c}}{U_o}$.

where $\phi = \phi(y)$ and $U = (1-y^2)$.

This is the way in which the Orr-Sommerfeld equation is usually developed, and the computing for this problem has been performed using this equation. However, in order to obtain results for fixed physical wall parameters, we wish to vary the Reynolds number of the flow by varying U_0, without altering the dimensionless parameters describing the flexible wall. In other words, we envisage a situation in which a given channel and fluid are employed, while the fluid velocity is increased until instability occurs. We therefore render our physical wall parameters dimensionless with respect to h, ν and ρ. In order that our computational results will be meaningful physically, it is found necessary to multiply the computational eigenvalue, c, by a factor R, to obtain a physical eigenvalue, c_p (i.e. $c_p = R.c$ is the wave speed made dimensionless for given wall and fluid properties). This is due to the fact that the previous equations have been made dimensionless using U_0, which is the parameter varied in order to vary R. In order to compare our eigenvalues with previous work we use c. Otherwise we use c_p, which gives results which are more meaningful, physically, in the present work.

Since our scheme of dimensionless variables is independent of U_0, and it is not proposed to consider any anisotropic wall properties in this work, the consideration of the two-dimensional problem (as opposed to the three-dimensional problem) is justified by reference to the work of Squire (1933).

2.2. Boundary conditions.

In dimensionless terms, we have flexible walls positioned at $y = \pm 1$ and a steady state flow of the form $U = (1-y^2)$. The flexible walls are assumed to be surfaces inextensible in the longitudinal (x) direction, with lateral motion governed by a dynamical equation which takes into account properties of mass, tension, elastic stiffness, viscous damping and flexural rigidity. We consider first the wall at $y = +1$. Let η[†] be the distance of displacement of the wall from its unperturbed state, $y = +1$. Assuming that there is no slip at the wall gives

$$U(y)\Big|_{y = 1+\eta} + \frac{d\phi(y)}{dy}\Big|_{y = 1+\eta} \exp\{-ia(x-ct)\} = 0 \quad .$$

Hence, substituting $U = (1-y^2)$, gives, to first order,

$$-2\eta + \frac{d\phi(+1)}{dy} \exp\{-ia(x-ct)\} = 0 \quad . \qquad 2.2.1$$

We now assume that the fluid stays in contact with the flexible wall and obtain

$$\frac{\partial \eta}{\partial t} = ia\phi(y)\Big|_{y = 1+\eta} \exp\{-ia(x-ct)\} \quad ,$$

and hence

$$\frac{\partial \eta}{\partial t} = ia\phi(+1)\exp\{-ia(x-ct)\} \quad . \qquad 2.2.2$$

---

† We make $\tilde{\eta}$ dimensionless by $\eta = \frac{\tilde{\eta}}{h}$.

Combining Equations 2.2.1 and 2.2.2 gives

$$\frac{d\phi(+1)}{dy} - \frac{2}{c}\phi(+1) = 0 \quad , \qquad 2.2.3$$

which is the first boundary condition, obtained from kinematic considerations. The equation of motion for normal forces on the wall at y = +1 is (see, for example, Timoshenko and Gere (1961))

$$\tilde{T}_1 \frac{\partial^2\tilde{\eta}}{\partial\tilde{x}^2} - \tilde{e}_1\tilde{\eta} - \tilde{d}_1 \frac{\partial\tilde{\eta}}{\partial\tilde{t}} - \tilde{s}_1 \frac{\partial^4\tilde{\eta}}{\partial\tilde{x}^4} - \tilde{I}_{\tilde{yy}} = \tilde{m}_1 \frac{\partial^2\tilde{\eta}}{\partial\tilde{t}^2} \quad , \qquad 2.2.4$$

where $\tilde{T}_1$ = the tension parameter,

$\tilde{e}_1$ = the elastic stiffness parameter,

$\tilde{d}_1$ = the damping parameter,

$\tilde{s}_1$ = the flexural rigidity parameter,

$\tilde{m}_1$ = the mass parameter

and $\tilde{I}_{\tilde{yy}}$ = the component of the fluid stress tensor normal to the wall at y = +1. (Suffix "1" denotes parameters for the wall at y = +1.) The above component of the stress tensor is

$$\tilde{I}_{\tilde{yy}} = -\tilde{p}' + 2\mu \frac{\partial\tilde{v}'}{\partial\tilde{y}}^{\dagger} \quad , \text{ and hence } \tilde{I}_{\tilde{yy}} = -\tilde{p}' - 2\mu \frac{\partial\tilde{u}'}{\partial\tilde{x}}^{\dagger} \text{ by continuity.}$$

(Here μ = viscosity and $\nu = \frac{\mu}{\rho}$ = kinematic viscosity.) The equation is now made dimensionless with respect to h, ρ, U_0 and μ by putting

---

† These expressions being evaluated at the wall y = +1.

$\eta = \frac{\tilde{\eta}}{h}$, $x = \frac{\tilde{x}}{h}$, $u' = \frac{\tilde{u}'}{U_0}$, $t = \frac{\tilde{t}\, U_0}{h}$, $T_1 = \frac{\tilde{T}_1\, \rho h}{\mu^2}$, $e_1 = \frac{\tilde{e}_1\, \rho h^3}{\mu^2}$,

$d_1 = \frac{\tilde{d}_1\, h}{\mu}$, $p' = \frac{\tilde{p}'}{\rho U_0^2}$, $m_1 = \frac{\tilde{m}_1}{\rho h}$ and $s_1 = \frac{\tilde{s}_1\, \rho}{\mu^2 h}$. We also use

$u'(+1) = \frac{d\phi(+1)}{dy} \exp\{-ia(x-ct)\}$ and Equations 2.2.1 and 2.2.3, and

substitute into Equation 2.2.4 to obtain

$$p'(+1) = \phi(+1) \left\{ \frac{a^2 T_1}{cR^2} + \frac{e_1}{cR^2} + \frac{iad_1}{R} + \frac{a^4 s_1}{cR^2} - a^2 cm_1 + \frac{4ia}{cR} \right\} \exp\{-ia(x-ct)\}.$$

Substituting this in the x momentum equation (Equation 2.1.3), evaluated at y = +1, gives

$$\frac{d^3\phi(+1)}{dy^3} + \frac{R}{E_1} \phi(+1) = 0 \quad , \qquad 2.2.5$$

where $E_1^{-1} = -\frac{a^2}{R} \left\{ d_1 + \frac{6}{c} \right\} + i \left\{ \frac{a}{cR^2} \left\{ e_1 + a^2 T_1 + a^4 s_1 \right\} - a^3 cm_1 \right\}$.

This is the second boundary condition, obtained from dynamical considerations.

The two remaining boundary conditions are the corresponding boundary conditions obtained at the wall at y = -1. These are

$$\frac{d\phi(-1)}{dy} + \frac{2}{c} \phi(-1) = 0 \qquad 2.2.6$$

and

$$\frac{d^3\phi(-1)}{dy^3} - \frac{R}{E_2} \phi(-1) = 0 \quad , \qquad 2.2.7$$

where $$E_2^{-1} = -\frac{a^2}{R}\left\{ d_2 + \frac{6}{c} \right\} + i\left\{ \frac{a}{cR^2}\left\{ e_2 + a^2 T_2 + a^4 s_2 \right\} - a^3 c m_2 \right\}.$$

(Suffix "2" denotes parameters for the wall at $y = -1$.)

These boundary conditions coincide with those of Hains and Price (1961a) except for the inclusions of the viscous component of the normal stress and flexural rigidity, the fact that there is no restriction to considering ϕ as symmetric and also that the problem of the two flexible walls having different physical properties may be considered in the present work. The similarity between the present boundary conditions and those of Hains and Price facilitates comparisons of results. It should be noted that, with this scheme of dimensionless parameters, the flow may be varied by changing its velocity without affecting the parameters describing the flexible walls. As explained in Section 2.1, the eigenvalue, c, in these boundary conditions is the computational eigenvalue.

The parameters E_1 and E_2 will now be rewritten to make them comparable with the parameters involved in other work in the field by putting

$$c_{oj}^2 = \frac{e_j + T_j a^2 + s_j a^4}{m_j a^2} \quad \text{and} \quad D_j = \frac{d_j}{m_j},$$

where $j = 1$ or 2 depending on whether the wall is taken at $y = +1$ or -1. c_{oj} is a dimensionless parameter representing the speed at which free waves would propagate along the undamped flexible walls when there is no fluid in the two-dimensional pipe. Hence we obtain

$$E_j^{-1} = -m_j D_j \frac{a^2}{R} - \frac{6a^2}{cR} + im_j \frac{a^3}{c}\left\{\frac{c_{oj}^2}{R^2} - c^2\right\} . \qquad 2.2.8$$

A wide class of physical boundaries may be approximated by this representation. For comparison with the work by Landahl and Kaplan (1965) on the boundary layer problem, taking into account the different schemes of dimensionless variables, the following table is useful. (Here, the suffix "j" is dropped for the moment.)

Landahl and Kaplan	present work
m	m
ω_o^2	$\frac{e}{mR^2}$
c_o^2	$\frac{T}{mR^2}$
d	$\frac{D}{R}$
not taken into account	s

In the work of Landahl and Kaplan, the parameters defining the wall properties are made dimensionless more appropriately in terms of U_∞ and δ. (U_∞ equals the steady velocity of the boundary layer as y tends to infinity and δ equals the boundary layer thickness, which is not constant in the x direction.) There is some difficulty in interpreting their results to obtain results for fixed physical situations unless a "tailored" wall is employed. (The term"tailored"

is used to describe a wall whose physical properties are altered to compensate for the change in thickness of the boundary layer. Of course, the wall equation itself is not changed so that this interpretation is unsound when the boundary layer thickness changes too rapidly: a situation which does not exist for the plane Poiseuille flow problem.) The variety of possible schemes of dimensionless variables has lead to some confusion in the past.

2.3. Related problems.

There are a number of problems closely related to the present problem, some of which are listed below. They are not only related physically, but also, their solution may be tackled by the technique which will be described later.

1). The same problem as at present, with the condition of wall inextensibility in the streamwise direction relaxed.

2). The problem of plane Couette flow with flexible walls.

3). The problem of plane Poiseuille flow of a dusty gas.

These problems can be considered seperately or in any combination and involve variations in the boundary conditions and steady velocity profile.

Chapter 3. The method of solution of the problem.

3.1. Outline of the method of solution.

We now have to solve the boundary value problem of the Orr-Sommerfeld equation (Equation 2.1.6)

$$\frac{d^4\phi}{dy^4} - 2a^2\frac{d^2\phi}{dy^2} + a^4\phi + iaR\left\{(U-c)\left\{\frac{d^2\phi}{dy^2} - a^2\phi\right\} - \frac{d^2U}{dy^2}\phi\right\} = 0 \quad ,$$

where $\phi = \phi(y)$ and $U = (1-y^2)$, with the boundary conditions (Equations 2.2.3, 2.2.5, 2.2.6, 2.2.7 and 2.2.8)

$$\frac{d\phi(+1)}{dy} - \frac{2}{c}\phi(+1) = 0 \quad ,$$

$$\frac{d^3\phi(+1)}{dy^3} + \frac{R}{E_1}\phi(+1) = 0 \quad ,$$

$$\frac{d\phi(-1)}{dy} + \frac{2}{c}\phi(-1) = 0 \quad \text{and}$$

$$\frac{d^3\phi(-1)}{dy^3} - \frac{R}{E_2}\phi(-1) = 0 \quad ,$$

where $$E_j^{-1} = -m_j D_j \frac{a^2}{R} - \frac{6a^2}{cR} + im_j\frac{a^3}{c}\left\{\frac{c_{oj}^2}{R^2} - c^2\right\} \quad .$$

We regard this as an eigenvalue problem for c and proceed to solve it to obtain numerical values of the eigenvalue for given values of the fluid parameters and physical wall parameters. Because the boundary conditions contain c in a rather complicated way, the most common and convenient way of coping with this difficulty is to first obtain eigenvalues for fixed values of the parameters E_1 and E_2. This we do using a new variational approach. We then use these results and adopt an iteration scheme, similar to the one used by Kaplan (1964), which gives us the eigenvalues in terms of fixed physical wall parameters. This approach to the problem provides an accurate and speedy solution from which we may easily obtain as many eigenvalues from the spectrum as we wish, within the space limitations of the computer being employed. We may also obtain the corresponding eigenvectors and hence the stream function and Reynolds stress distributions across the channel.

3.2. The variational formulation.

The variational formulation about to be presented is not peculiar to the particular problem associated with the present work and hence will be stated in general form. In essence, we merely extend the conventional variational problem to one which includes the boundary conditions as well as the governing equation, and we will therefore develop our general formulation in parallel with the conventional variational formulation.

Suppose we have a differential equation $L\phi = 0$, where L is a linear differential operator defined in the range $[y_1, y_2]$ and ϕ is some function of y. We denote the set of boundary conditions at y_1 and y_2 by $\{B\phi\} = 0$. The adjoint operator L^*, together with a set of adjoint boundary condition operators $\{B^*\}$, is defined such that, if u is any function satisfying $\{Bu\} = 0$ and v is any function satisfying $\{B^*v\} = 0$, then

$$\langle v, Lu\rangle - \langle L^*v, u\rangle = 0 \quad ,$$

where the inner product of a and b is defined as

$$\langle a, b\rangle = \frac{1}{y_2 - y_1} \int_{y_1}^{y_2} \bar{a}b \, dy \quad ,$$

the star denoting an adjoint and the bar a complex conjugate. Now, inserting the Orr-Sommerfeld equation and the flexible wall boundary conditions (see Section 3.1) for $L\phi = 0$ and $\{B\phi\} = 0$ respectively, we obtain the corresponding adjoint differential equation and adjoint boundary conditions (after integration by parts). The complex conjugate, adjoint differential equation is found to be

$$\frac{d^4\bar{\phi}^*}{dy^4} - 2a^2 \frac{d^2\bar{\phi}^*}{dy^2} + a^4\bar{\phi}^* + iaR\left\{\frac{d^2\bar{\phi}^*}{dy^2} - \frac{d^2(y^2\bar{\phi}^*)}{dy^2} + (2 - a^2 + a^2y^2)\bar{\phi}^*\right\}$$

$$- ciaR\left\{\frac{d^2\bar{\phi}^*}{dy^2} - a^2\bar{\phi}^*\right\} = 0 \quad , \qquad 3.2.1$$

where $\bar{\phi}^* = \bar{\phi}^*(y)$. The complex conjugate, adjoint boundary conditions

are found to be

$$\frac{d^3\bar{\phi}^*(+1)}{dy^3} - \frac{2}{c}\frac{d^2\bar{\phi}^*(+1)}{dy^2} + \left\{\frac{R}{E_1} + \frac{4a^2}{c}\right\}\bar{\phi}^*(+1) = 0 \quad ,$$

$$\frac{d\bar{\phi}^*(+1)}{dy} = 0 \quad ,$$

$$\frac{d^3\bar{\phi}^*(-1)}{dy^3} + \frac{2}{c}\frac{d^2\bar{\phi}^*(-1)}{dy^2} - \left\{\frac{R}{E_2} + \frac{4a^2}{c}\right\}\bar{\phi}^*(-1) = 0 \qquad \text{and}$$

$$\frac{d\bar{\phi}^*(-1)}{dy} \quad . \qquad 3.2.2$$

Now we consider vectors $\underline{f}(\underline{w})$ and $\underline{g}(\underline{w})$, both belonging to a Hilbert space and being quadratically integrable, where

$$\underline{w} = (w_1, w_2, \ldots, w_m),$$
$$\underline{f}(\underline{w}) = (f_1(\underline{w}), f_2(\underline{w}), \ldots, f_n(\underline{w})) \qquad \text{and}$$
$$\underline{g}(\underline{w}) = (g_1(\underline{w}), g_2(\underline{w}), \ldots, g_n(\underline{w})).$$

Corresponding to the inner product of two scalar functions, we define

$$\langle \underline{f}, \underline{g} \rangle = \sum_{i=1}^{n} \frac{1}{S} \int_V \bar{f}_i g_i \, dV \quad , \text{ where } S = \int_V dV \quad \text{and}$$

$dV = dw_1\, dw_2 \ldots dw_m$. We now define

$$\underline{H}(\underline{u}) = \begin{bmatrix} L\phi \\ B_1\phi \\ B_2\phi \\ B_3\phi \\ B_4\phi \end{bmatrix} \quad , \quad \underline{\bar{H}}^{\star}(\underline{\bar{u}}^{\star}) = \begin{bmatrix} \bar{L}^{\star}\bar{\phi}^{\star} \\ \bar{B}_1^{\star}\bar{\phi}^{\star} \\ \bar{B}_2^{\star}\bar{\phi}^{\star} \\ \bar{B}_3^{\star}\bar{\phi}^{\star} \\ \bar{B}_4^{\star}\bar{\phi}^{\star} \end{bmatrix} \quad , \quad \underline{u} = \begin{bmatrix} \phi \\ a_1 \\ b_1 \\ c_1 \\ d_1 \end{bmatrix} \quad \text{and} \quad \underline{\bar{u}}^{\star} = \begin{bmatrix} \bar{\phi}^{\star} \\ a_2 \\ b_2 \\ c_2 \\ d_2 \end{bmatrix} .$$

We shall interpret these equations with $L\phi = 0$ as the Orr-Sommerfeld equation, $\{B_i\phi\} = 0$ (i=1, 2, 3 and 4) as the corresponding boundary conditions, $\bar{L}^{\star}\bar{\phi}^{\star} = 0$ as the complex conjugate, adjoint equation and $\{\bar{B}_i^{\star}\bar{\phi}^{\star}\} = 0$ (i=1, 2, 3 and 4) as the complex conjugate, adjoint boundary conditions (see Section 3.1 and Equations 3.2.1 and 3.2.2). The a_i, b_i, c_i and d_i (i=1 and 2) are determined by demanding that

$\langle \underline{u}^{\star}, \underline{H}(\underline{u}) \rangle - \langle \underline{\bar{H}}^{\star}(\underline{u}^{\star}), \underline{u} \rangle = 0$ is satisfied, where, in our case $\phi = \phi(y)$ and $\int_V dV = \int_{-1}^{+1} dy$. These criteria establish the necessary structure of the Hilbert space.

We now return to the one-dimensional case. When ϕ and $\phi^{\star}$ are solutions of their respective problems, the functional I, which is equal to $\langle \phi^{\star}, L\phi \rangle$, is zero, and is stationary with respect to appropriately restricted arbitrary variations in ϕ and $\phi^{\star}$. The appropriate restrictions are that the variations must satisfy the boundary conditions of the appropriate problem. This is equivalent to saying that $L\phi = 0$ and $L^{\star}\phi^{\star} = 0$ are Euler equations of the problem under consideration.

If we now suppose that the operator L is of the form $L = P - \lambda Q$ (where λ is an eigenvalue), then we can show that the ratio

$\dfrac{\langle \phi^*, P\phi \rangle}{\langle \phi^*, Q\phi \rangle}$ is stationary with respect to the same variations as before, when ϕ and ϕ^* are eigenfunctions. Also, it takes on the value of the appropriate eigenvalue when ϕ and ϕ^* are eigenfunctions. For an error of order ϵ in ϕ and ϕ^*, the error in λ is of order ϵ^2. Hence, reasonably close approximations to the eigenfunctions may produce more accurate estimates of λ.

The conventional variational method takes series of approximating functions f_n and f_n^* which satisfy $\{Bf_n\} = 0$ and $\{B^*f_n^*\} = 0$ respectively. We put

$$\phi = \sum_{n=1}^{N} a_n f_n \qquad \text{and} \qquad \phi^* = \sum_{n=1}^{N} a_n^* f_n^* \quad , \text{ where } a_n \text{ and } a_n^* \text{ are}$$

undetermined constants. Substituting these series into

$$I = \langle \phi^*, (P-\lambda Q)\phi \rangle \quad , \text{ we obtain } \quad I = \sum_{n=1}^{N} \sum_{m=1}^{N} \bar{a}_n^* a_m (B_{nm} - \lambda D_{nm}) \quad ,$$

where

$$B_{nm} = \langle f_n^*, Pf_m \rangle \qquad \text{and} \qquad D_{nm} = \langle f_n^*, Qf_m \rangle \quad .$$

The constants, a_m and $\bar{a}_n^*$, are now determined by requiring I to be stationary with respect to variations in these constants. If I is stationary with respect to $\bar{a}_n^*$, we obtain

$$\sum_{m=1}^{N} a_m \left(B_{nm} - \lambda D_{nm}\right) = 0 \qquad (n=1, 2, \ldots, N).$$

If I is stationary with respect to a_m, we obtain

$$\sum_{n=1}^{N} \bar{a}_n^{\star} \left(B_{nm} - \lambda D_{nm}\right) = 0 \qquad (m=1, 2, \ldots, N).$$

We therefore have a set of N homogeneous, algebraic equations for the N a_m's and a seperate set of N equations for the N $\bar{a}_n^{\star}$'s. There are non-trivial solutions, if, and only if,

$$\left| B_{nm} - \lambda D_{nm} \right| = 0 \ .$$

This determines the eigenvalues, λ, and the eigenvectors, whose components are the a_m's and $a_n^{\star}$'s. We may truncate the series at any point and examine the convergence by incrementing N.

We now generalise the previous argument: when $\underline{u}$ and $\underline{u}^{\star}$ are solutions to their respective problems, we demand that

$$\langle \underline{u}^{\star}, \underline{H}(\underline{u}) \rangle \qquad \text{is zero and is stationary}$$

with respect to variations in $\underline{u}$ and $\underline{u}^{\star}$. Since the boundary conditions have been included in the $\underline{H}(\underline{u})$ and $\underline{H}^{\star}(\underline{u}^{\star})$, we choose the variations in $\underline{u}$ and $\underline{u}^{\star}$ arbitrarily and continue as in the one-dimensional case. This is equivalent to substituting some approximating series for ϕ in the differential equation and boundary conditions and, in some suitable manner, adding up the residues and setting them equal to zero. The

best choice of an approximating series would appear to be such that the series is complete, not too restrictive and rapidly convergent.

This technique for solving an eigenvalue problem, when the boundary conditions for the problem contain the eigenvalue, is suggested by Friedman (1956). It is also suggested indirectly by Finlayson and Scriven (1966).

3.3. The iterative scheme.

We now incorporate the previous variational technique (Section 3.2) into an iterative scheme, developed by Kaplan (1964), for finding the eigenvalues (c) in terms of fixed physical wall properties. We take identical walls, with $E_1^{-1} = E_2^{-1} = e$, and wish to find the eigenvalues for given values of a, R and the physical wall parameters. Employing a given (guessed) value of an eigenvalue ($c = c^o$) in our expression for e, as well as a, R and the physical wall parameters, we obtain an initial value for e ($= e^o$), for use in the variational part of the problem. From the resultant spectrum, we take the eigenvalue corresponding to c^o (c^1) and, from c^1, obtain a new value of e (e^1). The sense in which the eigenvalue chosen from the spectrum corresponds to c^o, depends on the particular eigenvalue sought. Usually, we are seeking the most unstable eigenvalue for a given physical situation, and so we choose the most unstable eigenvalue from the spectrum. If the initial eigenvalue guess had been a sufficiently good guess at an eigenvalue

of the problem, we would have $e^0 = e^1$ and $c^0 = c^1$ (these two conditions occuring together). More generally, for any given guessed eigenvalue, e^0 and e^1 would differ, and the iterative scheme is developed so that we may make this difference as small as we choose in finding an eigenvalue of the problem. (We use the difference between e^0 and e^1 as our error criterion for purely numerical reasons, explained in Section 4.5.) To do this we now define $K = e^0 - e^1$, and the zeros of K correspond to eigenvalues of the problem. Considering K as a Taylor series in c^1 and truncating the Taylor series, we have, approximately,

$K(c^1) = e^0 - e^1 = A + Bc^1$, where A and B are constants. The value of e^0 is calculated using the estimated eigenvalue, c^0, and two values of e, e_1^0 and e_2^0, lying on either side of e^0, and close to it, are employed in the variational part of the problem, giving c_1^1, e_1^1, c_2^1 and e_2^1. This gives us

$$e_1^0 - e_1^1 = A + Bc_1^1 = K(c_1^1) = K_1 \qquad \text{and}$$

$$e_2^0 - e_2^1 = A + Bc_2^1 = K(c_2^1) = K_2 \quad .$$

We therefore obtain

$$A = \frac{K_2 c_1^1 - K_1 c_2^1}{c_1^1 - c_2^1} \qquad \text{and} \qquad B = \frac{K_1 - K_2}{c_1^1 - c_2^1} \quad .$$

The next estimate of the eigenvalue of the problem, c^2, is given by

$$A + Bc^2 = 0 \ , \quad \text{i.e.} \quad c^2 = -\frac{A}{B} = \frac{K_1 c_2^1 - K_2 c_1^1}{K_1 - K_2} \quad .$$

Proceeding as before, we may use c^2 to calculate a value of e (e^2), and hence obtain an eigenvalue c^3 and then a value e^3. In assessing the proximity of c^2 to an eigenvalue of the problem, we compare e^2 and e^3. This is the basis of the iterative scheme for the case where we have identical walls. For different walls, we may adopt a similar iterative technique, but in this case the iterative technique would be based on changes in c, since e would take different values for each wall. Although it is possible to devise more sophisticated iterative schemes, the one outlined above is particularly straightforward and appears to present no difficulties with convergence in the numerical computations.

Chapter 4. Computational aspects of the problem.

4.1. The different variational formulations considered.

If the problem is set up using the general variational technique described (Section 3.2), it is found that there is a certain freedom in the representation of the problem. This can be explained by the fact that the technique involves substitution of an approximating series in the differential equation and boundary conditions, followed by a suitable combining of the resultant residues. The different representations of the problem which are possible, correspond to weighting the boundary conditions in different ways.

The problem was first set up as in Appendix A.1, with no preconceived ideas as to possible difficulties. Due to the complicated nature of the boundary conditions and differential equation, it was found that the latitude in choosing the formulation was small. In the second and third positions of the vector $\underline{\bar{u}}^*$, we find terms from the problem (ϕ), mixed with terms from the adjoint problem (ϕ^*). Consider the problem reduced to the form of a matrix to be solved, and consider the (m,n) position of this matrix. In our general approach, the $\underline{\bar{u}}^*$ is associated with the m, and the $\underline{H}(\underline{u})$ is associated with the n. It can be seen that there is difficulty in deciding whether to associate the mixed ϕ terms (in $\underline{\bar{u}}^*$) with the m or the n. The problem was done both ways, and these were called Formulations 1 and 2.

To overcome the difficulty of these mixed terms, the problem was reformulated, as in Appendix A.2, and this was called Formulation 3. It can be seen that the problem of mixed terms still occurs, but this time in the adjoint problem.

As will be seen, the adjoint problem will be required in finding the stream function and Reynolds stress distributions of the problem, and so, to remove these mixed terms altogether, Formulation 4 was calculated. Previously, we defined $\underline{H}(\underline{u})$, $\underline{\bar{H}}^{\star}$, $\underline{u}$ and $\underline{\bar{u}}^{\star}$ with a dimension of five (corresponding to the differential equation and the four boundary conditions). For Formulation 4, we redefine these as

$$\underline{H}(\underline{u}) = \begin{bmatrix} L\phi \\ B_1\phi \\ B_2\phi \\ B_3\phi \\ B_4\phi \\ B_1\phi \\ B_2\phi \end{bmatrix} , \quad \underline{\bar{H}}^{\star}(\underline{\bar{u}}^{\star}) = \begin{bmatrix} \bar{L}^{\star}\bar{\phi}^{\star} \\ \bar{B}_1^{\star}\bar{\phi}^{\star} \\ \bar{B}_2^{\star}\bar{\phi}^{\star} \\ \bar{B}_3^{\star}\bar{\phi}^{\star} \\ \bar{B}_4^{\star}\bar{\phi}^{\star} \\ \bar{B}_1^{\star}\bar{\phi}^{\star} \\ \bar{B}_2^{\star}\bar{\phi}^{\star} \end{bmatrix} , \quad \underline{u} = \begin{bmatrix} \phi \\ a_1 \\ b_1 \\ c_1 \\ d_1 \\ e_1 \\ f_1 \end{bmatrix} \quad \text{and} \quad \underline{\bar{u}}^{\star} = \begin{bmatrix} \bar{\phi}^{\star} \\ a_2 \\ b_2 \\ c_2 \\ d_2 \\ e_2 \\ f_2 \end{bmatrix} .$$

(N.B. The last two terms in the vectors $\underline{H}(\underline{u})$ and $\underline{\bar{H}}^{\star}(\underline{\bar{u}}^{\star})$ are the first pair of boundary conditions repeated.) The a_i, b_i, c_i, d_i, e_i and f_i (i=1 and 2) are found as before. Nothing new is involved in this enlarging the dimensions of the vectors. We are, in effect, adding up the differential equation residue and the boundary condition residues

in a different way. Formulation 4 is given in Appendix A.3 and, with this formulation, we eliminate the previous difficulty from both the problem under consideration and its adjoint.

4.2. The approximating series.

We choose trigonometric functions for the approximating functions for both ϕ and ϕ^*. These form a complete set and have no inherent disadvantages. Because of the more general formulation of the problem, these approximating functions do not have to satisfy the boundary conditions.

For the rigid wall problem, a variety of test functions have been employed. Lee and Reynolds (1967) solve the problem of plane Poiseuille flow by a variational method, using polynomial approximating functions which satisfy the rigid wall boundary conditions. Dolph and Lewis (1958), in their approach to the same problem, adopt approximating functions, ϕ_n, which are eigenfunctions of the boundary value problem

$$\frac{d^4\phi_n}{dy^4} - 2a^2\frac{d^2\phi_n}{dy^2} + a^4\phi_n = \lambda_n\left\{a^2\phi_n - \frac{d^2\phi_n}{dy^2}\right\} \quad ,$$

with $\phi_n(\pm 1) = \frac{d\phi_n}{dy}(\pm 1) = 0$, where λ_n is the eigenvalue and $\phi_n = \phi_n(y)$.

Grosch and Salwen (1968), in their paper on steady and time dependent

plane Poiseuille flow, adopted similar functions to Dolph and Lewis. In both of these latter papers, the approximating functions were a combination of hyperbolic and trigonometric functions. Chebyshev polynomials have also been used to solve related stability problems

For this analysis, a half range Fourier series was chosen as the approximating series, i.e. $\cos(n\pi y/2)$ (n = 0, 1, 2, . . .) and $\sin(n\pi y/2)$ (n = 0, 1, 2, . . .) . We may truncate the series, and the order of the terms in the truncated series is unimportant. In certain circumstances, it may be advantageous to take a different number of cosine terms to sine terms, in order to shorten the numerical work without affecting the accuracy of the results. In the case of symmetric disturbances, only the even cosine series is required.

It should be noted that the functions corresponding to a full range Fourier series for the interval, i.e. $\cos(n\pi y)$ (n = 0, 1, 2, . . .) and $\sin(n\pi y)$ (n = 0, 1, 2, . . .) , are too restrictive. This may be seen by substituting into the previous formulations, when it is found that dependence on the wall parameters, E_1 and E_2, reduces to dependence on $(E_1^{-1} - E_2^{-1})$ and $(E_1^{-1} + E_2^{-1})$ with the half range Fourier series, and $(E_1^{-1} - E_2^{-1})$ with the full range Fourier series. Hence, when $E_1 = E_2$ (i.e. the walls have the same properties), all dependence on the walls vanishes with the full range Fourier series; an unsatisfactory situation, which shows the inadequacy of this approximating series.

It would appear that a reasonable number of terms of the chosen series is suitable for approximating the stream function near the critical point ($y = y_c$, where $U(y_c) = 1-y_c^2 = c_r$ and $c = c_r + ic_i$) and the wall, where rapid changes might be expected (as for the stream function distribution given by Thomas (1953) for rigid wall, plane Poiseuille flow at a = 1 and R = 10000). This was not used as a criterion to establish our approximating series, but does give us reason to believe that our chosen series will converge rapidly. In fact, our series was chosen as generally as possible. Comparisons of stream functions will be given later (see Section 5.2).

4.3. Comparison of the formulations.

Since there is variability in the formulation of the approximate solution, it is of some interest to examine the effects that different formulations may have on the results. Therefore, using these approximating functions, the matrices corresponding to the different formulations were set up (as described later, in Section 4.4). The eigenvalues of these matrices were computed, and comparisons made between the different formulations. For symmetric disturbances only, a cosine series is necessary, and convergence of the most unstable eigenvalue was examined for $E_1 = E_2 = 10^{-4}$ at a = 1 and R = 1600 and 2500. As will be seen, this value of E_1 and E_2 corresponds to effectively rigid walls. Results for the different formulations are given in Tables 1 and 2, and these results are further discussed

in Section 5.2.

It can be seen that, apart from Formulation 2, there is very little difference in the convergence of the different formulations. It should be expected that any formulation which satisfies the criteria initially stated will converge to the correct result. We would hope to pick a formulation which converged reasonably quickly. Because of the complicated nature of the differential equation and boundary conditions, we have, in fact, very little latitude in choosing the formulations. The result is that, for the main part, the different formulations converge, in the eigenvalues, with equal speed. Formulation 4 is the one chosen, since it allows the adjoint problem to be calculated without the complication previously mentioned. Apart from providing a good check on the arithmetic, the solution of the adjoint problem proves to be the most satisfactory for calculating the stream function and Reynolds stress distributions (this point will be discussed in Section 4.5).

It can be seen from the definitions of E_1 and E_2, that rigid walls correspond to $|E_1|$ and $|E_2|$ tending to zero. Calculations, typically as given in Table 3 (and further discussed in Section 5.2) for Formulation 4 (the chosen formulation), show that a sufficiently small value of E_1 and E_2 to simulate a rigid wall (or to make the ratio of wall to fluid resistance very large) is 10^{-4}. The arguments of E_1 and E_2 are seen to be unimportant in this respect.

4.4. Calculations for the chosen formulation.

For the reasons given in Section 4.3, Formulation 4 is chosen. We return now to set up the approximate solution, using Formulation 4 as given in Appendix A.3. (The principles are the same for setting up the approximate solution using any of the other formulations.)

Continuing with Formulation 4 therefore, we have

$$I = \langle \underline{u}^{\star}, \underline{H}(\underline{u}) \rangle = \int_{-1}^{+1} \bar{\phi}^{\star} \left\{ \frac{d^4\phi}{dy^4} - 2a^2 \frac{d^2\phi}{dy^2} + a^4\phi + iaR \left\{ (1-y^2) \left\{ \frac{d^2\phi}{dy^2} - a^2\phi \right\} + 2\phi \right\} \right\} dy$$

$$+ 2\phi(+1) \left\{ -iaR\bar{\phi}^{\star}(+1) + \frac{1}{2} \frac{d^3\bar{\phi}^{\star}(+1)}{dy^3} + \frac{R}{2E_1} \bar{\phi}^{\star}(+1) \right\}$$

$$+ 2\phi(-1) \left\{ -iaR\bar{\phi}^{\star}(-1) - \frac{1}{2} \frac{d^3\bar{\phi}^{\star}(-1)}{dy^3} + \frac{R}{2E_2} \bar{\phi}^{\star}(-1) \right\}$$

$$+ \left\{ \frac{E_1}{R} \frac{d^3\phi(+1)}{dy^3} + \phi(+1) \right\} \left\{ -\frac{R}{E_1} \bar{\phi}^{\star}(+1) \right\}$$

$$+ \left\{ \frac{E_2}{R} \frac{d^3\phi(-1)}{dy^3} - \phi(-1) \right\} \left\{ \frac{R}{E_2} \bar{\phi}^{\star}(-1) \right\}$$

$$- c \left\{ \int_{-1}^{+1} \bar{\phi}^{\star} \left\{ iaR \left\{ \frac{d^2\phi}{dy^2} - a^2\phi \right\} \right\} dy \right.$$

$$\left. + \frac{d\phi(+1)}{dy} \left\{ -iaR\bar{\phi}^{\star}(+1) + \frac{1}{2} \frac{d^3\bar{\phi}^{\star}(+1)}{dy^3} + \frac{R}{2E_1} \bar{\phi}^{\star}(+1) \right\} \right.$$

$$- \frac{d\phi(-1)}{dy} \left\{ -iaR\bar{\phi}^{\star}(-1) - \frac{1}{2}\frac{d^3\bar{\phi}^{\star}(-1)}{dy^3} + \frac{R}{2E_2}\bar{\phi}^{\star}(-1) \right\} \Bigg\} \Bigg\} ,$$

where $\phi = \phi(y)$ and $\bar{\phi}^{\star} = \bar{\phi}^{\star}(y)$ in the integral terms. For our approximating series (see Section 4.2), we substitute

$$\phi(y) = \sum_{m=0}^{N-1} a_m \cos(m\pi y/2) + \sum_{m=N}^{N+M-1} a_m \sin((m-N)\pi y/2) \qquad \text{and}$$

$$\bar{\phi}^{\star}(y) = \sum_{n=0}^{N-1} \bar{a}_n^{\star} \cos(n\pi y/2) + \sum_{n=N}^{N+M-1} \bar{a}_n^{\star} \sin((n-N)\pi y/2) \quad .$$

Since the series have been truncated, we will get identical results for any order of the functions in the approximating series, so we order them as above. If we initially substitite

$$\phi(y) = \sum_{m=0}^{N+M-1} a_m g_m(y) \qquad \text{and} \qquad \bar{\phi}^{\star}(y) = \sum_{n=0}^{N+M-1} \bar{a}_n^{\star} f_n(y)$$

in $\langle \underline{u}^{\star}, \underline{H}(\underline{u}) \rangle$, we obtain

$$I = \langle \underline{u}^{\star}, \underline{H}(\underline{u}) \rangle = \sum_{n=0}^{N+M-1} \sum_{m=0}^{N+M-1} \bar{a}_n^{\star} a_m \left((B_{nm}) - c(D_{nm}) \right) \quad ,$$

where

$$B_{nm} = \int_{-1}^{+1} f_n \left\{ \frac{d^4 g_m}{dy^4} - 2a^2 \frac{d^2 g_m}{dy^2} + a^4 g_m + iaR \left\{ (1-y^2) \left\{ \frac{d^2 g_m}{dy^2} - a^2 g_m \right\} + 2g_m \right\} \right\} dy$$

$$+ 2g_m(+1) \left\{ -iaRf_n(+1) + \frac{1}{2} \frac{d^3 f_n(+1)}{dy^3} + \frac{R}{2E_1} f_n(+1) \right\}$$

$$+ 2g_m(-1) \left\{ -iaRf_n(-1) - \frac{1}{2} \frac{d^3 f_n(-1)}{dy^3} + \frac{R}{2E_2} f_n(-1) \right\}$$

$$+ \left\{ \frac{E_1}{R} \frac{d^3 g_m(+1)}{dy^3} + g_m(+1) \right\} \left\{ - \frac{R}{E_1} f_n(+1) \right\}$$

$$+ \left\{ \frac{E_2}{R} \frac{d^3 g_m(-1)}{dy^3} - g_m(-1) \right\} \left\{ \frac{R}{E_2} f_n(-1) \right\}$$

and

$$D_{nm} = \int_{-1}^{+1} f_n \left\{ iaR \left\{ \frac{d^2 g_m}{dy^2} - a^2 g_m \right\} \right\} dy$$

$$+ \frac{dg_m(+1)}{dy} \left\{ -iaRf_n(+1) + \frac{1}{2} \frac{d^3 f_n(+1)}{dy^3} + \frac{R}{2E_1} f_n(+1) \right\}$$

$$- \frac{dg_m(-1)}{dy} \left\{ -iaRf_n(-1) - \frac{1}{2} \frac{d^3 f_n(-1)}{dy^3} + \frac{R}{2E_2} f_n(-1) \right\} .$$

Now, if we substitute the trigonometric functions for f_n and g_m,

as defined, it can be seen that the matrices (B_{nm}) and (D_{nm}) may be partitioned in the following manner

$$(B_{nm}) = \left[\begin{array}{c|c} (B_{11}(p,q)) & (B_{12}(p,q)) \\ \hline (B_{21}(p,q)) & (B_{22}(p,q)) \end{array}\right] \qquad \text{and}$$

$$(D_{nm}) = \left[\begin{array}{c|c} (D_{11}(p,q)) & (D_{12}(p,q)) \\ \hline (D_{21}(p,q)) & (D_{22}(p,q)) \end{array}\right] .$$

Here, $(B_{11}(p,q))$ and $(D_{11}(p,q))$ correspond to $f_p(y) = \cos(p\pi y/2)$ $(p=0, 1, \ldots, N-1)$ and $g_q(y) = \cos(q\pi y/2)$ $(q=0, 1, \ldots, N-1)$, $(B_{12}(p,q))$ and $(D_{12}(p,q))$ correspond to $f_p(y) = \cos(p\pi y/2)$ $(p=0, 1, \ldots, N-1)$ and $g_q(y) = \sin(q\pi y/2)$ $(q=0, 1, \ldots, M-1)$, $(B_{21}(p,q))$ and $(D_{21}(p,q))$ correspond to $f_p(y) = \sin(p\pi y/2)$ $(p=0, 1, \ldots, M-1)$ and $g_q(y) = \cos(q\pi y/2)$ $(q=0, 1, \ldots, N-1)$ and $(B_{22}(p,q))$ and $(D_{22}(p,q))$ correspond to $f_p(y) = \sin(p\pi y/2)$ $(p=0, 1, \ldots, M-1)$ and $g_q(y) = \sin(q\pi y/2)$ $(q=0, 1, \ldots, M-1)$. The size of the matrices (B_{nm}) and (D_{nm}) is $(M+N, M+N)$, and the sizes of the smaller matrices are given by the maxima of the indices p and q. The entries for (B_{nm}) and (D_{nm}), after substitution of the approximating series, are given in Appendix B.1. It can be seen that the rows n=N and columns m=N of (B_{nm}) and (D_{nm}), corresponding to

sin(0) (i.e. zero), are identically zero. In the computations, these rows and columns are omitted.

Now we demand that the functional, I, is stationary with respect to variations in $\underline{u}$ and $\underline{\bar{u}}^{\star}$ (i.e. with respect to variations in a_m and $\bar{a}_n^{\star}$). Applying this, we obtain that

$$\frac{\partial I}{\partial \bar{a}_n^{\star}} = 0 \quad \text{leads to} \quad \sum_{m=0}^{N+M-1} a_m \left((B_{nm}) - c(D_{nm}) \right) = 0$$

$$(n=0,\ 1,\ \ldots,\ N+M-1)$$

and $$\frac{\partial I}{\partial a_m} = 0 \quad \text{leads to} \quad \sum_{n=0}^{N+M-1} \bar{a}_n^{\star} \left((B_{nm}) - c(D_{nm}) \right) = 0$$

$$(m=0,\ 1,\ \ldots,\ N+M-1).$$

This gives us (N+M) linear equations for the (N+M) a_m's, and (N+M) linear equations for the (N+M) $\bar{a}_n^{\star}$'s. We get non-trivial solutions if, and only if,

$$\left| (B_{nm}) - c(D_{nm}) \right| = 0 \ , \qquad 4.4.1$$

which defines our eigenvalues c.

As we shall be continuing with Formulation 4, the other formulations are not given. The matrices for the adjoint of our problem, using Formulation 4, were also calculated. The procedure was the same as that employed above, and the resulting entries of the matrices are given in Appendix B.2. For the adjoint problem, the functional taken is $I = \langle \underline{u}, \underline{H}^{\star}(\underline{u}^{\star}) \rangle$, instead of $I = \langle \underline{u}^{\star}, \underline{H}(\underline{u}) \rangle$. (Actually, we have considered the complex conjugate of the adjoint functional, $I = \langle \underline{\bar{u}}, \underline{\bar{H}}^{\star}(\underline{\bar{u}}^{\star}) \rangle$.)

4.5. Numerical considerations.

To obtain numerical results, we must determine the eigenvalues (c) of the characteristic equation (Equation 4.4.1)

$$| (B_{nm}) - c(D_{nm}) | = 0 \quad ,$$

the entries of the matrices (B_{nm}) and (D_{nm}) in this characteristic equation being given in Appendix B.1. Standard numerical eigenvalue procedures are normally based on (D_{nm}) being a unit matrix. It is therefore necessary, having computed the entries of (B_{nm}) and (D_{nm}), to multiply the characteristic equation by the inverse of (D_{nm}) ($(D_{nm})^{-1}$). This gives us

$$| ((D_{nm})^{-1}(B_{nm})) - c(I) | = 0 \quad ,$$

where (I) is the unit matrix. In order to obtain accurate inverses of the matrices involved, a double precision matrix inversion routine was used. The eigenvalue routine, which also found the eigenvectors, was a FORTRAN coded program; Share number SDA 3441. Another routine, Share number SDA 3099, which only evaluated the eigenvalues, was also adapted for use with the program.

Checks may be kept on the accuracy of the inversion and eigenvalue routines. The number of eigenvalues obtained, and their accuracy, is determined by the number of terms used in the approximating series. We consider only symmetric disturbances, employing an approximating series of cosines only, and find that a thirty term approximating

series gives us the most unstable eigenvalue with sufficient accuracy. We gauge our accuracy by comparison with previous rigid wall work, and by incrementing our approximating series until the resultant stability curves and stream function and Reynolds stress distributions become insensitive to further increase. We obtain results accurate to four decimal places, and results showing the accuracy of the present computations are described in Chapter 5. The complete spectrum of eigenvalues and eigenvectors is obtained from this part of the program.

The necessary stability curves may be obtained from the eigenvalues. When difficulty was encountered in obtaining accurate results for the eigenvalues, it was found that use of an eigenvalue pivot was very beneficial. Lee and Reynolds (1967) employed such a technique in their study of the rigid wall problem. When eigenvalue routines find the eigenvalue of largest modulus first (and most accurately), the characteristic equation, $| (B) - c(D) | = 0$, can be rewritten as

$$| (D) - \frac{1}{(c-\lambda_o)} (B-\lambda_o D) | = 0 .$$

The eigenvalue pivot, λ_o, may be chosen as complex (all the matrices involved are complex and non-symmetric) and is chosen fairly close to the desired eigenvalue c. In our case, $\lambda_o = .2$ produced adequate results for the rigid wall problem. The eigenvalue routine is used to find the eigenvalues of $((B-\lambda_o D)^{-1}(D))$, after which, the effects of the pivot are removed to give the correct eigenvalues.

From the eigenvectors, the components of which are simply the coefficients in the approximating series for $\phi(y)$, the stream function and Reynolds stress distributions may be obtained by substitution. The stream function distributions, hence obtained, are unique apart from an arbitrary multiplying factor. This (complex) factor is used to normalise the stream functions such that $\phi_r(0) = 1$ and $\phi_i(0) = 0$, where the stream function $= \phi(y) = \phi_r(y) + i\phi_i(y)$. The Reynolds stress distributions are obtained by substituting the normalised stream function distributions into the expression

$$2\left\{ \phi_r(y) \frac{d\phi_i(y)}{dy} - \phi_i(y) \frac{d\phi_r(y)}{dy} \right\}$$

(see, for example, Stuart (1963)). This expression represents the correct Reynolds stress for the problem, when multiplied by $\left\{ -\frac{\rho a}{4} \right\}$. The results are normalised in this manner to facilitate comparisons with previous results for the rigid wall problem.

Although the direct formulation gave accurate eigenvalue results, when the stream function and Reynolds stress distributions were sought it was found that the resultant distributions did not converge well with incrementation of the approximating series, did not give good agreement with previous rigid wall results and did not satisfy the relevant boundary conditions. However, when the transpose of the direct formulation was used to find the adjoint stream function and Reynolds stress distributions, good results were obtained (when

judged by the previous criteria). When the adjoint formulation was used, it gave poor results for the adjoint distributions, but good results for the distributions of the problem under consideration (obtained by transposing the matrices in the adjoint formulation). These inaccuracies would appear to be due to numerical ill-conditioning. Lee and Reynolds(1964) appear to have had the same trouble, although, using their approach to the rigid wall problem, they obtained good results for the problem and poor results for the adjoint problem. For the present results, the transpose of the adjoint formulation was used to obtain results for the problem, and the transpose of the direct formulation was used to obtain results for the adjoint problem.

The variational part of the solution is incorporated into the iterative scheme (which is set up as described in Section 3.3), as shown in the simple flow diagram given in Appendix C. Accuracy may be controlled by the choice of the eigenvalue guess (c^o), how close to e^o we choose the values e_1^o and e_2^o and the number of iterations performed. We take $e_1^o = e^o + pe^o$ and $e_2^o = e^o - pe^o$, where p is a small constant ($0<p<<1$), which depends on the estimated sensitivity to changes in e of the eigenvalue sought and the accuracy of the eigenvalue guess. We may choose a different value of p for each iteration performed in a particular eigenvalue search. In the computer program, a typical value of p for the first iteration was .01, decreasing by .0025 with each successive iteration. Each iteration involved three uses of the variational part of the solution. It was unusual to take more than

three iterations, and, with a good eigenvalue guess, convergence could be obtained with one iteration. If the program exceeded four iterations, then it was better to start the program again with a new eigenvalue guess, and so a limit of four iterations was kept for each eigenvalue search. We judge convergence by examining the changes in e, since this, generally, changes more rapidly than c. In the present work, satisfactory convergence of the eigenvalues was obtained when the two values of e compared (e^2 and e^3), differed by less than .1%. This gave us the eigenvalues accurate to four decimal places.

The computations were programmed in FORTRAN for the CDC 6600 computer, and all the results presented herein were obtained on this computer. Some initial work was performed on an IBM 7094 computer. It was only found necessary to employ the eigenvalue pivoting technique when working on the IBM 7094 computer. On the CDC 6600 computer, it took approximately 11 seconds to obtain a spectrum of thirty eigenvalues in terms of fixed values of the parameters E_1 and E_2. The times taken in the present work are roughly equivalent to those taken in previous computations, taking into account the improvements in computer storage and speed.

Chapter 5. Discussion of numerical results.

5.1. Introduction.

The numerical results obtained from the computer program, set up as described previously, are presented in figures and tables at the end of the thesis. These results, consisting partly of checks on accuracy, and partly of solutions to representative flexible wall situations, will be described and discussed in the present chapter. The notation used in the figures and tables is defined in the relevant part of the thesis, and further given at the beginning of the thesis.

5.2. Rigid wall results.

In Tables 1 and 2, the most unstable eigenvalue, c, is given for the different formulations considered, showing the convergence of c with increases in the number of terms in the approximating series (at a value a = 1 and values R = 1600 and 2500). The chosen values of E_1 and E_2 simulate rigid walls, and convergence to the results given by Thomas (1953), for the chosen formulation (Formulation 4), is obtained with sixteen and eighteen term series respectively. Lee and Reynolds (1964, 1967) use an approximating series especially suited to their variational solution of the rigid wall problem, and they obtain convergence to Thomas's results at (a,R) = (1,1600) (table 1) with

an eleven term series. In their first paper (1964), higher eigenvalues are given at (a,R) = (1,100), and these agree well with present results. Apart from the Tollmien-Schlichting modes, numbers of spurious modes occurred in the present eigenvalue spectrums, these spurious modes being non-convergent with increases in the number of terms in the approximating series. Unfortunately, Lee and Reynolds did not give a neutral stability curve in their results, and so comparisons with the present rigid wall neutral stability curve are impossible. It should be remembered that the approximating series in the present work has been chosen as generally as possible. From these tables, it may also be seen that the real part of c, c_r, converged more rapidly than the imaginary part, c_i. This is a feature of all the present results. Table 3 gives the most unstable eigenvalue at (a,R) = (1,2500), using a twenty cosine series, showing how suitable values of E_1 and E_2 may be chosen to simulate rigid walls. Tables 1, 2 and 3 are further discussed in Section 4.3.

Table 4 gives values of the imaginary part of the most unstable eigenvalue, c_i, for different values of the fluid parameters (a,R), using a thirty cosine series. Curves of c_i versus R, for fixed values of a, are plotted in Figure 3. As described in Section 1.2, neutral stability is found where $c_i = 0$ (in the temporal sense). Points on the rigid wall neutral stability curve are determined by plotting curves of c_i versus R for fixed a, and then finding the values of R at which $c_i = 0$. In this way, values of the fluid parameters, (a,R), defining the neutral stability curves for both the rigid wall and

flexible wall problems, were determined. (In cases where portions of the neutral stability curve lie parallel to the R axis, it is more accurate to determine these portions of the neutral stability curve by using curves of c_i versus a for fixed R.) Points on the constant amplification curves are found where c_i takes a constant value. Points on the rigid wall neutral stability and constant amplification curves, using a thirty cosine series, are given in Table 5. Points on the rigid wall neutral stability curve, using a twenty cosine series, are given in Table 7. The neutral stability and constant amplification curves are plotted in Figure 4. In Figure 5, convergence of the present work and comparisons with previous results are shown. Values of the real part of the most unstable eigenvalue, c_r, using a thirty cosine series, are given in Table 6, and these values are used to plot the curves in Figure 6. The neutral stability curve of c_r versus R (i.e. the spatial neutral stability curve) is obtained from these curves by finding the values of c_r corresponding to the values of a and R lying on the temporal neutral stability curve. Points on the spatial neutral stability curves, for twenty and thirty cosine series, are given in Table 8, and the curves are plotted in Figure 7. For both the temporal and spatial stability curves, results are given accurate to three decimal places.

All of the previous curves are very smooth, and give good agreement with previous work. The curves in Figure 5 show how good the exact agreement is, comparing the present with previous work. The earlier,

asymptotic curve, obtained by Shen (1954), agrees well with the low a part of the present curve, but at higher values of a, a fairly large discrepancy may be seen, as would be expected considering the limitations of the asymptotic analysis. The neutral stability curve of Grosch and Salwen (1968), which is obtained computationally by using a similar technique to the present, but for rigid walls, gives excellent agreement with the present curve. It is believed that Grosch and Salwen employed a thirty term series in obtaining their curve. The present curve, obtained using a thirty cosine series, is insensitive to further increase in the number of terms used in the approximating series. Comparisons with the curve obtained by using a twenty cosine series, show that the latter curve gives a very similar critical Reynolds number and reasonable agreement for small values of a, but that, at larger values of a, the discrepancy becomes more marked, and the latter stability curve falls too low. Convergence of the spatial neutral stability curve is shown in Figure 7, and the same convergence trends may be noted as in the temporal neutral stability curve (Figure 5). In this case, however, the convergence is more rapid, since, as already pointed out, c_r converges more rapidly than c_i.

Rigid wall stream function and Reynolds stress distributions will now be presented. In Tables 9(a), 10(b) and 12(a), points are given, and in Figures 8, 9 and 10, the corresponding graphs plotted, for the rigid wall distributions at a = 1 and R = 100, 1600 and 10000, using a thirty cosine series. It should be noted that, as stated in

Section 4.5, the stream function, $\phi(y)$, is normalised such that $\phi_r(0) = 1$ and $\phi_i(0) = 0$, and also that the Reynolds stress plotted is equal to the correct Reynolds stress divided by a factor$(-\rho a/4)$. This means that a positive sign for the plotted Reynolds stress implies conversion of energy from the mean flow into the disturbance. The rigid wall boundary conditions are $\phi(+1) = 0$ and $\frac{d\phi(+1)}{dy} = 0$, and it may be observed that the stream functions satisfy these conditions to high accuracy. The Reynolds stresses are zero at the wall, as required, and have a peak (at which the Reynolds stress is positive) near the critical point, $y = y_c$ (where $U(y_c) = (1-y_c^2) = c_r$). This latter fact would be expected, since, for the rigid wall problem, the critical point is close to the wall and the jump in the value of the Reynolds stress, expected at the critical point, is quickly brought to zero by the viscous forces at the wall. In Tables 9(b), 10(a), 11(a) and 11(b), points are given, and, in Figures 11, 12, 13, 14 and 15, the corresponding graphs are plotted, by means of which we examine the distributions for convergence at values of $(a,R) = (1,1600)$, using ten and twenty cosine series, and $(a,R) = (1,6400)$, using twenty and thirty cosine series. It can be seen that the real parts of the stream functions have already converged with the smaller numbers of terms in the series, while the imaginary parts of the stream functions and the Reynolds stresses have almost converged, although the increases in the numbers of terms in

the series produce slight alterations of the curves. As pointed out earlier, the variational approach would be expected to give the eigenvalues more accurately than the eigenvectors. It may be observed in these convergence results that, the higher the value of R used, the larger the number of terms required in the approximating series, for given accuracy. Figures 16, 17 and 18 show comparisons of present results with those of Lee and Reynolds at (a,R) a (1,1600), and with those of Thomas at (a,R) = (1,10000). At (a,R) = (1,1600), a ten cosine series is employed for the present results, to give a direct comparison with Lee and Reynolds, and at (a,R) = (1,10000), a thirty cosine series was used, although no direct comparison can be made with Thomas from the point of view of the number of terms used in the approximating series. In both cases, the comparisons are very favourable. In Table 12(b), points are given, and in Figure 19, the corresponding graphs plotted, for the stream function and Reynolds stress distributions for the adjoint rigid wall problem at (a,R) = (1,100), using a thirty cosine series. These are very smooth and agree exactly with curves given by Lee and Reynolds. As mentioned in Section 4.5, the transpose of the direct formulation is used to obtain the adjoint stream function and Reynolds stress distributions. The eigenvalues of the problem are obtained using the direct formulation, and their accuracy is related to the accuracy of these distributions. The adjoint results are therefore included to show the accuracy of these distributions.

At this stage it is possible to conclude that the problem set up generally to solve the flexible wall problem is capable of giving excellent results for the rigid wall situation. As there is no particular bias in the modes towards rigid or non-rigid walls, we may now anticipate, with some optimism, equally satisfactory results in the flexible wall case.

5.3. Flexible wall results.

There are a number of results available from the publications of Hains and Price (1961a and b, 1962a and b) which may be used to check the present calculations. The simplest calculations are for fixed values of E_1 and E_2, corresponding to rather artificial flexible walls, since the physical wall parameters will vary along the stability curves (due to the a, R and c dependence in the definitions of E_1 and E_2). Stability curves were calculated for a value of $E_1^{-1} = E_2^{-1} = -10$, and we first examine the convergence of the present curves at this value. Points on the stability curves, obtained using thirty and twenty cosine series respectively, are given in Tables 13 and 14. In Figure 20, we compare the neutral stability curves obtained with twenty and thirty cosine series. It can be seen that, at small a, the curves have already converged with a twenty cosine series. Along the high a portions of the curves, there is a small difference when the number of terms in the approximating series is increased, the largest difference being

about 4 °/o. There is insignificant change for more than thirty terms in the approximating series. In Figure 21, it can be seen that the spatial stability curves have already converged with a twenty cosine series (as pointed out in Section 5.2, more rapid convergence may be expected with spatial stability than with temporal stability curves). Also in Figures 20 and 21, we compare the present stability curves with those of Hains and Price, for this value of E_1 and E_2. Good agreement is obtained in both comparisons, the largest discrepancy between the present neutral stability curve for a thirty cosine series and the neutral stability curve of Hains and Price being about 2 °/o.

It is possible to examine the effect of omitting the viscous component of the normal stress (Hains and Price, and Landahl and Kaplan (1965) omit this term in their respective calculations). This omission is equivalent to subtracting a factor $(-4a^2/cR)$ from the expression for E_j^{-1} $(j = 1,2)$ (see Section 2.2), and the largest modification of E_j^{-1} is expected when the smallest value of damping is used. In the present results, the smallest value of damping used was D = 250, and, with this value of damping, omission of the above term caused an increase of about 1 °/o in the critical Reynolds number of the class A mode. Changes would generally be expected to be smaller than this, and, with a tension of $.5\times10^9$ for the case of walls with tension only, an increase in critical Reynolds number of about .2 °/o was experienced.

For certain flexible wall situations, it is possible to transform, quite readily, the neutral stability curve for rigid wall, plane

Poiseuille flow into neutral stability curves for the flexible wall problem, by use of the asymptotic analysis developed by Lin (1945, 1955). The basis of such a transformation lies in the analysis of Benjamin (1960) for the qualitative behaviour of the stability curves for the flexible wall, boundary layer problem. For the present problem of flexible wall, plane Poiseuille flow, we take that analysis a stage further to establish a precise form for the transformation of the Tollmien-Schlichting stability curve for a rigid wall to that for a membrane wall with no structural damping. We start with the characteristic equation in the usual form and notation (see Benjamin (1960), where $\lambda = 0$, and Landahl (1962)):

$$u + iv + \alpha = \frac{\mathcal{J}(z)}{1 + \lambda(1 - \mathcal{J}(z))} \quad , \qquad 5.3.1$$

where, in our notation (see Section 2.2), for a membrane without structural damping,

$$\alpha = - \frac{\frac{dU(-1)}{dy}\, c}{ma^2 \left\{ \frac{c_0^2}{R^2} - c^2 \right\}}$$

and (from Lin (1955), pages 37, 38 and 40)

$$u = \frac{v}{\pi} \log c + O(1) + \frac{\frac{dU(-1)}{dy}\, c}{a^2 \int_{-1}^{0} (U-c)^2 \, dy} \left(1 + O(a^2)\right) \quad ,$$

$$v = -\pi c \frac{dU(-1)}{dy} \frac{\frac{d^2U(y_c)}{dy^2}}{\left\{\frac{dU(y_c)}{dy}\right\}^3} (1 + O(c^3)) \quad ,$$

$$\lambda = \frac{(y_c + 1)}{c} \frac{dU(-1)}{dy} - 1 \quad , \mathcal{J}(z) \text{ is the modified Tietjens function}$$

and $z = \left\{ aR \frac{dU(y_c)}{dy} \right\}^{\frac{1}{3}} (y_c + 1)$. These terms are given, and will be

used, to the order of accuracy employed in the calculations of the rigid wall stability curve (Lin (1945)), which is known to be quite accurate. Since λ and v are functions of c alone, $\mathcal{J}$ is a function of z alone, z is a function of aR and c alone and α is real, the parameters a_o, R_o and c, defining the rigid wall, neutral stability curve (corresponding to $\alpha = 0$), may be used to obtain the parameters a, R and c, defining the flexible wall, neutral stability curves, by keeping c and z constant and only changing u through a (see Benjamin (1960)), i.e. $u(a,c) + \alpha = u(a_o,c)$ and $z(a,R,c) = z(a_o,R_o,c)$. (N.B. c_o is the free wave speed in the undamped membrane walls and not the value of c on the rigid wall, neutral stability curve.) Hence we obtain

$$\frac{\frac{dU(-1)}{dy} c}{a^2 \int_{-1}^{0} (U - c)^2 dy} + \alpha = \frac{\frac{dU(-1)}{dy} c}{a_o^2 \int_{-1}^{0} (U - c)^2 dy}$$

and $a_o R_o = aR$. Hence, on substituting for U and α, and performing the integration, we obtain

$$\frac{1}{a^2}\left\{ f(c)^{-1} - \left\{ m \left\{ \frac{c_o^2}{R^2} - c^2 \right\} \right\}^{-1} \right\} = \frac{1}{a_o^2} f(c)^{-1} \qquad 5.3.2$$

and $aR = a_o R_o$, where $f(c) = \left\{ \frac{8}{15} - \frac{4}{3}c + c^2 \right\}$. As Hains and Price (1961b, 1962b) have calculated stability curves for membranes under tension only, it is of interest to examine that case in more detail. Hence, substituting $mc_o^2 = T$ and $m = 0$ in the above two equations and eliminating R, we obtain

$$a^2 = a_o^2 \left\{ \frac{1}{2} \pm \left\{ \frac{1}{4} - \frac{R_o^2}{T} f(c) \right\}^{\frac{1}{2}} \right\} . \qquad 5.3.3$$

The two roots of this equation imply that each point on the rigid wall curve has a double image in the transformed plane. It may further be deduced that the neutral stability curve would be expected to close, since, for sufficiently large R_o, a becomes complex, contradicting our initial assumption that a is real. The neutral stability curves, obtained by Hains and Price for membranes under tension only, do, in fact, close. The neutral stability curve given by Lin (1945), for rigid wall, plane Poiseuille flow, is used in the above transformation to give a neutral stability curve for the case when $T = .5 \times 10^9$. (Accurate points on the flexible wall curve are found by using the table of rigid

wall points given by Lin, more approximate points being obtained by using Lin's curve to give the rigid wall points.) This curve is compared with the neutral stability curve obtained from the present program and also that of Hains and Price, for this value of T. The curves are compared in Figure 22 (the points for the present curve and the asymptotic curve being given in Table 15). It may be seen that agreement is good along the low R portions of the curves, while there is a marked discrepancy between the curve of Hains and Price and the other two curves along the high R portions. The curve for the present work is not completed, since the program is unsuited to examine stability at the low values of a and high values of R involved. Since, for the asymptotic analysis, that part of the rigid wall stability curve needed in the transformation is known to be quite accurate, and since the same order of accuracy is employed in the transformation, we would expect the flexible wall stability curve to be of the same accuracy. It is therefore unexpected to find the Hains and Price results in such disagreement with the asymptotic theory and our calculations.

From Equation 5.3.3, we may further deduce that, at the value of T for which

$$\frac{1}{4} - \frac{R_o^2}{T} f(c) = 0$$ when R_o is the rigid wall

critical Reynolds number (R_{o_c}), the region of instability shrinks to a point, and, for T less than this value, there is no transformed stability curve. Inserting the values given by Lin (1945) for a_o, R_o

and c, corresponding to the rigid wall critical Reynolds number, we find that the asymptotic theory predicts the curves closing to a point for $T = 2.8 \times 10^7$. This value of T is less than half that obtained by Hains and Price ($T = 6.65 \times 10^7$). Further, the point at which the curves disappear is given as $(a,R) = (.74,7500)$ by the asymptotic theory and as $(a,R) = (.85,8240)$ by Hains and Price. The present program was used to search the neighbourhood of these points. Again, the asymptotic theory was found to be more accurate. These results show that, for limited physical wall situations, where there is obviously no class B instability, the asymptotic theory can give very good stability results. They also cast doubt on the accuracy of the computations of Hains and Price.

We now examine a more general wall situation: the general effects of variations in free wave speed, c_o, and damping, D, in the walls, for representative values of these parameters. First, we examine the effect of changing c_o (or tension, for a membrane), keeping other properties constant. The mass parameter, m, for all these curves, is fixed at a representative value of unity. A value of c_o, suitable to simulate a rigid wall, was found to be $c_o = 10^5$, stability curves being insensitive to further increase in this parameter. Stability curves were found for values of c_o chosen to represent walls departing from rigidity down to a value $c_o = 3000$. For a free, damped membrane, the wave speed, c_p ($c_p = R \times c$, see Section 2.1), is given by the expression

$$c_p = \frac{iD}{2a} \pm \left\{ c_o^2 - \frac{D^2}{4a^2} \right\}^{\frac{1}{2}} \quad ,$$

and underdamped waves exist provided the damping ratio, $\frac{D}{2ac_o}$, is less than unity. The value of damping chosen for the present results was $D = 1000$, and, for wave numbers in the range associated with the critical Reynolds numbers, the present values of c_o give underdamped waves in the membrane, the situation closest to critical damping ($D/2ac_o = 1$) occuring when $c_o = 3000$ (for this value of c_o, a must be less than $1/6$ before the waves are overdamped; larger values of D, causing waves to be overdamped at higher a, are of less interest since the damping would then begin to swamp the effect of variations in c_o). The parameters chosen for the present model are qualitatively similar to those chosen by Kaplan (1964) and Landahl and Kaplan (1965), for the boundary layer problem. (Taking into account the different schemes of dimensionless variables, their values of D ranged from 20 to 3000, and their values of c_o ranged from 1000 to 3000, while m was fixed at unity.) In the present work, stability results were found for $c_o = 3000$, 5000, 10000 and 10^5. The points on the stability curves are given in Tables 16, 18 and 20. The neutral stability curves are compared in Figure 23. In this figure, it can be seen that, for the values $c_o = 3000$ and 5000, the neutral stability curves have two (joined) parts exhibiting different natures. These two parts will be referred to as the lower part and the

upper part (from their position in the a versus R diagram). The neutral stability curve for c_o = 10000 also exhibited this characteristic, although its upper part was at a Reynolds number of roughly 15000. Curves for large values of c_o, close to the rigid wall curve (as typified by the curve at c_o = 10000), have lower parts whose behaviour is predicted by Benjamin (1960) in his description of the class A mode. However, as c_o decreases further away from its rigid wall value, the damping starts to have a greater influence and the lower parts of the neutral stability curves become more unstable (in the sense of critical Reynolds number). Spatial stability curves are given in Figure 24, and it can be seen that, in the vicinity of the critical Reynolds number, the walls are stiffness controlled, and hence (damped) free wave speeds are always larger than wave speeds associated with neutral stability curves. At significantly lower values of c_o, the walls would become inertia controlled in the vicinity of the critical Reynolds number and this, combined with the damping effect, would cause an even faster shift to the left.

The upper parts of the neutral stability curves become steadily more unstable as the flexibility of the walls is increased (i.e. c_o decreases). The class B mode of unstable disturbance (Benjamin (1960)), corresponding to unstable waves in the flexible walls, would be expected when the wave speed, c_{pr}, is near the free wave speed in the flexible walls. It may be seen from Figure 24 that, as we move from the lower parts to the upper parts of the neutral stability curves, c_{pr} is steadily increasing, supporting the classification of the upper parts

of the curves as class B disturbances. Another marked difference between the lower parts and the upper parts of the neutral stability curves, is the different rate of amplification experienced when crossing the stability boundaries of these two parts. This property is illustrated in Figure 25, where a constant amplification curve is shown, calculated for $c_o = 5000$, representing a constant rate of amplification of $c_{pi} = -2.5$ (points for this curve are given in Table 19). At $a = .925$ on the lower part of the curve, it took an increase in R of roughly 400 to achieve this amplification rate, while at all points on the upper part of the curve, the amplification rate was so rapid as to make distinction from the neutral curve impossible. In general, amplification rates increased by a factor of between 10 and 100 when moving from the lower to the upper parts of the stability curves. The above difference between the magnitudes of the amplification rates, experienced when crossing the two parts of the neutral stability curves, is typified by a rapid change of slope in curves of c_{pi} versus R at fixed a, this rapid change occuring in the neighbourhood of $c_{pi} = 0$. An illustration of this behaviour is shown in Figure 26, where curves of c_{pi} versus R for fixed a are plotted at $c_o = 3000$ (points on these curves are given in Table 17). The curve at $a = 1.05$ shows the changes in c_{pi} when crossing the upper part, and the curve at $a = .95$ shows the changes in c_{pi} when crossing the lower part of the neutral stability curve. Results for other neutral stability curves are similar. Another important aspect, shown here, is that the region in which the amplification rate increases rapidly, lies not only

behind the upper part but also behind the lower part of the neutral stability curve. Since the class B mode of disturbance is essentially a resonance effect at values of c_{pr} near c_o, it might be expected that a rapid amplification rate was experienced across a class B stability boundary. The critical Reynolds number may be associated with either the lower or the upper parts of a neutral stability curve (for the flexible wall parameters $(m,D,c_o) = (1,250,5000)$, the upper part of the neutral stability curve exhibited a critical Reynolds number marginally smaller than that of the lower part). It would appear that, in order to obtain reduction of the amplification rates, inhibition of the upper parts of the stability curves would be far more important than inhibition of the lower parts. Kaplan (1964) gave a class B stability boundary for the boundary layer over a membrane wall, although he later reported an error in this result (Landahl and Kaplan (1965)). He found this stability curve in a similar region of the (a,R) plane to the region in which the upper parts of the present curves are found. He did not, however, find a large difference in amplification rate between class A and class B modes, his results showing that the amplification rates were of the same magnitude for both modes.

There is a strong suggestion in the nature of the present results that, in the terminology of Benjamin, the two parts of the curves represent class A and class B instabilities. This is a situation not unlike that indicated elsewhere, although other results show two seperate neutral stability curves for class A and class B instabilities: in the

present case the curves have merged to form a continuous stability curve.

We now investigate the effect of damping variation, with other properties remaining constant. The mass is again kept at unity, and a moderate value for the free wave speed, $c_0 = 5000$, is chosen, at which to make comparison. Results for these values, with a value for damping of $D = 1000$, have been given above. A reduced value of the damping, $D = 250$, giving a lightly damped wall, is chosen, at which to make comparison with these above curves. For the lower value of the damping, the stability results were taken to a very high value of a, in order to examine more fully the behaviour of the upper part of the curve, and points on this curve are given in Table 21 ((a) and (b)). Figures 27 and 28 show the stability curves in the usual (a,R) region, and, in Figure 27, the partitioning effect of the neutral stability curve is again encountered. It can be seen that, the decrease in damping has stabilised the lower part of the stability curve, while destabilising the upper part. These alterations are again in line with the predictions of Benjamin (1960), classifying the lower and upper parts of the curves as classes A and B respectively. In Figures 29 and 30, the upper parts of the stability curves, at $(m,D,c_0) = (1,250.5000)$, are plotted more fully. The classical asymptotic analysis would be completely inadequate at these high values of wave number. In Figure 29, the upper part of the neutral stability curve is seen to exhibit a critical Reynolds number (slightly lower than that of the lower part), and, for even

higher values of a, the curve becomes somewhat wavy. This waviness is due to the accuracy of the results dropping off at the high value of a involved. A few points calculated for the stability curve with a thirty-five term series, instead of the usual thirty, showed that this waviness may be smoothed out. An interesting fact, noted from Figure 30, is that c_{pr} reaches an almost constant value on the upper part of the neutral stability curve, this constant value being slightly less than the value of c_o being used. This would again lead to the conclusion that the upper part of the stability curve should be classified as a class B mode.

Further insight into the nature of the different parts of the stability curves may be gained by examining the spatial distribution of the disturbance between the walls. Stream function and Reynolds stress distributions were found at values of $(m,D,c_o) = (1,1000,5000)$ for the flexible wall parameters, and at different points on the corresponding stability curve. The first set of distributions (Table 22) were taken at a point on the front of the lower part, the second (Table 23) at a point on the back of the lower part and the third (Table 24) at a point on the upper part of the neutral stability curve. The real parts of the stream functions are compared in Figure 31, the imaginary parts of the stream functions in Figure 32 and the Reynolds stresses in Figure 33. A further check on the accuracy of the calculations may be made by investigating how closely the computed stream function distributions

satisfy the boundary condition, $\frac{d\phi(+1)}{dy} - \frac{2}{c}\phi(+1) = 0$ (see Section 2.2). By substituting the values of $\phi_r(+1)$, $\phi_i(+1)$ and c into this boundary condition, we may predict the values which the gradients of the stream functions would be expected to take at the wall. These predicted gradients are shown alongside the stream function distributions in Figures 31 and 32, and a detailed examination of the stream functions at the wall shows that they change rapidly near the wall to produce the predicted gradients with high accuracy. The Reynolds stresses are zero (or almost zero) at the wall, ~~as expected~~. A marked difference may be noticed between the three sets of distributions, and this is particularly noticeable and relevant in the Reynolds stress distributions. All of these Reynolds stresses indicate a conversion of energy from the mean flow to the disturbance. The first distribution is very similar to that obtained at neutral stability for a rigid wall, being virtually zero nearly up to the critical point ($y = y_c$), where a rapid increase takes place, this increase being brought to zero at the wall. A double peak is just noticeable in this curve. The other two distributions broaden out, and the double peak becomes more obvious, the first peak occuring near the critical point and the second (larger) very close to the wall. This second peak becomes more pronounced in the third curve. Reynolds stresses for other values of the flexible wall parameters exhibit similar behaviour. This behaviour confirms earlier statements by Benjamin (1960) and Landahl (1962) about the decrease in the

thickness of the viscous wall layer caused by wall compliance. The viscous and critical layers overlap at neutral stability in the rigid wall problem, causing the maximum Reynolds stress to occur at (or near) the critical point. However, when the thickness of the wall layer decreases, the jump in the Reynolds stress occurs at $y = y_c$ (as predicted by inviscid theory). The sharp peak in the Reynolds stress near the wall may be explained in terms of the rapidly oscillating and decaying wall layer (Lin (1955)). Kaplan (1964) gives Reynolds stresses for class A and B modes exhibiting similar behaviour to that of the first and third curves in the present work. Again, the classification of the lower and upper parts of the neutral stability curves as class A and B modes appears justified.

The effect of variation in free wave speed (c_o) with a, may be obtained, in principle, by a cross plotting of constant c_o neutral stability curves. However, unless the variation of c_o with a is very large, the present stability curves (Figure 23) are too widely spaced (in terms of c_o) to be useful in this way. Nevertheless, the general behaviour may be predicted, and this is illustrated for the case of thin plates. In this case, c_o increases with a, and, for thin plate neutral stability curves roughly coincident at a = .9 with the membrane neutral stability curve for $(m,D,c_o) = (1,1000,5000)$, we would expect the upper parts of the neutral stability curves to be stabilised, while the lower parts are destabilised. (By "stabilised", we mean that, for the same value of a, the thin plate curve is found at higher values

of R than those at which the membrane curve for $(m,D,c_o) = (1,1000,5000)$ is found, and vice versa for "destabilised".) Results were found for two such thin plates, the first at $(m,D,c_o) = (1,1000,(4000^2 + 10^7 a^2)^{\frac{1}{2}})$ (Table 25(a)) and the second, a plate with no mid-plane tension, at $(m,D,c_o) = (1,1000,(3\times10^7 a^2)^{\frac{1}{2}})$ (Table 25(b)). The resultant curves are compared with those for a membrane at $(m,D,c_o) = (1,1000,5000)$ in Figures 34 and 35, and the predicted behaviour is seen to be confirmed. Flexural rigidity may thus be seen to be beneficial in promoting stability by moving the regions of high amplification rate (associated with the upper parts of the neutral stability curves) to higher values of R.

Chapter 6. Conclusions.

The results presented in the previous chapter, and conclusions drawn from them, support a general classification of the lower parts of the neutral stability curves as class A, and the upper parts as class B. Although the classification of possible disturbances into classes A, B and C is very convenient, the present work demonstrates that, in practical situations, this exact classification may cease to be of importance since unstable disturbances may represent mergers of behaviour typical of all three modes. For example, it might be argued that the upper parts of the neutral stability curves are class C (or Kelvin-Helmholtz) modes, since they become more unstable with increased flexibility of the wall, are associated with regions of large amplification rate, and c_p is almost insensitive to changes in R along the corresponding high a portions of the spatial stability curves (see Figure 30). In fact, Kaplan (1964) reported, without details, unstable class C modes in the region in which he presented stability curves for other modes.

With regard to class A waves, it was established in Section 5.3 that a simple transformation existed to convert the rigid wall, neutral stability curve into the tension-only membrane stability curves. It was also established that the results of this transformation were more accurate than previously computed stability curves. It therefore seems

worthwhile to return to this analysis and examine it for more general situations. The fundamental idea (both for the boundary layer and plane Poiseuille flow problems) is that if the right hand side of Equation 5.3.1 is kept constant, then the net left hand side result must also be constant, i.e. $u_o + iv_o = u + iv + \alpha$ or, in real and imaginary parts, $u_o = u + \alpha_r$ and $v_o = v + \alpha_i$, where the subscript "$_o$" denotes conditions on the rigid wall. These two equations may be thought of as defining values of (a, c) (for flexible wall) in terms of (a_o, c) (for rigid wall); the constancy of the right hand side then determining the new R. Unfortunately, the functional dependence on a and c is often so complicated that explicit forms for these variables are not possible, and the only course open is a numerical evaluation of the above equations; the problem falls into this category if $\alpha_i \neq 0$. Hence, all deductions that can be made readily are for surfaces with no structural dissipation. When $\alpha_i = 0$, v is unchanged, which, because of its approximate form, requires c to be unchanged. Hence, $u_o = u + \alpha_r$ reduces to an equation for a, which, for undamped membrane walls enclosing plane Poiseuille flow, has the form given by Equation 5.3.2:

$$\frac{1}{a^2}\left\{ f(c)^{-1} - \left\{ m\left\{ \frac{c_o^2}{R^2} - c^2 \right\}\right\}^{-1} \right\} = \frac{1}{a_o^2}\, f(c)^{-1} \quad ,$$

where $f(c) = \left\{ \frac{8}{15} - \frac{4}{3}c + c^2 \right\}$. (N.B. c_o is the free wave speed

in the undamped membrane walls and should not be identified with (a_o, R_o).) Therefore, the complete transformation becomes

$$\frac{a^2}{a_o^2} = \frac{R_o^2}{2c_o^2}\left\{ c^2 + \frac{c_o^2}{R_o^2} \right\} \pm \frac{R_o^2}{2c_o^2}\left\{ \left\{ c^2 - \frac{c_o^2}{R_o^2} \right\}^2 - \frac{4c_o^2 f(c)}{mR_o^2} \right\}^{\frac{1}{2}}$$

and $R = \frac{a_o}{a} R_o$. Depending upon the membrane properties, c_o and m, and also upon the fact that R_o may not be less than the critical Reynolds number of the rigid wall stability curve, it can be seen that the discriminant, $\left\{ \left\{ c^2 - \frac{c_o^2}{R_o^2} \right\}^2 - \frac{4c_o^2 f(c)}{mR_o^2} \right\}$, may, or may not, be negative. Unlike the transformation for inertialess membranes, the discriminant must become positive for sufficiently large R_o, although, in a certain closed range of R_o, the discriminant may be negative. If, for example, m and c_o are so large that the discriminant is always positive, there will be a double image of all rigid wall points but no closed loop. Again, if the discriminant is negative at the critical rigid wall Reynolds number (R_{o_c}), no closed loop exists, but, on the other hand, if the discriminant goes negative after R_{o_c} (say at R_1), that part of the rigid wall, neutral stability curve up to R_1, will map into a closed loop in the transformed (a,R) plane. When the discriminant becomes positive again, the mapping gives stability curves which eventually extend into regions where the asymptotic theory

breaks down. There is no reason to suppose, in this general discussion, that the various regions of instability would not, in some cases, overlap. Nevertheless, it can be stated that the closed stability loop is not a unique product of the inertialess wall situation (although a wall with a purely inertial response, $c_0 = 0$, cannot exhibit such behaviour). For all these curves, c is less than .3 , and the class B curves, which would be expected in these cases, cannot be generated by such a transformation. (N.B. All the stability curves obtained from the present program have upper parts which exhibit values of c greater than .3 (sometimes markedly greater).)

The same observations may be made in the Blasius boundary layer situation, when the appropriate definitions of u and v are used and alterations in the scheme of dimensionless variables are taken into account. Considering a membrane under tension only, and making the tension dimensionless in the same manner as Hains (1965), we have

$$\alpha = -\frac{dU(w)}{dy}\frac{cR}{Ta^2} \quad , \text{ where } \frac{dU(w)}{dy} \text{ is the steady state velocity}$$

gradient evaluated at the wall, and T is the wall tension made dimensionless with the free-stream flow velocity. When u is taken for the Blasius boundary layer in the form

$$u = \frac{dU(w)}{dy}\frac{c}{a(1-c)^2}$$ (Lin (1955)), a transformation

equivalent to those obtained for plane Poiseuille flow may be derived,

$$\text{i.e.} \quad \left\{\frac{a}{a_o}\right\}^3 - \left\{\frac{a}{a_o}\right\}^2 + \frac{R_o}{a_o T}(1-c)^2 = 0 \quad \text{and} \quad R = \frac{a_o}{a} R_o \ .$$

This transformation predicts that the rigid wall neutral stability curve is again transformed into closed loops which disappear at $(a,R) = (1.1,2900)$ when $T = 2800$, whereas Hains (1965), in his calculations for this problem, obtained closed loops disappearing at $(a,R) = (1.0,4000)$ when $T = 4025$. Hains (1965) has commented that, if the tension were made dimensionless by using the boundary layer thickness instead of the free-stream velocity, the curves would probably not close. Such a prediction is not born out by this analysis, since making the tension dimensionless in this manner merely changes the form of α to $-\frac{dU(w)}{dy}\frac{cR^2}{Ta^2}$ and the resulting transformation still predicts the closure of the stability curves.

The low wave number region always causes some difficulty for the boundary layer situation because the dominant term in the perturbation pressure is the inviscid pressure (as expected when the boundary layer thickness becomes insignificant on a wave length scale) and the stability is then governed by the classical Kelvin-Helmholtz analysis. A pure membrane loses its stiffness for large wave lengths (because of the very small surface curvature) and is unstable when coupled to an inviscid

flow. This has lead to considerable discussion (Benjamin (1960), Landahl(1962)) and the employment of "local" stiffness terms in the membrane formulation (Landahl (1962), Kaplan (1964)). Such a difficulty does not arise for plane Poiseuille flow since the coupling of the membranes to the flow does not necessarily cause instability in this case. To show this, the leading term from the asymptotic expression for the pressure must be derived (by use of the results of Lin (1955)) and then inserted into the membrane equation (see Section 2.2), giving

$$c^2(1+m) - c\left\{\frac{4}{3} + i\frac{Dm}{aR}\right\} + \left\{\frac{8}{15} - m\frac{c_o^2}{R^2}\right\} = 0 \quad .$$

This equation is equivalent to that used by Landahl (1962) to study the role of damping in the boundary layer problem, and it predicts instability to occur, for $D \neq 0$, when

$$(1+m)\left\{\frac{8}{15} - m\frac{c_o^2}{R^2}\right\} > 0 \quad \text{or} \quad R > \left\{\frac{15}{8}mc_o^2\right\}^{\frac{1}{2}} \quad ,$$

and, for $D = 0$, when

$$(1+m)\left\{\frac{8}{15} - m\frac{c_o^2}{R^2}\right\} > \frac{4}{9} \quad \text{or} \quad R > \left\{\frac{1}{mc_o^2}\left\{\frac{8}{15} - \frac{4}{9(1+m)}\right\}\right\}^{-\frac{1}{2}} .$$

It can be seen therefore, that, as a tends to zero, the stability boundaries in the (a,R) plane become parallel to the a axis, eventually intercepting the R axis, and also that the effect of damping is

destabilising. Inserting in these formulae the values of m and c_0 considered in the present calculations, we obtain the following values at which the R axis is intercepted

c_0 (m = 1)	R (D ≠ 0)	R (D = 0)
3000	4110	5370
5000	6850	8950
10^4	13700	17900
10^5	137000	179000

A major point which can be made is that the asymptotic curves, for very small a, are at greater Reynolds numbers than the critical Reynolds numbers of the respective flexible wall curves, and hence R_c is still determined by the computed portions of the curves. Computations performed to check the stability boundaries predicted by this asymptotic analysis were inconclusive, because the program is not well suited for examining small a conditions.

It should, perhaps, be added that this argument is of limited practical interest, since the parameters describing the flexible walls would not be expected to hold in any real physical situation on a length scale where details of the overall wall support conditions become important. Further, when the wave length becomes much greater than the width of the pipe, the physical limitations on the length of the pipe would introduce the important effects of the ends.

Another region of interest in the present stability problem is that of low Reynolds number. Landahl (1962) has found regions of class B instability here, and Nonweiler (1963), using a similar approach to Benjamin's to obtain qualitative information on the stability of the boundary layer over various flexible walls, has obtained results for a membrane, similar in nature to those of Landahl (i.e. he predicted regions of class B instability at low R). (Lock (1954), using an asymptotic analysis to study the flow in the laminar boundary layer between parallel streams, also gives neutral stability curves at very low R.) All these results, based on the asymptotic analysis, assume that aR is large. From the appearance of these curves, it may be more informative to investigate small R solutions in order to see if the wall waves can be excited by very small fluid velocities. Such an approach may be summarized as follows. If we assume that the wall damping is zero, and expand the wave speed, c_p (the physical wave speed is used since it has not been made dimensionless with the fluid velocity), in terms of R, and then of m^{-1}, in order to study the most unstable class B disturbances at small R and small departures from wall rigidity, we obtain

$$c_p = (c_{11} + c_{12}/m + O(1/m^2)) + R(c_{21} + c_{22}/m + O(1/m^2)) + O(R^2) .$$

In this series, $c_{11} = c_0$ (purely real), and, letting m tend to infinity, we see that the remaining terms independent of m (c_{21}, c_{31}, . . . etc.) must be zero since m tending to infinity corresponds to a free flexible

wall. At R = 0 (zero flow velocity) there is no energy supply to feed a wall disturbance, and so the imaginary part of c_{12} must be positive, indicating stability. It may be seen that, for large values of m (corresponding to class B modes, since m is made dimensionless with the fluid density, ρ), there must be a region of stability for low enough R (R_c strictly speaking, much less than unity). This result may be derived analytically.

As regards possible favourable effects on flow stability as a result of using flexible walls, we may see in the present results that increases in R_c are possible, although not large, and that the regions of high amplification rate, associated with the upper parts of the neutral stability curves, may be moved to higher Reynolds number by a suitable choice of surface flexural rigidity. However, we must echo the conclusions of previous papers, that the new modes of instability introduced by the wall flexibility produce a generally more complex situation, where no substantial improvement in stability appears to be possible.

The computer program has been used to study the present stability problem for symmetric stream function distributions between two identical walls. For the rigid wall problem, symmetric stream functions have been demonstrated to be the most unstable, and no change is anticipated in this respect, when the flexible walls are introduced. It is possible that dissimilar walls could improve stability, and the present program has been set up to cope with this situation. However, no radical improvements in stability would be expected, and no computations have

been performed for this case.

We may finally remark on the approach employed in the present work. This has proved very satisfactory, and no complications are envisaged in applications of this method to other problems. Indeed, given the computing facilities, a general system of programs, with the same status as that of Landahl's programs (1966), could be constructed. With further computing scope, the present method of solution could be modified to solve directly for the eigenvalues. Noting that c occurs quadratically in the present problem (see Sections 2.2 and 4.4), the retention of c in explicit form when setting up the matrix equations would have generated a matrix equation of the form

$$\left((A)c^2 + (B)c + (D) \right) \underline{x} = 0 \quad ,$$ where (A), (B) and (C) are matrices

of the same order as those used in the present method, c is the eigenvalue and $\underline{x}$ the eigenvector. This may be converted to standard form by substituting $(I)c\underline{x} = (I)\underline{x_1}$, where (I) is the unit matrix and $\underline{x_1}$ a vector, and solving the above as two simultaneous equations to give

$$\left\{ \begin{bmatrix} (0) & -(I) \\ (A)^{-1}(D) & (A)^{-1}(B) \end{bmatrix} + c \begin{bmatrix} (I) & (0) \\ (0) & (I) \end{bmatrix} \right\} \begin{bmatrix} \underline{x} \\ \underline{x_1} \end{bmatrix} = 0 \quad .$$

In this standard form, the matrices are of twice the order of those involved in the present method. The great advantage is that this would

provide directly the complete spectrum of eigenvalues of the physical problem, and would eliminate the need for an iterative scheme, as used in the present solution.

Appendix A. The different formulations.

A.1. Formulations 1 and 2.

The operator ($\underline{H}$), for Formulations 1 and 2, is given by

$$\underline{H}(\underline{u}) = \begin{bmatrix} \dfrac{d^4\phi}{dy^4} - 2a^2\dfrac{d^2\phi}{dy^2} + a^4\phi + iaR\left\{(1-y^2)\left\{\dfrac{d^2\phi}{dy^2} - a^2\phi\right\} + 2\phi\right\} \\ 2\phi(+1) \\ 2\phi(-1) \\ \dfrac{E_1}{R}\dfrac{d^3\phi(+1)}{dy^3} + \phi(+1) \\ \dfrac{E_2}{R}\dfrac{d^3\phi(-1)}{dy^3} - \phi(-1) \end{bmatrix}$$

$$- c\begin{bmatrix} iaR\left\{\dfrac{d^2\phi}{dy^2} - a^2\phi\right\} \\ \dfrac{d\phi(+1)}{dy} \\ -\dfrac{d\phi(-1)}{dy} \\ 0 \\ 0 \end{bmatrix} ,$$

where $\underline{u} =$

$$\begin{bmatrix} 2\phi \\ -iaR\phi(+1) + \dfrac{d\phi(+1)}{dy}\left\{-a^2 + \dfrac{1}{2\phi(+1)} \cdot \dfrac{d^2\phi(+1)}{dy^2}\right\} \\ iaR\phi(-1) + \dfrac{d\phi(-1)}{dy}\left\{-a^2 + \dfrac{1}{2\phi(-1)} \cdot \dfrac{d^2\phi(-1)}{dy^2}\right\} \\ -\dfrac{1}{2} \cdot \dfrac{d\phi(+1)}{dy} \\ -\dfrac{1}{2} \cdot \dfrac{d\phi(-1)}{dy} \end{bmatrix} ,$$

and $\phi = \phi(y)$ in the first entries of the vectors.

The complex conjugate adjoint operator ($\underline{\underline{H}}^{\star}$), for Formulations 1 and 2, is given by

$$\underline{\underline{H}}^{\star}(\underline{\bar{u}}^{\star}) = \begin{bmatrix} \dfrac{d^4\bar{\phi}^{\star}}{dy^4} - 2a^2\dfrac{d^2\bar{\phi}^{\star}}{dy^2} + a^4\bar{\phi}^{\star} + iaR\left\{\dfrac{d^2\bar{\phi}^{\star}}{dy^2} - \dfrac{d^2(y^2\bar{\phi}^{\star})}{dy^2} + (2-a^2+a^2y^2)\bar{\phi}^{\star}\right\} \\ 0 \\ 0 \\ -2\dfrac{d^2\bar{\phi}^{\star}(+1)}{dy^2} + 4a^2\bar{\phi}^{\star}(+1) \\ 2\dfrac{d^2\bar{\phi}^{\star}(-1)}{dy^2} - 4a^2\bar{\phi}^{\star}(-1) \end{bmatrix}$$

$$- c \begin{bmatrix} iaR\left\{\dfrac{d^2\bar{\phi}^*}{dy^2} - a^2\bar{\phi}^*\right\} \\ \dfrac{d\bar{\phi}^*(+1)}{dy} \\ \dfrac{d\bar{\phi}^*(-1)}{dy} \\ -\dfrac{d^3\bar{\phi}^*(+1)}{dy^3} - \dfrac{R}{E_1}\bar{\phi}^*(+1) \\ -\dfrac{d^3\bar{\phi}^*(-1)}{dy^3} + \dfrac{R}{E_2}\bar{\phi}^*(-1) \end{bmatrix} ,$$

where

$$\bar{\underline{u}}^* = \begin{bmatrix} 2\bar{\phi}^* \\ \dfrac{1}{2}\dfrac{d^3\bar{\phi}^*(+1)}{dy^3} - \left\{iaR - \dfrac{R}{2E_1}\right\}\bar{\phi}^*(+1) + \dfrac{d\phi^*(+1)}{dy}\left\{-a^2 + \dfrac{d^2\phi(+1)}{dy^2}\cdot\dfrac{1}{2\phi(+1)}\right\} \\ -\dfrac{1}{2}\dfrac{d^3\bar{\phi}^*(-1)}{dy^3} - \left\{iaR - \dfrac{R}{2E_2}\right\}\bar{\phi}^*(-1) - \dfrac{d\bar{\phi}^*(-1)}{dy}\left\{-a^2 + \dfrac{d^2\phi(-1)}{dy^2}\cdot\dfrac{1}{2\phi(-1)}\right\} \\ -\dfrac{R}{E_1}\bar{\phi}^*(+1) \\ \dfrac{R}{E_2}\bar{\phi}^*(-1) \end{bmatrix} ,$$

and $\bar{\phi}^* = \bar{\phi}^*(y)$ in the first entries of the vectors.

A.2. Formulation 3.

The operator ($\underline{H}$), for Formulation 3, is given by

$$\underline{H}(\underline{u}) = \begin{bmatrix} \dfrac{d^4\phi}{dy^4} - 2a^2\dfrac{d^2\phi}{dy^2} + iaR\left\{(1-y^2)\left\{\dfrac{d^2\phi}{dy^2} - a^2\phi\right\} + 2\phi\right\} \\ 2\phi(+1) \\ 2\phi(-1) \\ \dfrac{E_1}{R}\dfrac{d^3\phi(+1)}{dy^3} + \phi(+1) \\ \dfrac{E_2}{R}\dfrac{d^3\phi(-1)}{dy^3} + \phi(-1) \end{bmatrix}$$

$$- c \begin{bmatrix} iaR\left\{\dfrac{d^2\phi}{dy^2} - a^2\phi\right\} \\ \dfrac{d\phi(+1)}{dy} \\ -\dfrac{d\phi(-1)}{dy} \\ 0 \\ 0 \end{bmatrix},$$

where $\underline{u} = \begin{bmatrix} 2\phi \\ 1 \\ 1 \\ -\frac{1}{2}\frac{d\phi(+1)}{dy} \\ -\frac{1}{2}\frac{d\phi(-1)}{dy} \end{bmatrix}$,

and $\phi = \phi(y)$ in the first entries of the vectors.

The complex conjugate adjoint operator ($\bar{\underline{H}}^{\star}$), for Formulation 3, is given by

$$\bar{\underline{H}}^{\star}(\bar{\underline{u}}^{\star}) = \begin{bmatrix} \frac{d^4\bar{\phi}^{\star}}{dy^4} - 2a^2\frac{d^2\bar{\phi}^{\star}}{dy^2} + a^4\bar{\phi}^{\star} + iaR\left\{\frac{d^2\bar{\phi}^{\star}}{dy^2} - \frac{d^2(y^2\bar{\phi}^{\star})}{dy^2} + (2-a^2+a^2y^2)\bar{\phi}^{\star}\right\} \\ -\frac{d^2\phi(+1)}{dy^2}\cdot\frac{d\bar{\phi}^{\star}(+1)}{dy} \\ \frac{d^2\phi(-1)}{dy^2}\cdot\frac{d\bar{\phi}^{\star}(-1)}{dy} \\ -2\frac{d^2\bar{\phi}^{\star}(+1)}{dy^2} + 4a^2\bar{\phi}^{\star}(+1) \\ 2\frac{d^2\bar{\phi}^{\star}(-1)}{dy^2} - 4a^2\bar{\phi}^{\star}(-1) \end{bmatrix}$$

$$
- c \begin{bmatrix}
iaR \left\{ \dfrac{d^2\bar{\phi}^*}{dy^2} - a^2\bar{\phi}^* \right\} \\
\left(-iaR\phi(+1) - a^2 \dfrac{d\phi(+1)}{dy}\right) \dfrac{d\bar{\phi}^*(+1)}{dy} \\
\left(iaR\phi(-1) - a^2 \dfrac{d\phi(-1)}{dy}\right) \dfrac{d\bar{\phi}^*(-1)}{dy} \\
- \dfrac{d^3\bar{\phi}^*(+1)}{dy^3} - \dfrac{R}{E_1}\bar{\phi}^*(+1) \\
- \dfrac{d^3\bar{\phi}^*(-1)}{dy^3} + \dfrac{R}{E_2}\bar{\phi}^*(-1)
\end{bmatrix} ,
$$

where

$$
\underline{\bar{u}}^* = \begin{bmatrix}
2\bar{\phi}^* \\
\dfrac{1}{2}\dfrac{d^3\bar{\phi}^*(+1)}{dy^3} - a^2 \dfrac{d\bar{\phi}^*(+1)}{dy} + \left\{ \dfrac{R}{2E_1} - iaR \right\} \bar{\phi}^*(+1) \\
- \dfrac{1}{2}\dfrac{d^3\bar{\phi}^*(-1)}{dy^3} + a^2 \dfrac{d\bar{\phi}^*(-1)}{dy} + \left\{ \dfrac{R}{2E_2} - iaR \right\} \bar{\phi}^*(-1) \\
- \dfrac{R}{E_1}\bar{\phi}^*(+1) \\
\dfrac{R}{E_2}\bar{\phi}^*(-1)
\end{bmatrix} ,
$$

and $\bar{\phi}^* = \bar{\phi}^*(y)$ in the first entries of the vectors.

A.3. Formulation 4.

The operator $(\underline{H})$, for Formulation 4, is given by

$$\underline{H}(\underline{u}) = \begin{bmatrix} \dfrac{d^4\phi}{dy^4} - 2a^2\dfrac{d^2\phi}{dy^2} + a^4\phi + iaR\left\{(1-y^2)\left\{\dfrac{d^2\phi}{dy^2} - a^2\phi\right\} + 2\phi\right\} \\ 2\phi(+1) \\ 2\phi(-1) \\ \dfrac{E_1}{R}\dfrac{d^3\phi(+1)}{dy^3} + \phi(+1) \\ \dfrac{E_2}{R}\dfrac{d^3\phi(-1)}{dy^3} - \phi(-1) \\ 0 \\ 0 \end{bmatrix} - c \begin{bmatrix} iaR\left\{\dfrac{d^2\phi}{dy^2} - a^2\phi\right\} \\ \dfrac{d\phi(+1)}{dy} \\ -\dfrac{d\phi(-1)}{dy} \\ 0 \\ 0 \\ 0 \\ 0 \end{bmatrix},$$

where $\underline{u} =$

$$\begin{bmatrix} 2\phi \\ -iaR\phi(+1) \\ iaR\phi(-1) \\ -\frac{1}{2}\frac{d\phi(+1)}{dy} \\ -\frac{1}{2}\frac{d\phi(-1)}{dy} \\ -\frac{d^2\phi(+1)}{dy^2} + (2a^2 + iaR)\,\phi(+1) \\ \frac{d^2\phi(-1)}{dy^2} - (2a^2 + iaR)\,\phi(-1) \end{bmatrix},$$

and $\phi = \phi(y)$ in the first entries of the vectors.

The complex conjugate adjoint operator $(\underline{\bar{H}}^{\star})$, for Formulation 4, is given by

$$\underline{\bar{H}}^{\star}(\underline{\bar{u}}^{\star}) = \begin{bmatrix} \frac{d^4\bar{\phi}^{\star}}{dy^4} - 2a^2\frac{d^2\bar{\phi}^{\star}}{dy^2} + a^4\bar{\phi}^{\star} + iaR\left\{\frac{d^2\bar{\phi}^{\star}}{dy^2} - \frac{d^2(y^2\bar{\phi}^{\star})}{dy^2} + (2-a^2+a^2y^2)\bar{\phi}^{\star}\right\} \\ \frac{d\phi^{\star}(+1)}{dy} \\ \frac{d\phi^{\star}(-1)}{dy} \\ -2\frac{d^2\bar{\phi}^{\star}(+1)}{dy^2} + 4a^2\bar{\phi}^{\star}(+1) \\ 2\frac{d^2\bar{\phi}^{\star}(-1)}{dy^2} - 4a^2\bar{\phi}^{\star}(-1) \\ \frac{d\bar{\phi}^{\star}(+1)}{dy} \\ \frac{d\bar{\phi}^{\star}(-1)}{dy} \end{bmatrix}$$

$$
- c \begin{bmatrix}
iaR \left\{ \dfrac{d^2\bar{\phi}^*}{dy^2} - a^2\bar{\phi}^* \right\} \\
\dfrac{d\bar{\phi}^*(+1)}{dy} \\
\dfrac{d\bar{\phi}^*(-1)}{dy} \\
- \dfrac{d^3\bar{\phi}^*(+1)}{dy^3} - \dfrac{R}{E_1}\,\bar{\phi}^*(+1) \\
- \dfrac{d^3\bar{\phi}^*(-1)}{dy^3} + \dfrac{R}{E_2}\,\bar{\phi}^*(-1) \\
0 \\
0
\end{bmatrix} ,
$$

where

$$
\bar{u}^* = \begin{bmatrix}
2\bar{\phi}^* \\
\dfrac{1}{2}\dfrac{d^3\bar{\phi}^*(+1)}{dy^3} + \left\{ \dfrac{R}{2E_1} - iaR \right\} \bar{\phi}^*(+1) \\
- \dfrac{1}{2}\dfrac{d^3\bar{\phi}^*(-1)}{dy^3} + \left\{ \dfrac{R}{2E_2} - iaR \right\} \bar{\phi}^*(-1) \\
- \dfrac{R}{E_1}\,\bar{\phi}^*(+1) \\
\dfrac{R}{E_2}\,\bar{\phi}^*(-1) \\
C \\
C
\end{bmatrix} ,
$$

and $\bar{\phi}^* = \bar{\phi}^*(y)$ in the first entries of the vectors.

Appendix B. The chosen formulation (Formulation 4).

B.1. Matrix entries for Formulation 4.

The (p,q) positions in the matrices for Formulation 4 are given by

$$B_{11}(p,q) = \left\{\frac{p^3\pi^3}{16}(1-(-1)^p)(-1)^{\frac{p-1}{2}} - iaR(1+(-1)^p)(-1)^{\frac{p}{2}}\right\}\left\{(1+(-1)^q)(-1)^{\frac{q}{2}}\right\}$$
$$- \left\{(1+(-1)^p)(-1)^{\frac{p}{2}}\right\}\left\{\frac{q^3\pi^3}{16}(1-(-1)^q)(-1)^{\frac{q-1}{2}}\right\}$$
$$+ \left\{\left\{\frac{q^2\pi^2}{4} + a^2\right\}^2 + iaR\left\{2 - \frac{q^2\pi^2}{4} - a^2\right\}\right\} I_4$$
$$+ \left\{iaR\left\{\frac{q^2\pi^2}{4} + a^2\right\}\right\} I_1 \quad ,$$

$$D_{11}(p,q) = -\left\{\frac{p^3\pi^3}{16}(1-(-1)^p)(-1)^{\frac{p-1}{2}} - iaR(1+(-1)^{\frac{p}{2}})\right\}\left\{\frac{q\pi}{4}(1-(-1)^q)(-1)^{\frac{q-1}{2}}\right\}$$
$$- \left\{\frac{qaR}{16}\left\{\frac{1}{E_1} + \frac{1}{E_2}\right\}(1+(-1)^p)(1-(-1)^q(-1)^{\frac{p+q-1}{2}}\right\}$$
$$- \left\{iaR\left\{\frac{q^2\pi^2}{4} + a^2\right\}\right\} I_4 \quad ,$$

$$B_{12}(p,q) = \left\{\left\{\frac{q^2\pi^2}{4} + a^2\right\}^2 + iaR\left\{2 - \frac{q^2\pi^2}{4} - a^2\right\}\right\} I_5$$
$$+ \left\{iaR\left\{\frac{q^2\pi^2}{4} + a^2\right\}\right\} I_6 \quad ,$$

$$D_{12}(p,q) = \left\{\frac{q\pi R}{16}\left\{\frac{1}{E_1} - \frac{1}{E_2}\right\}(1+(-1)^p)(1+(-1)^q)(-1)^{\frac{p+q}{2}}\right\}$$

$$- \left\{iaR\left\{\frac{q^2\pi^2}{4} + a^2\right\}\right\} I_5 \quad ,$$

$$B_{21}(p,q) = \left\{\left\{\frac{q^2\pi^2}{4} + a^2\right\}^2 + iaR\left\{2 - \frac{q^2\pi^2}{4} - a^2\right\}\right\} I_7$$

$$+ \left\{iaR\left\{\frac{q^2\pi^2}{4} + a^2\right\}\right\} I_8 \quad ,$$

$$D_{21}(p,q) = -\left\{\frac{q\pi R}{16}\left\{\frac{1}{E_1} - \frac{1}{E_2}\right\}(1-(-1)^p)(1-(-1)^q)(-1)^{\frac{p+q-2}{2}}\right\}$$

$$- \left\{iaR\left\{\frac{q^2\pi^2}{4} + a^2\right\}\right\} I_7 \quad ,$$

$$B_{22}(p,q) = \left\{-\frac{p^3\pi^3}{16}(1+(-1)^p)(-1)^{\frac{p}{2}} - iaR(1-(-1)^p)(-1)^{\frac{p-1}{2}}\right\}\left\{(1-(-1)^q)(-1)^{\frac{q-1}{2}}\right\}$$

$$+ (1-(-1)^p)(-1)^{\frac{p-1}{2}}\left\{\frac{q^3\pi^3}{16}(1+(-1)^q)(-1)^{\frac{q}{2}}\right\}$$

$$+ \left\{\left\{\frac{q^2\pi^2}{4} + a^2\right\}^2 + iaR\left\{2 - \frac{q^2\pi^2}{4} - a^2\right\}\right\} I_3$$

$$+ \left\{iaR\left\{\frac{q^2\pi^2}{4} + a^2\right\}\right\} I_2 \qquad \text{and}$$

$$D_{22}(p,q) = \left\{ -\frac{p^3\pi^3}{16}(1+(-1)^p)(-1)^{\frac{p}{2}} - iaR(1-(-1)^p)(-1)^{\frac{p-1}{2}} \right\} \cdot \left\{ \frac{q\pi}{4}(1+(-1)^q)(-1)^{\frac{q}{2}} \right\}$$

$$+ \left\{ \frac{qR\pi}{16}\left\{ \frac{1}{E_1} + \frac{1}{E_2} \right\}(1-(-1)^p)(1+(-1)^q)(-1)^{\frac{p+q-1}{2}} \right\}$$

$$- \left\{ iaR\left\{ \frac{q^2\pi^2}{4} + a^2 \right\} \right\} I_3 \qquad \text{, where}$$

$$I_1 = \int_{-1}^{+1} y^2 \cos(p\pi y/2)\cos(q\pi y/2)\,dy$$

$$= \frac{1}{(p+q)\pi}\left\{ 1 - \frac{8}{(p+q)^2\pi^2} \right\}(1-(-1)^{p+q})(-1)^{\frac{p+q-1}{2}}$$

$$\frac{1}{(p-q)\pi}\left\{ 1 - \frac{8}{(p-q)^2\pi^2} \right\}(1-(-1)^{p-q})(-1)^{\frac{p-q-1}{2}}$$

$$+ \frac{4}{(p+q)^2\pi^2}(1+(-1)^{p+q})(-1)^{\frac{p+q}{2}} + \frac{4}{(p-q)^2\pi^2}(1+(-1)^{p-q})(-1)^{\frac{p-q}{2}}$$

for $p \neq q$,

$$= \frac{1}{3} + \frac{2(-1)^q}{q^2\pi^2} \qquad \text{for } p = q \neq 0,$$

$$= \frac{2}{3} \qquad \text{for } p = q = 0,$$

$$I_2 = \int_{-1}^{+1} y^2 \sin(p\pi y/2) \sin(q\pi y/2)\, dy$$

$$= -\frac{1}{(p+q)\pi}\left\{1 - \frac{8}{(p+q)^2\pi^2}\right\}(1-(-1)^{p+q})(-1)^{\frac{p+q-1}{2}}$$

$$+ \frac{1}{(p-q)\pi}\left\{1 - \frac{8}{(p-q)^2\pi^2}\right\}(1-(-1)^{p-q})(-1)^{\frac{p-q-1}{2}}$$

$$- \frac{4}{(p+q)^2\pi^2}(1+(-1)^{p+q})(-1)^{\frac{p+q}{2}} + \frac{4}{(p-q)^2\pi^2}(1+(-1)^{p-q})(-1)^{\frac{p-q}{2}}$$

for $p \neq q$,

$$= \frac{1}{3} - \frac{2(-1)^q}{q^2\pi^2} \qquad \text{for } p = q \neq 0,$$

$$= 0 \qquad \text{for } p = q = 0,$$

$$I_3 = \int_{-1}^{+1} \sin(p\pi y/2) \sin(q\pi y/2)\, dy$$

$$= \frac{1}{(p-q)\pi}(1-(-1)^{p-q})(-1)^{\frac{p-q-1}{2}} - \frac{1}{(p+q)\pi}(1-(-1)^{p+q})(-1)^{\frac{p+q-1}{2}}$$

for $p \neq q$,

$$= 1 \qquad \text{for } p = q \neq 0,$$

$$= 0 \qquad \text{for } p = q = 0,$$

$$I_4 = \int_{-1}^{+1} \cos(p\pi y/2)\cos(q\pi y/2)\,dy$$

$$= \frac{1}{(p+q)\pi}(1-(-1)^{p+q})(-1)^{\frac{p+q-1}{2}} + \frac{1}{(p-q)\pi}(1-(-1)^{p-q})(-1)^{\frac{p-q-1}{2}}$$

for $p \neq q$,

$$= 1 \qquad \text{for } p = q \neq 0,$$

$$= 2 \qquad \text{for } p = q = 0,$$

$$I_5 = \int_{-1}^{+1} \cos(p\pi y/2)\sin(q\pi y/2)\,dy = 0\,,$$

$$I_6 = \int_{-1}^{+1} y^2 \cos(p\pi y/2)\sin(q\pi y/2)\,dy = 0\,,$$

$$I_7 = \int_{-1}^{+1} \sin(p\pi y/2)\cos(q\pi y/2)\,dy = 0 \qquad \text{and}$$

$$I_8 = \int_{-1}^{+1} y^2 \sin(p\pi y/2)\cos(q\pi y/2)\,dy = 0\,.$$

B.2. Matrix entries for the complex conjugate adjoint of Formulation 4.

The (p,q) positions in the matrices for the complex conjugate adjoint of Formulation 4 are given by

$$B_{11}(p,q) = \frac{p\pi}{8}\left\{\frac{q^2\pi^2}{2} + 4a^2\right\}(1-(-1)^p)(1+(-1)^q)(-1)^{\frac{p+q-1}{2}}$$

$$- \left\{\frac{p^2\pi^2}{4}(1+(-1)^p)(-1)^{\frac{p}{2}} + 2a^2(1+(-1)^p)(-1)^{\frac{p}{2}}\right\}\left\{\frac{q\pi}{4}(1-(-1)^q)(-1)^{\frac{q-1}{2}}\right.$$

$$+ \left\{\left\{\frac{q^2\pi^2}{4} + a^2\right\}^2 - iaR\left\{\frac{q^2\pi^2}{4} + a^2\right\}\right\} I_4$$

$$+ \left\{iaR\left\{\frac{q^2\pi^2}{4} + a^2\right\}\right\} I_1 + \left\{2\pi qiaR\right\} T_1 \quad ,$$

$$D_{11}(p,q) = iaR\frac{q\pi}{4}(1+(-1)^p)(1-(-1)^q)(-1)^{\frac{p+q-1}{2}}$$

$$+ \frac{pq^3\pi^4}{64}(1-(-1)^p)(1-(-1)^q)(-1)^{\frac{p+q}{2}}$$

$$- \frac{p\pi R}{16}\left\{\frac{1}{E_1} + \frac{1}{E_2}\right\}(1-(-1)^p)(1+(-1)^q)(-1)^{\frac{p+q-1}{2}}$$

$$- iaR\left\{\frac{q^2\pi^2}{4} + a^2\right\} I_4 \quad ,$$

$$B_{12}(p,q) = \left\{ \left\{ \frac{q^2\pi^2}{4} + a^2 \right\}^2 - iaR \left\{ \frac{q^2\pi^2}{4} + a^2 \right\} \right\} I_5$$

$$+ iaR \left\{ \frac{q^2\pi^2}{4} + a^2 \right\} I_6 - \left\{ 2q\pi iaR \right\} T_3 \quad ,$$

$$D_{12}(p,q) = + \frac{p\pi R}{16} \left\{ \frac{1}{E_1} - \frac{1}{E_2} \right\} (1-(-1)^p)(1-(-1)^q(-1)^{\frac{p+q}{2}}$$

$$- iaR \left\{ \frac{q^2\pi^2}{4} + a^2 \right\} I_5 \quad ,$$

$$B_{21}(p,q) = \left\{ \left\{ \frac{q^2\pi^2}{4} + a^2 \right\}^2 - iaR \left\{ \frac{q^2\pi^2}{4} + a^2 \right\} \right\} I_7$$

$$+ iaR \left\{ \frac{q^2\pi^2}{4} + a^2 \right\} I_8 + \left\{ 2q\pi iaR \right\} T_4 \quad ,$$

$$D_{21}(p,q) = \frac{p\pi R}{16} \left\{ \frac{1}{E_1} - \frac{1}{E_2} \right\} (1+(-1)^p)(1+(-1)^q)(-1)^{\frac{p+q}{2}}$$

$$- iaR \left\{ \frac{q^2\pi^2}{4} + a^2 \right\} I_7 \quad ,$$

$$B_{22}(p,q) = -\frac{p\pi}{4}\left\{\frac{q^2\pi^2}{4} + 2a^2\right\}(1+(-1)^p)(1-(-1)^q)(-1)^{\frac{p+q-1}{2}}$$

$$+\frac{q\pi}{4}\left\{\frac{p^2\pi^2}{4} + 2a^2\right\}(1-(-1)^p)(1+(-1)^q)(-1)^{\frac{p+q-1}{2}}$$

$$+\left\{\left\{\frac{q^2\pi^2}{4} + a^2\right\}^2 - iaR\left\{\frac{q^2\pi^2}{4} + a^2\right\}\right\} I_3$$

$$+ iaR\left\{\frac{q^2\pi^2}{4} + a^2\right\} I_2 - \left\{2\pi qiaR\right\} T_2 \qquad \text{and}$$

$$D_{22}(p,q) = -iaR\,\frac{q\pi}{4}(1-(-1)^p)(1+(-1)^q)(-1)^{\frac{p+q-1}{2}}$$

$$-\frac{pq^3\pi^4}{64}(1+(-1)^p)(1+(-1)^q)(-1)^{\frac{p+q}{2}}$$

$$+\frac{p\pi R}{16}\left\{\frac{1}{E_1} + \frac{1}{E_2}\right\}(1+(-1)^p)(1-(-1)^q)(-1)^{\frac{p+q-1}{2}}$$

$$-iaR\left\{\frac{q^2\pi^2}{4} + a^2\right\} I_3 \qquad ,$$

where the integrals from I_1 up to I_8 are given in Appendix B.1 and the integrals from T_1 up to T_4 are given by

$$T_1 = \int_{-1}^{+1} y \cos(p\pi y/2) \sin(q\pi y/2)\, dy$$

$$= -\frac{1}{(p+q)\pi}(1+(-1)^{p+q})(-1)^{\frac{p+q}{2}} + \frac{2}{(p+q)^2\pi^2}(1-(-1)^{p+q})(-1)^{\frac{p+q-1}{2}}$$

$$+\frac{1}{(p-q)\pi}(1+(-1)^{p-q})(-1)^{\frac{p-q}{2}} - \frac{2}{(p-q)^2\pi^2}(1-(-1)^{p-q})(-1)^{\frac{p-q-1}{2}}$$

$$= \frac{(-1)^{q-1}}{q\pi} \quad \text{for } p \neq q, \text{ for } p = q \neq 0,$$

$$= 0 \quad \text{for } p = q = 0,$$

$$T_2 = \int_{-1}^{+1} y \sin(p\pi y/2) \cos(q\pi y/2)\, dy$$

$$= -\frac{1}{(p+q)\pi}(1+(-1)^{p+q})(-1)^{\frac{p+q}{2}} + \frac{2}{(p+q)^2\pi^2}(1-(-1)^{p+q})(-1)^{\frac{p+q-1}{2}}$$

$$-\frac{1}{(p-q)\pi}(1+(-1)^{p-q})(-1)^{\frac{p-q}{2}} + \frac{2}{(p-q)^2\pi^2}(1-(-1)^{p-q})(-1)^{\frac{p-q-1}{2}}$$

$$= \frac{(-1)^{q-1}}{q\pi} \quad \text{for } p \neq q, \text{ for } p = q \neq 0,$$

$$= 0 \quad \text{for } p = q = 0,$$

$$T_3 = \int_{-1}^{+1} y \cos(p\pi y/2) \cos(q\pi y/2)\, dy = 0 \qquad \text{and}$$

$$T_4 = \int_{-1}^{+1} y \sin(p\pi y/2) \sin(q\pi y/2)\, dy = 0 .$$

Appendix C. A simple flow diagram for the computer program.

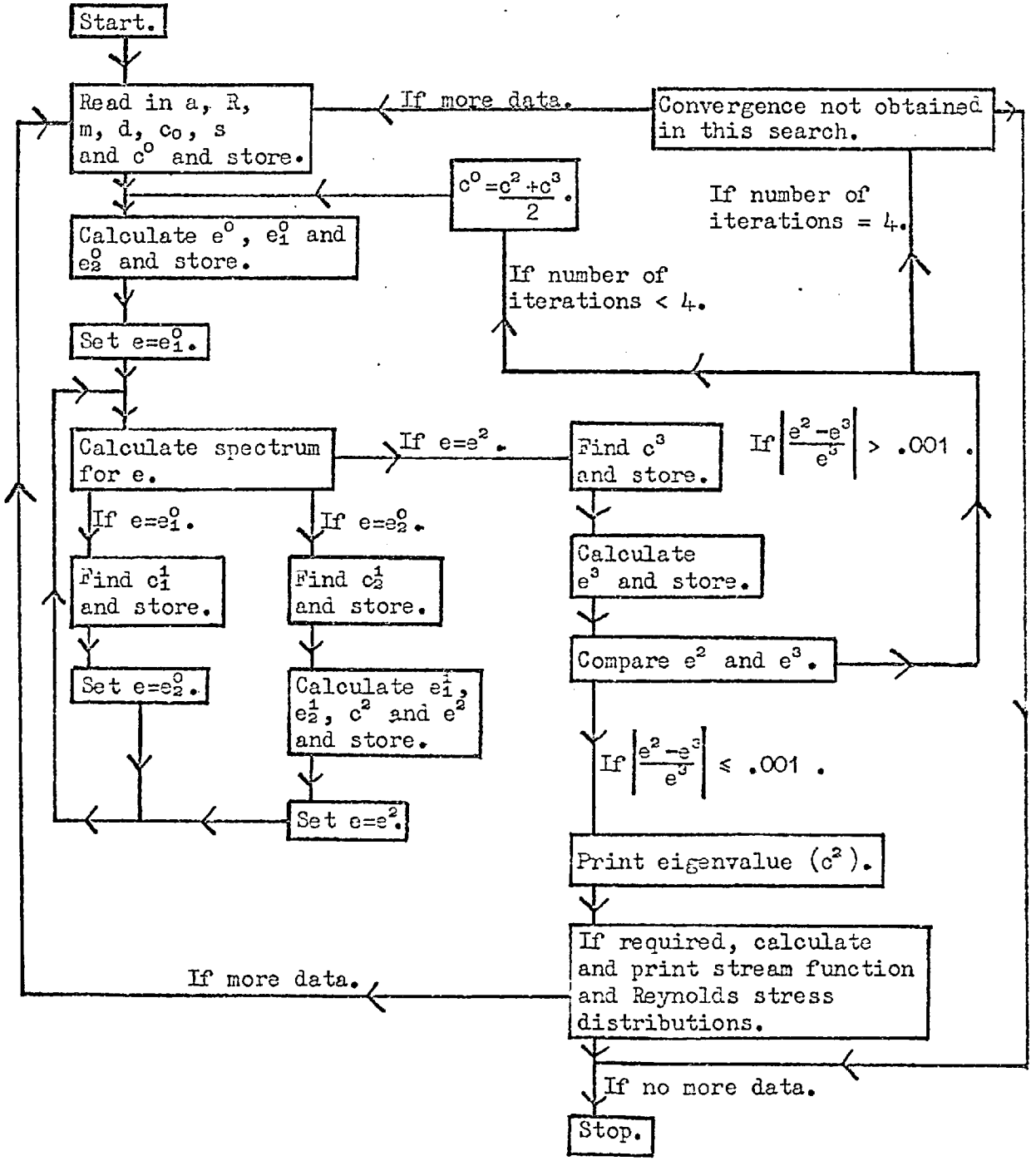

Number of cosine terms in series.	Formulation 1. Real part.	Imaginary part.	Formulation 2. Real part.	Imaginary part.	Formulation 3. Real part.	Imaginary part.	Formulation 4. Real part.	Imaginary part.	Formulation 4. (Adjoint problem.) Real part.	Imaginary part.
8	.3186,	.0292	.3455,	.0163	.3187,	.0292	.3187,	.0292	.3187,	.0292
10	.3231,	.0247	.3364,	.0184	.3230,	.0246	.3230,	.0245	.3230,	.0248
12	.3234,	.0256	.3234,	.0269	.3228,	.0241	.3227,	.0241	.3235,	.0258
14	.3231,	.0261	.3231,	.0267	.3231,	.0261	.3231,	.0261	.3231,	.0261
16	.3231,	.0262	.3232,	.0264	.3231,	.0262	.3231,	.0262	.3231,	.0262
18	.3231,	.0262	.3231,	.0262	.3231,	.0262	.3231,	.0262	.3231,	.0262
20	.3231,	.0262	.3232,	.0263	.3231,	.0262	.3231,	.0262	.3231,	.0262

Table 1. Convergence of the most unstable eigenvalue, using the different formulations at $a = 1$, $R = 1600$ and $E_1 = E_2 = 10^{-4}$. (For this case, Thomas obtained an eigenvalue $c = .3231 + .0262i$ and Lee and Reynolds, using an eleven term series, obtained an eigenvalue $c = .3231 + .0262i$.)

Number of cosine terms in series.	Formulation 1.		Formulation 2.		Formulation 3.		Formulation 4.		Formulation 4. (Adjoint problem.)	
	Real part.	Imaginary part.	Real part.	Imaginary part.	Real part.	Imaginary part.	Real part.	Imaginary part.	Real part.	Imaginary part.
8	.2870,	.0051	.3324,	.0089	.2873,	.0055	.2873,	.0055	.2873,	.0055
10	.2955,	.0138	.3331,	.0062	.2954,	.0139	.2954,	.0139	.2955,	.0139
12	.3014,	.0145	.3006,	.0169	.2994,	.0147	.2994,	.0147	.3014,	.0145
14	.3016,	.0143	.3003,	.0152	.3015,	.0143	.3015,	.0143	.3015,	.0143
16	.3013,	.0141	.3010,	.0149	.3013,	.0141	.3013,	.0141	.3013,	.0141
18	.3012,	.0142	.3007,	.0135	.3012,	.0142	.3012,	.0142	.3012,	.0142
20	.3011,	.0142	.3008,	.0140	.3012,	.0142	.3012,	.0142	.3012,	.0142

Table 2. Convergence of the most unstable eigenvalue, using the different formulations at $a = 1$, $R = 2500$ and $E_1 = E_2 = 10^{-4}$. (For this case, Thomas obtained an eigenvalue $c = .3011 + .0142i$ and Lee and Reynolds, using a twelve term series, obtained an eigenvalue $c = .3010 + .0143i$.)

$E_1^{-1} = E_2^{-1}$		Eigenvalue.		$E_1^{-1} = E_2^{-1}$		Eigenvalue.	
Real part.	Imaginary part.	Real part.	Imaginary part.	Real part.	Imaginary part.	Real part.	Imaginary part.
10^2,	0	.3013,	.0148	-10^2,	0	.3010,	.0135
0 ,	10^2	.3018,	.0140	0 ,	-10^2	.3005,	.0143
10^2,	10^2	.3016,	.0144	-10^2,	-10^2	.3007,	.0139
10^3,	0	.3012,	.0142	-10^3,	0	.3011,	.0141
0 ,	10^3	.3012,	.0142	0 ,	-10^3	.3011,	.0142
10^3,	10^3	.3012,	.0142	-10^3,	-10^3	.3011,	.0141
10^4,	0	.3012,	.0142	-10^4,	0	.3012,	.0142
0 ,	10^4	.3012,	.0142	0 ,	-10^4	.3011,	.0142
10^4,	10^4	.3012,	.0142	-10^4,	-10^4	.3012,	.0142
10^5,	0	.3012,	.0142	-10^5,	0	.3012,	.0142
0 ,	10^5	.3012,	.0142	0 ,	-10^5	.3011,	.0142
10^5,	10^5	.3012,	.0142	-10^5,	-10^5	.3011,	.0142

Table 3. Calculations to determine the values of E_1 and E_2 at which the walls are, effectively, rigid. For the above results we use a twenty cosine series and tabulate the most unstable eigenvalue at a = 1 and R = 2500.

a	R 1000	2000	3000	4000	5000	6000	7000	8000	9000	10000
.800	.0638	.0388	.0260	.0181	.0127	.0087	.0057	.0033	.0014	-.0002
.850	.0578	.0329	.0207	.0133	.0085	.0049	.0023	.0002	-.0013	-.0026
.900	.0521	.0278	.0163	.0096	.0052	.0022	-.0001	-.0017	-.0030	-.0040
.950	.0469	.0234	.0128	.0068	.0030	.0004	-.0014	-.0027	-.0037	-.0044
1.000	.0421	.0198	.0102	.0050	.0018	-.0003	-.0017	-.0027	-.0033	-.0037
1.025	.0400	.0184	.0092	.0044	.0015	-.0003	-.0015	-.0023	-.0028	-.0031
1.050	.0380	.0171	.0085	.0041	.0014	-.0001	-.0011	-.0017	-.0020	-.0022
1.075	.0363	.0161	.0080	.0039	.0017	.0003	-.0005	-.0009	-.0010	-.0010
1.100	.0346	.0153	.0077	.0040	.0020	.0009	.0004	.0002	.0002	.0003

Table 4. The imaginary part of the most unstable eigenvalue of the rigid wall problem, for different values of the fluid parameters (a,R), obtained using a thirty cosine series.

	c_i = .002		c_i = .001		c_i = .000		c_i = -.001		c_i = -.002	
a	R	R	R	R	R	R	R	R	R	R
.800	8650		9250		9850					
.850	7100		7600		8150		8850		9600	
.900	6050		6500		6950		7550		8250	
.950	5350		5750		6200		6700		7400	
1.000	4900		5350		5850		6400		7300	
1.025	4750		5200		5800		6500		7500	
1.050	4700		5200		5900		6850		9000	
1.075	4800		5500		6350					
1.100	5000		5800							
R	a	a	a	a	a	a	a	a	a	a
5000	.988	1.100								
6000	.905		.930	1.105	.970	1.060				
7000	.855		.875		.895	1.093	.930	1.055		
8000	.820		.835		.855	1.095	.880	1.070	.910	1.040
9000			.805		.825	1.094	.845	1.075	.865	1.050
10000						1.094	.815	1.075	.830	1.055

Table 5. Points on the rigid wall neutral stability and constant amplification curves, obtained using a thirty cosine series.

a	R 1000	2000	3000	4000	5000	6000	7000	8000	9000	10000
.800	.3064	.2772	.2606	.2490	.2400	.2328	.2268	.2216	.2171	.2131
.850	.3170	.2868	.2693	.2571	.2477	.2401	.2339	.2285	.2239	.2198
.900	.3272	.2957	.2775	.2647	.2549	.2471	.2406	.2351	.2303	.2261
.950	.3370	.3042	.2851	.2718	.2617	.2537	.2470	.2413	.2364	.2320
1.000	.3463	.3121	.2923	.2785	.2681	.2598	.2529	.2471	.2420	.2375
1.025	.3508	.3159	.2957	.2818	.2712	.2627	.2558	.2498	.2447	.2401
1.050	.3551	.3195	.2990	.2848	.2742	.2656	.2585	.2524	.2472	.2426
1.075	.3593	.3231	.3023	.2879	.2770	.2683	.2610	.2549	.2496	.2449
1.100	.3634	.3265	.3054	.2907	.2796	.2708	.2635	.2572	.2518	.2470

Table 6. The real part of the most unstable eigenvalue of the rigid wall problem, for different values of the fluid parameters (a,R), obtained using a thirty cosine series.

a	R	R	R	a	a
.85	8600		6000	.980	1.040
.90	7350		7000	.910	1.058
.95	6300		8000	.870	1.048
1.00	5800		9000	.838	1.030
1.05	6500	7800	10000	.818	1.015

Table 7. Points on the rigid wall neutral stability curve, obtained using a twenty cosine series.

20 cosine series.			30 cosine series.		
R	c_r	c_r	R	c_r	c_r
8600	.226		9850	.213	
7350	.239		8150	.228	
6300	.253		6950	.241	
5800	.262		6200	.252	
6500	.263		5850	.261	
7800		.254	5800	.263	
6000	.258	.265	5900	.266	
7000	.242	.260	6350	.266	
8000	.231	.253	6000	.256	.267
9000	.222	.246	7000	.240	.262
10000	.215	.239	8000	.229	.257
			9000	.221	.250
			10000		.246

Table 8. Points on the spatial neutral stability curves, obtained using twenty and thirty cosine series for the rigid wall problem.

y	Stream function. Real part.	Stream function. Imaginary part.	Reynolds stress.
.00	1.0000	.0000	.0000
.05	.9960	-.0021	-.1666
.10	.9841	-.0082	-.3231
.15	.9640	-.0181	-.4597
.20	.9353	-.0309	-.5674
.25	.8978	-.0459	-.6388
.30	.8513	-.0618	-.6689
.35	.7958	-.0773	-.6564
.40	.7318	-.0909	-.6045
.45	.6602	-.1012	-.5206
.50	.5825	-.1070	-.4164
.55	.5007	-.1073	-.3057
.60	.4172	-.1019	-.2022
.65	.3348	-.0911	-.1170
.70	.2564	-.0758	-.0561
.75	.1846	-.0579	-.0198
.80	.1220	-.0395	-.0032
.85	.0706	-.0229	.0012
.90	.0322	-.0100	.0008
.95	.0083	-.0024	.0001
1.00	.0000	.0000	.0000

(a)

y	Stream function. Real part.	Stream function. Imaginary part.	Reynolds stress.
.00	1.0000	.0000	.0000
.05	.9974	-.0001	-.0084
.10	.9899	-.0004	-.0181
.15	.9775	-.0010	-.0302
.20	.9603	-.0020	-.0448
.25	.9381	-.0033	-.0600
.30	.9106	-.0050	-.0722
.35	.8773	-.0069	-.0795
.40	.8381	-.0089	-.0853
.45	.7932	-.0111	-.0982
.50	.7422	-.0139	-.1257
.55	.6846	-.0177	-.1634
.60	.6188	-.0225	-.1901
.65	.5430	-.0273	-.1767
.70	.4564	-.0296	-.1094
.75	.3607	-.0265	-.0107
.80	.2608	-.0167	.0662
.85	.1644	-.0029	.0786
.90	.0815	.0074	.0393
.95	.0229	.0066	.0052
1.00	.0005	.0002	.0000

(b)

Table 9. Stream function and Reynolds stress distributions obtained for the rigid wall problem at

(a) $(a,R) = (1,100)$ using a thirty cosine series, and

(b) $(a,R) = (1,1600)$ using a ten cosine series.

y	Stream function.		Reynolds stress.
	Real part.	Imaginary part.	
.00	1.0000	.0000	.0000
.05	.9976	-.0001	-.0111
.10	.9902	-.0006	-.0230
.15	.9780	-.0013	-.0348
.20	.9607	-.0023	-.0462
.25	.9383	-.0036	-.0584
.30	.9105	-.0052	-.0714
.35	.8774	-.0072	-.0841
.40	.8385	-.0094	-.0969
.45	.7936	-.0120	-.1121
.50	.7425	-.0151	-.1332
.55	.6846	-.0189	-.1625
.60	.6187	-.0236	-.1916
.65	.5432	-.0286	-.1911
.70	.4566	-.0316	-.1310
.75	.3605	-.0290	-.0252
.80	.2601	-.0190	.0624
.85	.1642	-.0045	.0780
.90	.0821	.0064	.0384
.95	.0230	.0061	.0050
1.00	.0000	.0000	.0000

(a)

y	Stream function.		Reynolds stress.
	Real part.	Imaginary part.	
.00	1.0000	.0000	.0000
.05	.9976	-.0001	-.0114
.10	.9902	-.0006	-.0229
.15	.9780	-.0013	-.0346
.20	.9607	-.0023	-.0464
.25	.9382	-.0036	-.0586
.30	.9105	-.0052	-.0712
.35	.8774	-.0072	-.0840
.40	.8385	-.0094	-.0972
.45	.7936	-.0120	-.1121
.50	.7425	-.0151	-.1330
.55	.6846	-.0189	-.1627
.60	.6187	-.0236	-.1917
.65	.5432	-.0286	-.1909
.70	.4566	-.0316	-.1310
.75	.3605	-.0290	-.0253
.80	.2601	-.0190	.0625
.85	.1642	-.0045	.0780
.90	.0821	.0064	.0384
.95	.0230	.0061	.0050
1.00	.0000	.0000	.0000

(b)

Table 10. Stream function and Reynolds stress distributions obtained for the rigid wall problem at

(a) $(a,R) = (1,1600)$ using a twenty cosine series, and

(b) $(a,R) = (1,1600)$ using a thirty cosine series.

y	Stream function.		Reynolds stress.
	Real part.	Imaginary part.	
.00	1.0000	.0000	.0000
.05	.9980	.0000	.0014
.10	.9917	.0000	.0001
.15	.9809	.0000	-.0006
.20	.9659	.0000	.0014
.25	.9466	.0001	.0022
.30	.9224	.0001	.0003
.35	.8934	.0001	.0003
.40	.8598	.0002	.0029
.45	.8207	.0002	.0026
.50	.7759	.0003	-.0003
.55	.7254	.0002	.0012
.60	.6686	.0003	.0048
.65	.6042	.0004	-.0008
.70	.5322	.0001	-.0117
.75	.4508	-.0004	-.0010
.80	.3558	.0012	.0580
.85	.2497	.0081	.1346
.90	.1423	.0186	.1248
.95	.0464	.0170	.0289
1.00	.0001	-.0001	.0000

(a)

y	Stream function.		Reynolds stress.
	Real part.	Imaginary part.	
.00	1.0000	.0000	.0000
.05	.9979	.0000	.0003
.10	.9915	.0000	.0008
.15	.9809	.0000	.0009
.20	.9659	.0001	.0015
.25	.9464	.0001	.0017
.30	.9224	.0002	.0020
.35	.8936	.0002	.0024
.40	.8598	.0003	.0026
.45	.8208	.0003	.0031
.50	.7762	.0004	.0031
.55	.7256	.0005	.0034
.60	.6688	.0006	.0036
.65	.6048	.0006	.0024
.70	.5329	.0005	-.0050
.75	.4512	.0001	-.0031
.80	.3568	.0014	.0585
.85	.2509	.0087	.1440
.90	.1425	.0193	.1247
.95	.0466	.0170	.0283
1.00	.0000	.0000	.0000

(b)

Table 11. Stream function and Reynolds stress distributions obtained for the rigid wall problem at

(a) (a,R) = (1,6400) using a twenty cosine series, and

(b) (a,R) = (1,6400) using a thirty cosine series.

y	Stream function. Real part.	Stream function. Imaginary part.	Reynolds stress.
.00	1.0000	.0000	.0000
.05	.9980	.0000	.0011
.10	.9919	.0001	.0029
.15	.9817	.0001	.0035
.20	.9673	.0003	.0055
.25	.9486	.0004	.0064
.30	.9255	.0006	.0079
.35	.8978	.0008	.0096
.40	.8654	.0010	.0104
.45	.8280	.0013	.0127
.50	.7852	.0017	.0136
.55	.7367	.0020	.0156
.60	.6820	.0024	.0173
.65	.6206	.0029	.0189
.70	.5516	.0034	.0199
.75	.4737	.0036	.0135
.80	.3841	.0040	.0372
.85	.2799	.0084	.1288
.90	.1665	.0190	.1542
.95	.0582	.0198	.0458
1.00	.0000	.0000	.0000

(a)

y	Stream function. Real part.	Stream function. Imaginary part.	Reynolds stress.
.00	1.0000	.0000	.0000
.05	1.0060	.0069	.5557
.10	1.0230	.0280	1.1405
.15	1.0479	.0642	1.7760
.20	1.0755	.1163	2.4681
.25	1.0992	.1846	3.1996
.30	1.1113	.2675	3.9260
.35	1.1038	.3612	4.5757
.40	1.0701	.4593	5.0592
.45	1.0057	.5525	5.2865
.50	.9098	.6300	5.1907
.55	.7861	.6807	4.7515
.60	.6426	.6952	4.0116
.65	.4912	.6681	3.0766
.70	.3455	.5991	2.0962
.75	.2184	.4948	1.2258
.80	.1196	.3677	.5809
.85	.0531	.2349	.2005
.90	.0167	.1163	.0399
.95	.0025	.0318	.0022
1.00	.0000	.0000	.0000

(b)

Table 12. Stream function and Reynolds stress distributions

(a) obtained for the rigid wall problem at $(a,R) = (1,10000)$ using a thirty cosine series, and

(b) obtained for the adjoint rigid wall problem at $(a,R) = (1,100)$ using a thirty cosine series.

R	a	c_r	a	R	c_r
3000	1.268	.326	.80	7250	.224
3500	1.288	.319	.85	5750	.240
4000	1.293	.313	.90	4750	.256
4500	1.293	.306	.95	4000	.271
5000	1.288	.303	1.00	3450	.284
5500	1.285	.297	1.05	3100	.296
6000	1.278	.292	1.10	2800	.308
6500	1.270	.288	1.15	2650	.318
7500	1.258	.281	1.20	2700	.323
8000	1.253	.276	1.25	2850	.327

Table 13. Points on the stability curves, calculated for $E_1^{-1} = E_2^{-1} = -10$, using a thirty cosine series.

R	a	c_r	a	R	c_r
3500	1.290	.321	.80	7400	.223
4000	1.300	.315	.85	5800	.240
4500	1.300	.309	.90	4750	.256
5000	1.293	.304	.95	4000	.271
5500	1.283	.298	1.00	3500	.284
6000	1.270	.294	1.05	3100	.297
6500	1.258	.289	1.10	2750	.308
7000	1.240	.285	1.15	2650	.318
7500	1.220	.280	1.20	2650	.325
8000	1.205	.275	1.25	2750	.329

Table 14. Points on the stability curves, calculated for $E_1^{-1} = E_2^{-1} = -10$, using a twenty cosine series.

a	R
.109	42500
.146	41500
.184	40000
.379	32500
.483	27000
.595	20000
.723	12500
.800	9280
.850	7900
.900	6840
.950	6170
1.000	5820
1.050	6040
1.081	7500
1.068	10000
1.042	12500
.930	20000
.790	27000
.648	32500
.370	40000
.302	41500
.258	42500
.200	44000

(a)

a	R
.713	12700
.917	6170
1.003	5410
1.034	5350
1.075	5750
1.079	5970
1.088	6680
1.077	9520
.235	38300
.131	43200
.122	44400
.124	44700
.137	44800
.144	44700
.164	44300
.241	42600

(b)

a	R
.38	32500
.51	24700
.62	17400
.97	17000
.83	24700
.70	30100
.51	36500

(c)

Table 15. Points on the neutral stability curve for a membrane with tension only. The value of the tension is $.5 \times 10^9$ and the three tables correspond to

(a) the present work,

(b) accurate points for the asymptotic transformation and

(c) approximate points for the asymptotic transformation.

a	R	c_r	c_{pr}	a	R	c_r	c_{pr}
.800	3680	.293	1080	.998	4200	.335	1410
.825	3650	.297	1080	1.000	4450	.346	1540
.850	3630	.301	1090	1.013	4790	.375	1800
.875	3600	.305	1100	1.025	4860	.388	1880
.900	3600	.308	1110	1.050	4900	.398	1950
.925	3620	.312	1130	1.075	4910	.417	2050
.950	3650	.315	1150	1.100	4910	.428	2100
.975	3775	.321	1210	1.125	4920	.438	2150
.988	3880	.324	1260				

Table 16. Points on the flexible wall stability curves, calculated for $(m,D,c_o) = (1,1000,3000)$ using a thirty cosine series (i.e. damped membrane curves).

(a)

R	c_i	c_{pi}
3000	.0060	18.0
3300	.0030	9.9
3500	.0012	4.2
3800	-.0013	-4.9
4000	-.0028	-11.2
4200	-.0043	-18.1
4400	-.0059	-26.0
4500	-.0070	-31.5
4600	-.0085	-39.2
4800	-.0139	-66.7
5000	-.0270	-135.0

(b)

R	c_i	c_{pi}
3000	.0060	18.0
3250	.0048	15.6
3500	.0042	14.7
3750	.0041	15.4
4000	.0046	18.4
4200	.0056	23.5
4400	.0075	33.0
4550	.0095	43.2
4600	.0104	47.9
4650	.0113	52.6
4700	.0121	56.9
4750	.0126	59.9
4800	.0116	55.7
4850	.0072	34.9
4900	.0000	00.0
4950	-.0079	-39.1
5000	-.0154	-77.0

Table 17. Points on the curves of c_{pi} versus R for (a) a=.95 and (b) a=1.05, calculated for flexible walls with $(m,D,c_o)=(1,1000,3000)$ using a thirty cosine series (i.e. damped membrane curves).

a	R	c_r	c_{pr}	a	R	c_r	c_{pr}
.600	6560	.247	1620	.840	8000	.333	2660
.650	6320	.252	1610	.839	8100	.341	2760
.700	6060	.258	1560	.843	8200	.354	2900
.750	5800	.263	1530	.850	8250	.362	2990
.800	5560	.269	1500	.875	8300	.382	3170
.825	5450	.273	1490	.900	8300	.397	3300
.850	5380	.274	1470	.925	8285	.409	3390
.875	5270	.277	1460	.950	8265	.420	3470
.900	5270	.281	1480	.975	8250	.430	3550
.925	5350	.284	1520	1.000	8220	.439	3610
.934	5500	.286	1570	1.025	8195	.448	3670
.934	6000	.290	1740	1.050	8170	.457	3740
.917	6500	.294	1910	1.075	8140	.465	3790
.892	7000	.300	2100	1.100	8110	.473	3830
.863	7500	.310	2330	1.125	8085	.480	3880

Table 18. Points on the flexible wall stability curves, calculated for $(m,D,c_o) = (1,1000,5000)$ using a thirty cosine series (i.e. damped membrane curves).

a	R	a	R	a	R
.800	5630	.924	6000	.839	8000
.850	5470	.911	6500	.900	8300
.900	5470	.889	7000	1.000	8220
.910	5500	.862	7500	1.100	8110
.925	5750				

Table 19. Points on the constant amplification curve for $c_{pi} = -2.5$, calculated for a flexible wall with $(m,D,c_o) = (1,1000,5000)$ using a thirty cosine series (i.e. a damped membrane curve).

a	R	c_r	c_{pr}
.800	7880	.237	1870
.850	7030	.245	1720
.900	6400	.253	1620
.950	6000	.262	1570
.975	5940	.264	1570
1.000	6050	.267	1620
1.022	6500	.268	1740
1.023	7000	.265	1850
1.018	7500	.264	1980
1.011	8000	.261	2090
.999	8500	.259	2200
.987	9000	.259	2330

(a)

a	R	c_r	c_{pr}
.800	9850	.213	2100
.825	9000	.221	1990
.850	8150	.228	1860
.855	8000	.229	1830
.895	7000	.240	1680
.900	6950	.241	1670
.950	6200	.252	1560
.970	6000	.256	1540
1.000	5850	.261	1530
1.025	5800	.263	1540
1.050	5900	.266	1570
1.060	6000	.267	1600
1.075	6350	.266	1690
1.093	7000	.262	1830
1.095	8000	.257	2060
1.094	9000	.250	2250

(b)

Table 20. Points on the flexible wall stability curves, calculated for (a) $(m,D,c_o) = (1,1000,10^4)$ and (b) $(m,D,c_o) = (1,1000,10^5)$, using a thirty cosine series (i.e. damped membrane curves).

a	R	c_r	c_{pr}	a	R	c_r	c_{pr}
.600	7140	.263	1880	.675	8500	.423	3600
.625	7025	.264	1860	.690	8470	.433	3660
.650	6900	.266	1840	.700	8440	.438	3700
.675	6760	.267	1810	.725	8380	.451	3780
.700	6670	.269	1790	.750	8320	.464	3860
.725	6540	.271	1770	.800	8190	.486	3980
.750	6400	.273	1750	.850	8070	.504	4070
.775	6300	.273	1720	.900	7940	.523	4160
.800	6250	.276	1730	.950	7820	.541	4230
.810	6500	.282	1830	1.000	7700	.557	4290
.800	6775	.285	1930	1.050	7590	.572	4340
.783	7000	.287	2010	1.100	7490	.585	4380
.750	7390	.293	2170	1.150	7390	.597	4420
.738	7500	.294	2200	1.250	7200	.621	4470
.725	7630	.298	2270	1.350	7040	.641	4510
.700	7880	.304	2390	1.450	6900	.659	4550
.686	8000	.309	2470	1.550	6770	.674	4570
.675	8090	.313	2530	1.650	6660	.689	4590
.660	8230	.320	2630	1.750	6570	.701	4610
.650	8320	.326	2710	1.850	6480	.712	4620
.638	8400	.335	2810	1.950	6410	.724	4640
.628	8500	.349	2970	2.050	6350	.731	4640
.625	8545	.360	3080	2.150	6300	.738	4650
.625	8555	.362	3100	2.250	6250	.745	4660
.650	8540	.407	3480	2.350	6220	.751	4670
.665	8510	.422	3590	2.450	6200	.755	4680

Table 21(a). Points on the stability curves for damped membrane walls, calculated for $(m,D,c_0) = (1,250,5000)$ using a thirty cosine series.

a	R	c_r	c_{pr}	a	R	c_r	c_{pr}
2.550	6190	.756	4680	3.480	7200	.662	4770
2.650	6190	.758	4690	3.520	7300	.654	4780
2.750	6210	.757	4700	3.540	7400	.646	4780
2.850	6260	.752	4710	3.560	7500	.638	4780
2.950	6340	.744	4720	3.600	7600	.630	4790
3.050	6460	.732	4720	3.660	7700	.623	4800
3.120	6600	.718	4730	3.730	7800	.615	4800
3.180	6750	.703	4740	3.790	7900	.608	4800
3.260	6900	.689	4750	3.830	8000	.601	4810
3.340	7000	.680	4760	3.830	8100	.594	4810
3.420	7100	.671	4760	3.810	8200	.588	4820

Table 21(b). Points on the stability curves for damped membrane walls, calculated for $(m,D,c_0) = (1,250,5000)$ using a thirty cosine series.

y	Stream function.		Reynolds stress.	y	Stream function.		Reynolds stress.
	Real part.	Imaginary part.			Real part.	Imaginary part.	
.000	1.0000	.0000	.0000	.800	.2796	.0016	.0620
.050	.9975	.0000	.0000	.810	.2581	.0027	.0746
.100	.9901	.0000	.0001	.820	.2362	.0040	.0860
.150	.9778	.0000	-.0001	.830	.2140	.0056	.0955
.200	.9603	.0000	.0000	.840	.1920	.0073	.1027
.250	.9378	.0000	-.0001	.850	.1692	.0092	.1071
.300	.9100	.0000	-.0001	.860	.1466	.0112	.1087
.350	.8768	.0000	-.0001	.870	.1240	.0131	.1076
.400	.8381	.0000	-.0003	.880	.1015	.0150	.1043
.450	.7935	.0000	-.0003	.890	.0791	.0167	.0995
.500	.7429	.0000	-.0006	.900	.0569	.0181	.0938
.525	.7152	.0000	-.0008	.910	.0350	.0191	.0883
.550	.6858	-.0001	-.0008	.920	.0136	.0196	.0838
.575	.6548	-.0001	-.0010	.930	-.0073	.0195	.0810
.600	.6219	-.0001	-.0016	.940	-.0275	.0188	.0801
.625	.5873	-.0001	-.0032	.950	-.0467	.0174	.0807
.650	.5507	-.0002	-.0062	.960	-.0648	.0155	.0816
.675	.5120	-.0004	-.0101	.970	-.0812	.0132	.0798
.700	.4711	-.0006	-.0124	.980	-.0968	.0108	.0708
.725	.4275	-.0009	-.0090	.990	-.1081	.0090	.0474
.750	.3812	-.0009	.0048	1.000	-.1178	.0086	.0000
.775	.3318	-.0002	.0300				

Table 22. Points on the stream function and Reynolds stress distributions, calculated at $(a,R) = (.9,5270)$ for damped membranes with $(m,D,c_0) = (1,1000,5000)$ using a thirty cosine series. The relevant eigenvalue is $c = .281$.

y	Stream function.		Reynolds stress.	y	Stream function.		Reynolds stress.
	Real part.	Imaginary part.			Real part.	Imaginary part.	
.000	1.0000	.0000	.0000	.800	.2196	.0006	.0456
.050	.9973	.0000	.0000	.810	.1958	.0017	.0593
.100	.9892	.0000	.0001	.820	.1715	.0032	.0725
.150	.9757	.0000	-.0001	.830	.1468	.0050	.0842
.200	.9566	.0000	.0001	.840	.1216	.0072	.0940
.250	.9320	.0000	.0000	.850	.0961	.0097	.1015
.300	.9017	.0000	.0000	.860	.0702	.0126	.1066
.350	.8656	.0000	.0000	.870	.0441	.0156	.1097
.400	.8234	.0000	-.0002	.880	.0178	.0188	.1111
.450	.7750	.0000	-.0001	.890	-.0088	.0221	.1119
.500	.7200	.0000	-.0005	.900	-.0355	.0253	.1131
.525	.6900	.0000	-.0006	.910	-.0623	.0284	.1158
.550	.6582	.0000	-.0006	.920	-.0892	.0312	.1211
.575	.6246	.0000	-.0007	.930	-.1161	.0337	.1299
.600	.5892	-.0001	-.0009	.940	-.1429	.0356	.1424
.625	.5517	-.0001	-.0018	.950	-.1693	.0370	.1575
.650	.5123	-.0001	-.0041	.960	-.1952	.0377	.1719
.675	.4707	-.0003	-.0086	.970	-.2201	.0381	.1787
.700	.4267	-.0006	-.0140	.980	-.2437	.0382	.1663
.725	.3800	-.0010	-.0160	.990	-.2654	.0386	.1158
.750	.3301	-.0013	-.0081	1.000	-.2850	.0402	.0001
.775	.2767	-.0010	.0134				

Table 23. Points on the stream function and Reynolds stress distributions, calculated at $(a,R) = (.863,7500)$ for damped membranes with $(m,D,c_0) = (1,1000,5000)$ using a thirty cosine series. The relevant eigenvalue is $c = .310$.

y	Stream function.		Reynolds stress.	y	Stream function.		Reynolds stress.
	Real part.	Imaginary part.			Real part.	Imaginary part.	
.000	1.0000	.0000	.0000	.800	.0725	.0171	.1556
.050	.9969	.0000	.0002	.810	.0450	.0216	.1623
.100	.9874	.0000	.0007	.820	.0174	.0267	.1657
.150	.9717	.0000	.0008	.830	-.0103	.0321	.1665
.200	.9495	.0001	.0013	.840	-.0381	.0380	.1653
.250	.9209	.0001	.0014	.850	-.0659	.0441	.1629
.300	.8855	.0001	.0018	.860	-.0938	.0506	.1602
.350	.8433	.0002	.0021	.870	-.1218	.0572	.1578
.400	.7941	.0002	.0022	.880	-.1499	.0639	.1566
.450	.7375	.0003	.0025	.890	-.1783	.0708	.1570
.500	.6731	.0004	.0025	.900	-.2068	.0777	.1599
.525	.6379	.0004	.0027	.910	-.2356	.0846	.1663
.550	.6006	.0004	.0029	.920	-.2648	.0914	.1772
.575	.5611	.0004	.0023	.930	-.2942	.0981	.1938
.600	.5194	.0004	-.0005	.940	-.3239	.1045	.2165
.625	.4752	.0003	-.0062	.950	-.3538	.1107	.2442
.650	.4284	.0000	-.0127	.960	-.3837	.1164	.2722
.675	.3784	-.0004	-.0140	.970	-.4133	.1216	.2894
.700	.3248	-.0006	-.0012	.980	-.4421	.1267	.2758
.725	.2672	.0000	.0309	.990	-.4698	.1318	.1975
.750	.2054	.0026	.0774	1.000	-.4957	.1379	.0038
.775	.1402	.0081	.1240				

Table 24. Points on the stream function and Reynolds stress distributions, calculated at $(a,R) = (.9,8300)$ for damped membranes with $(m,D,c_o) = (1,1000,5000)$ using a thirty cosine series. The relevant eigenvalue is $c = .397$.

a	R	c_r	c_{pr}
.800	5330	.272	1450
.825	5280	.274	1450
.850	5225	.276	1440
.875	5200	.279	1450
.900	5210	.281	1460
.925	5300	.284	1510
.934	5500	.287	1580
.933	6000	.290	1740
.914	6500	.295	1920
.887	7000	.304	2130
.858	7500	.322	2420
.853	7625	.330	2520
.850	7750	.339	2630
.852	7875	.351	2760
.865	8000	.368	2940
.875	8058	.379	3050
.900	8143	.394	3210
.925	8210	.409	3360
.950	8270	.419	3470
.975	8330	.430	3580
1.000	8380	.441	3690
1.025	8430	.451	3800
1.050	8490	.460	3910
1.075	8540	.468	4000
1.100	8590	.479	4120

(a)

a	R	c_r	c_{pr}
.800	5050	.276	1390
.825	5070	.276	1400
.850	5120	.279	1430
.875	5140	.281	1450
.900	5220	.281	1470
.925	5400	.284	1530
.938	5750	.286	1640
.936	6000	.288	1730
.925	6330	.290	1840
.917	6500	.294	1910
.888	7000	.305	2130
.866	7300	.321	2340
.861	7400	.328	2430
.858	7500	.337	2530
.858	7600	.345	2620
.863	7750	.358	2770
.875	7940	.376	2990
.900	8180	.397	3250
.925	8390	.410	3440
.950	8600	.424	3650
.975	8800	.435	3830
1.000	9000	.447	4020
1.025	9190	.457	4210
1.050	9370	.469	4400
1.075	9550	.479	4580
1.100	9720	.489	4760

(b)

Table 25. Points on the stability curves for thin plates, calculated for (a) $(m,D,c_o) = (1,1000,(4000^2+10^7a^2)^{\frac{1}{2}})$ and (b) $(m,D,c_o) = (1,1000,(3\times10^7a^2)^{\frac{1}{2}})$, using a thirty cosine series.

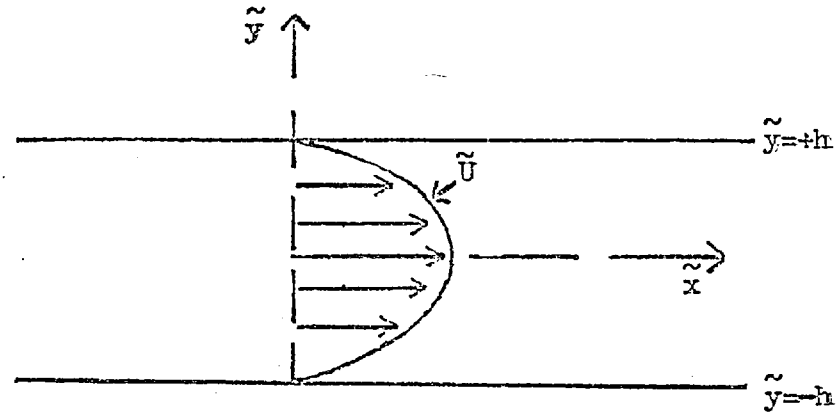

Figure 1. The coordinate system for plane Poiseulle flow with flexible walls.

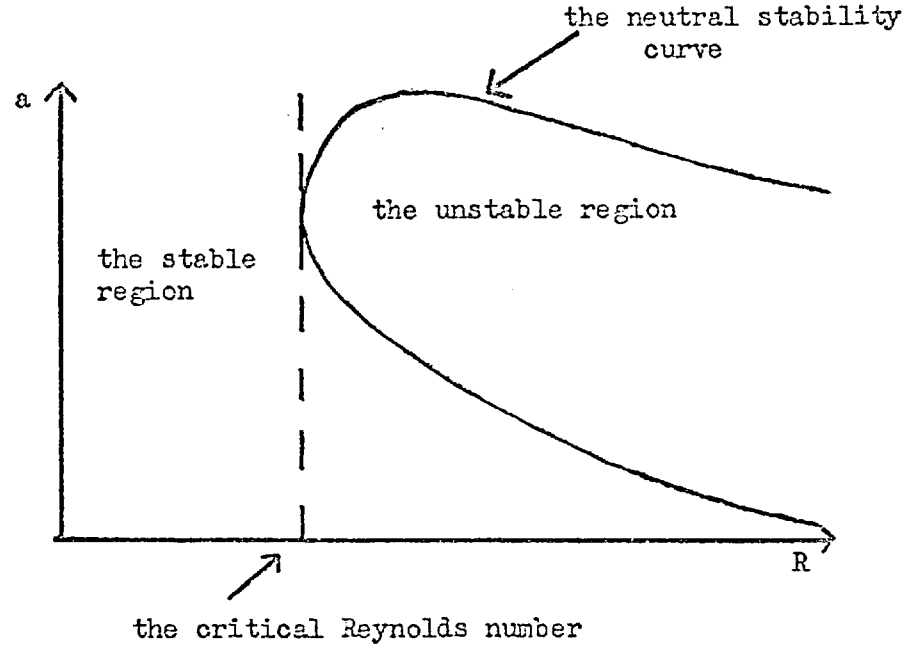

Figure 2. A typical neutral stability curve.

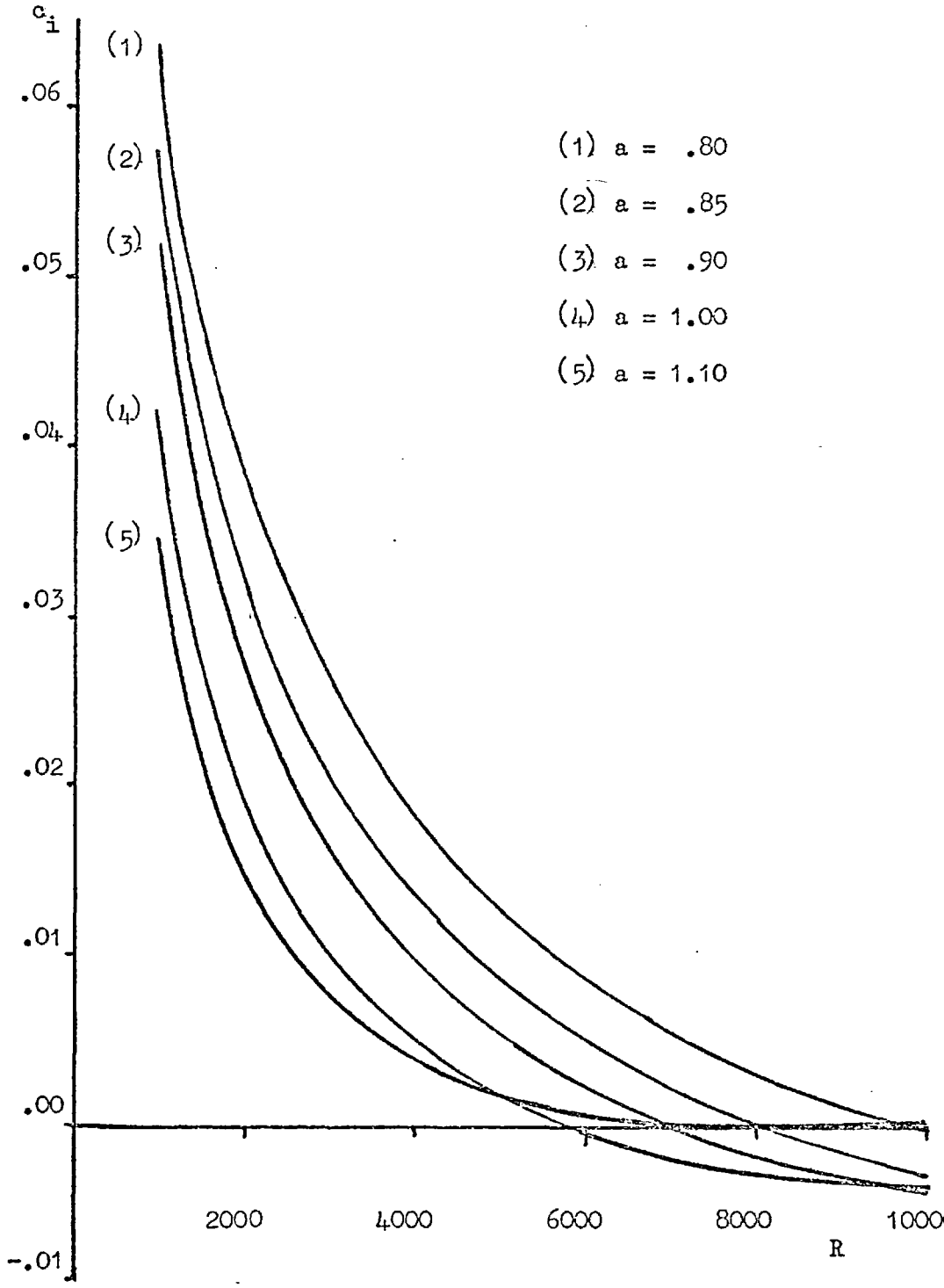

Figure 3. Curves of c_i versus R, at fixed values of a, obtained for the rigid wall problem using a thirty cosine series.

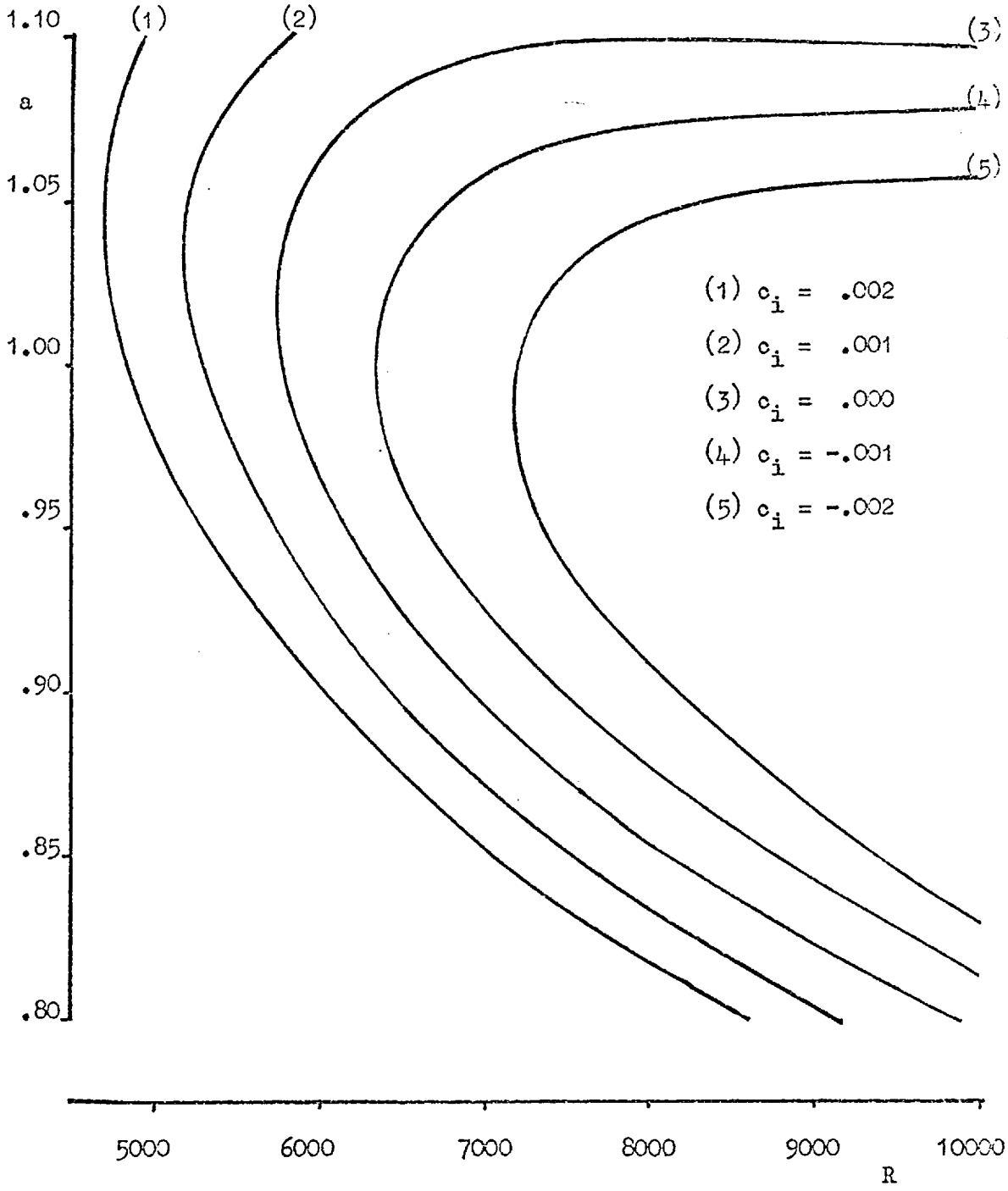

Figure 4. The neutral stability and constant amplification curves for the rigid wall problem, obtained using a thirty cosine series.

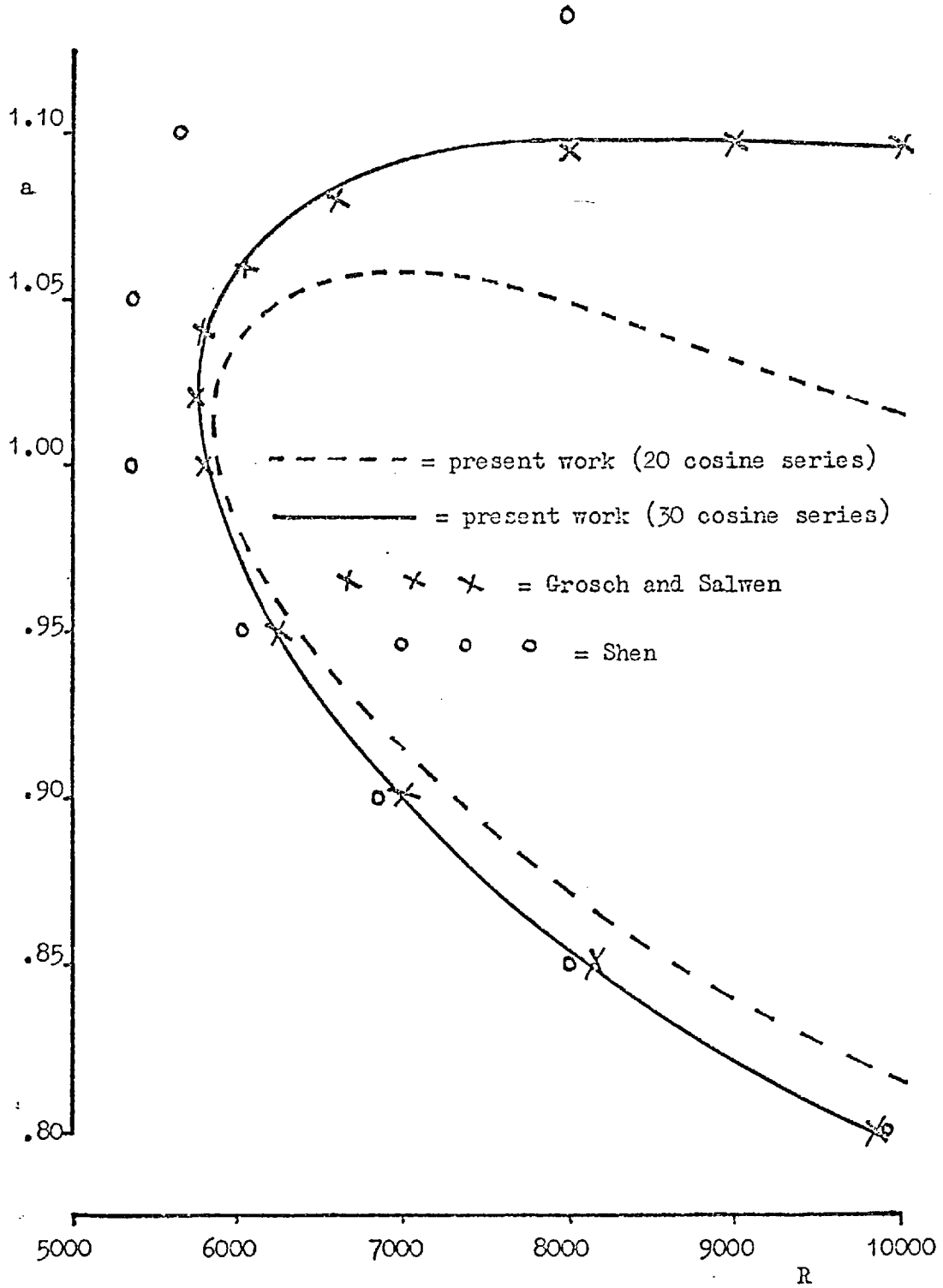

Figure 5. Convergence of the present rigid wall neutral stability curve and comparisons with previous neutral stability curves.

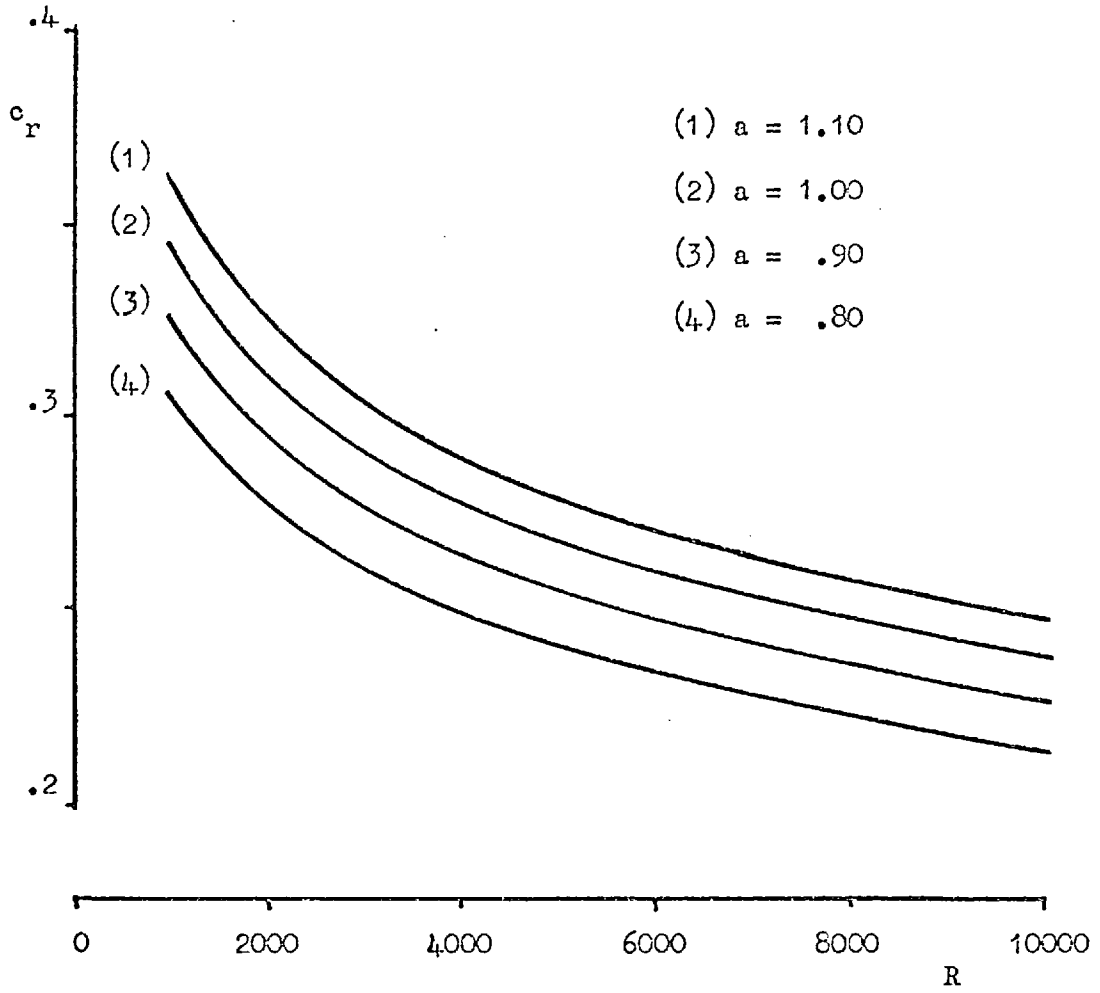

Figure 6. Curves of c_r versus R, at fixed values of a, obtained for the rigid wall problem using a thirty cosine series.

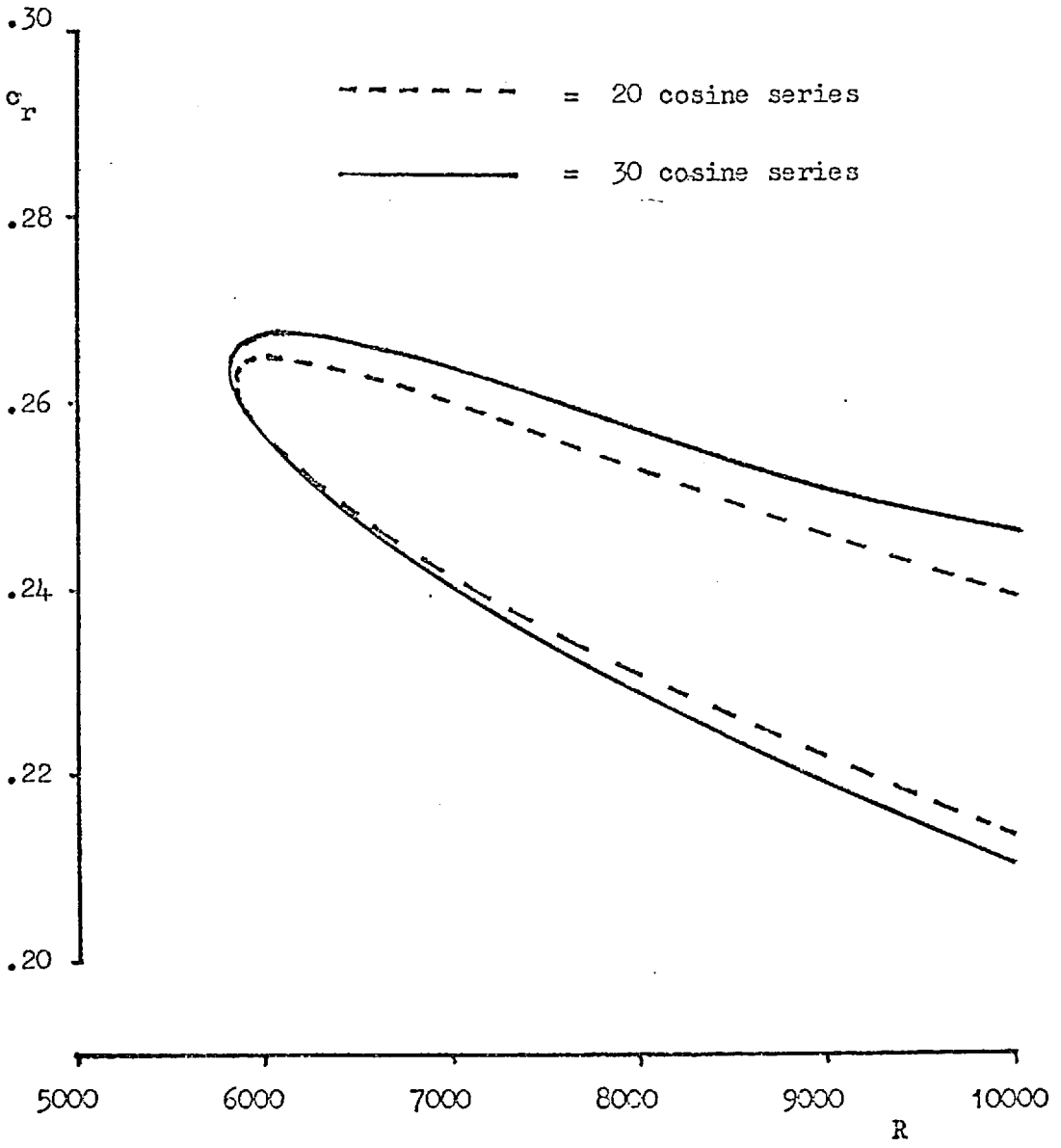

Figure 7. Convergence of the spatial neutral stability curve for the rigid wall problem.

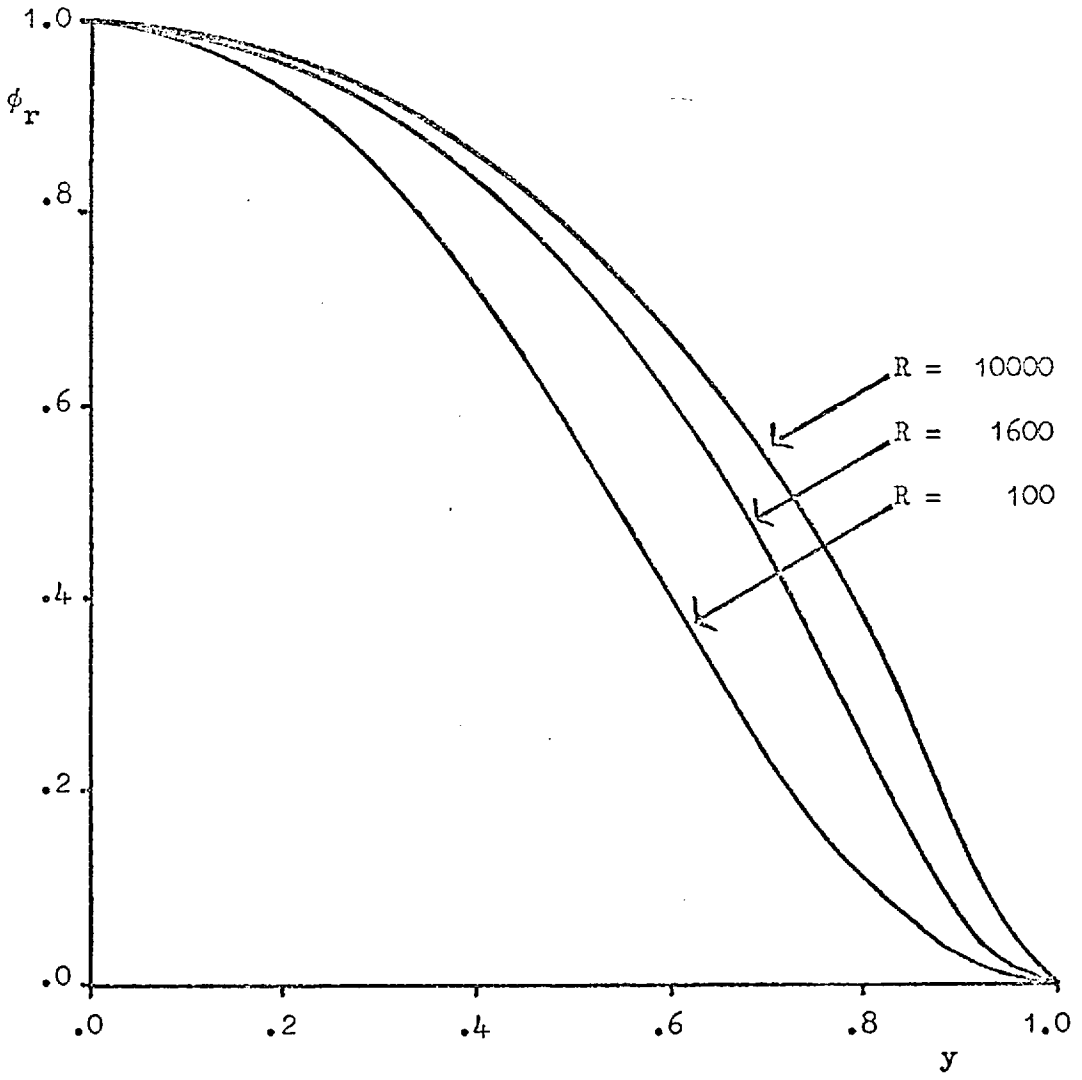

Figure 8. Comparison of the real parts of the rigid wall stream function distributions, obtained using a thirty cosine series.

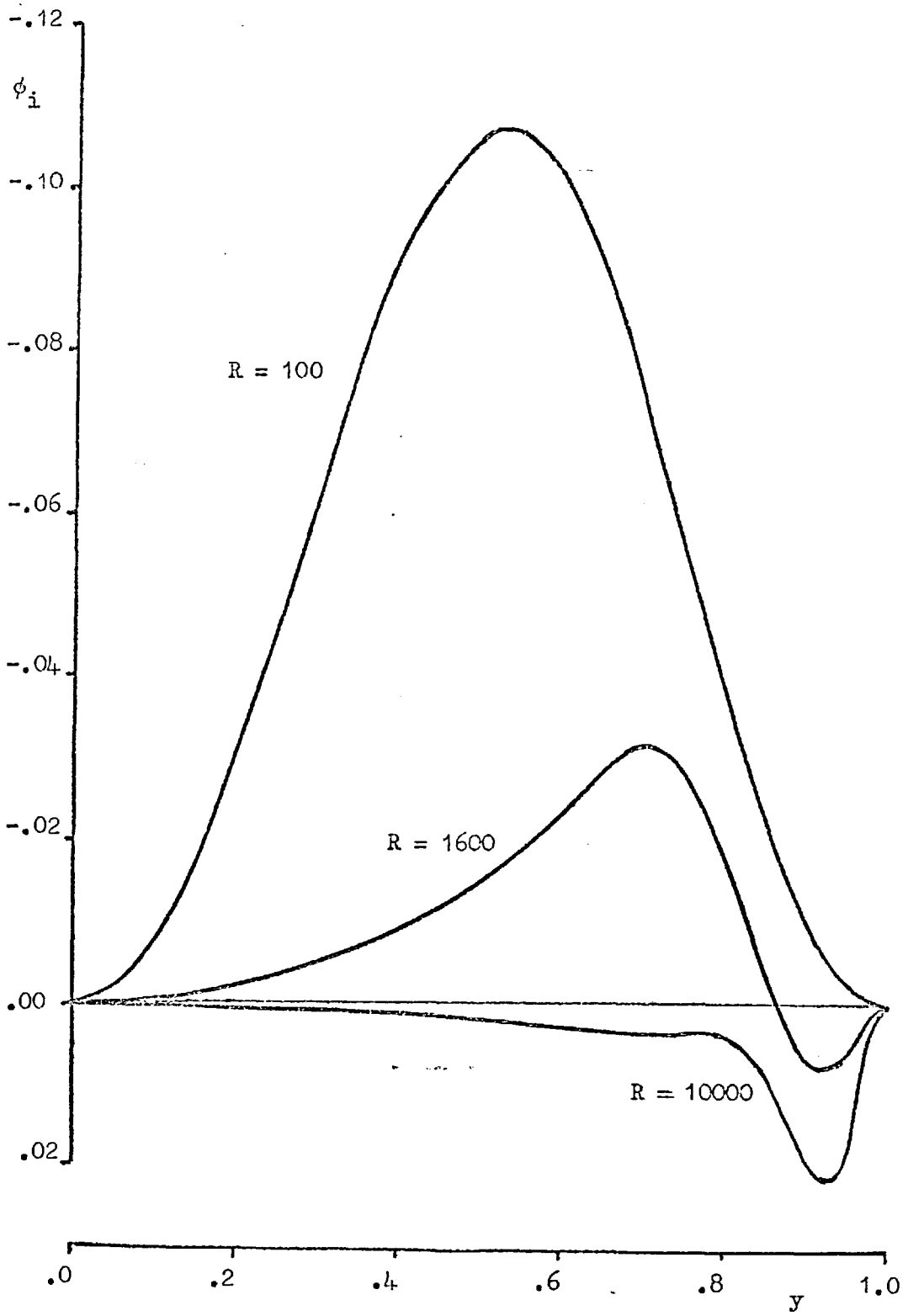

Figure 9. Comparison of the imaginary parts of the rigid wall stream function distributions, obtained using a thirty cosine series.

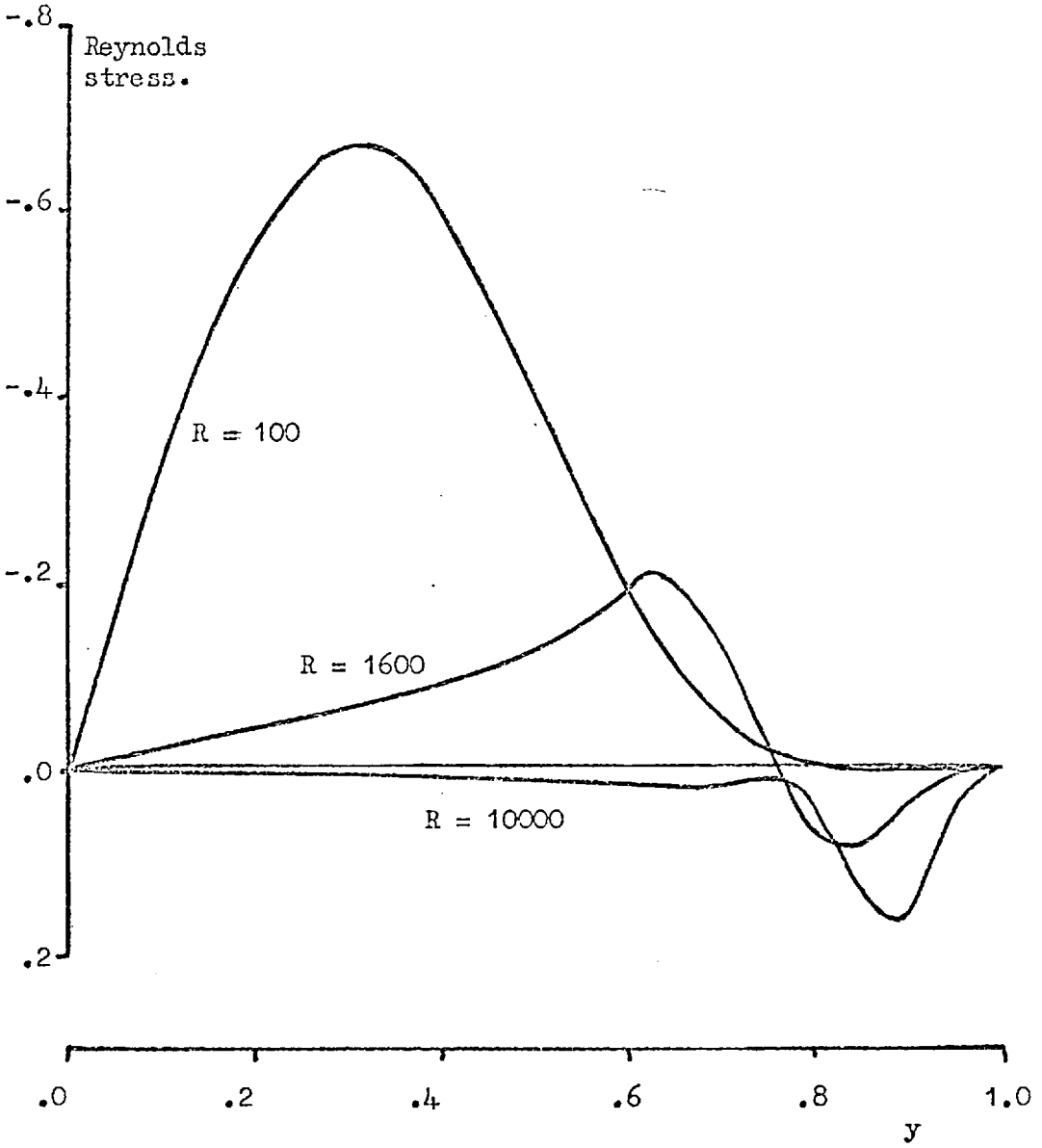

Figure 10. Comparison of the rigid wall Reynolds stress distributions, obtained using a thirty cosine series.

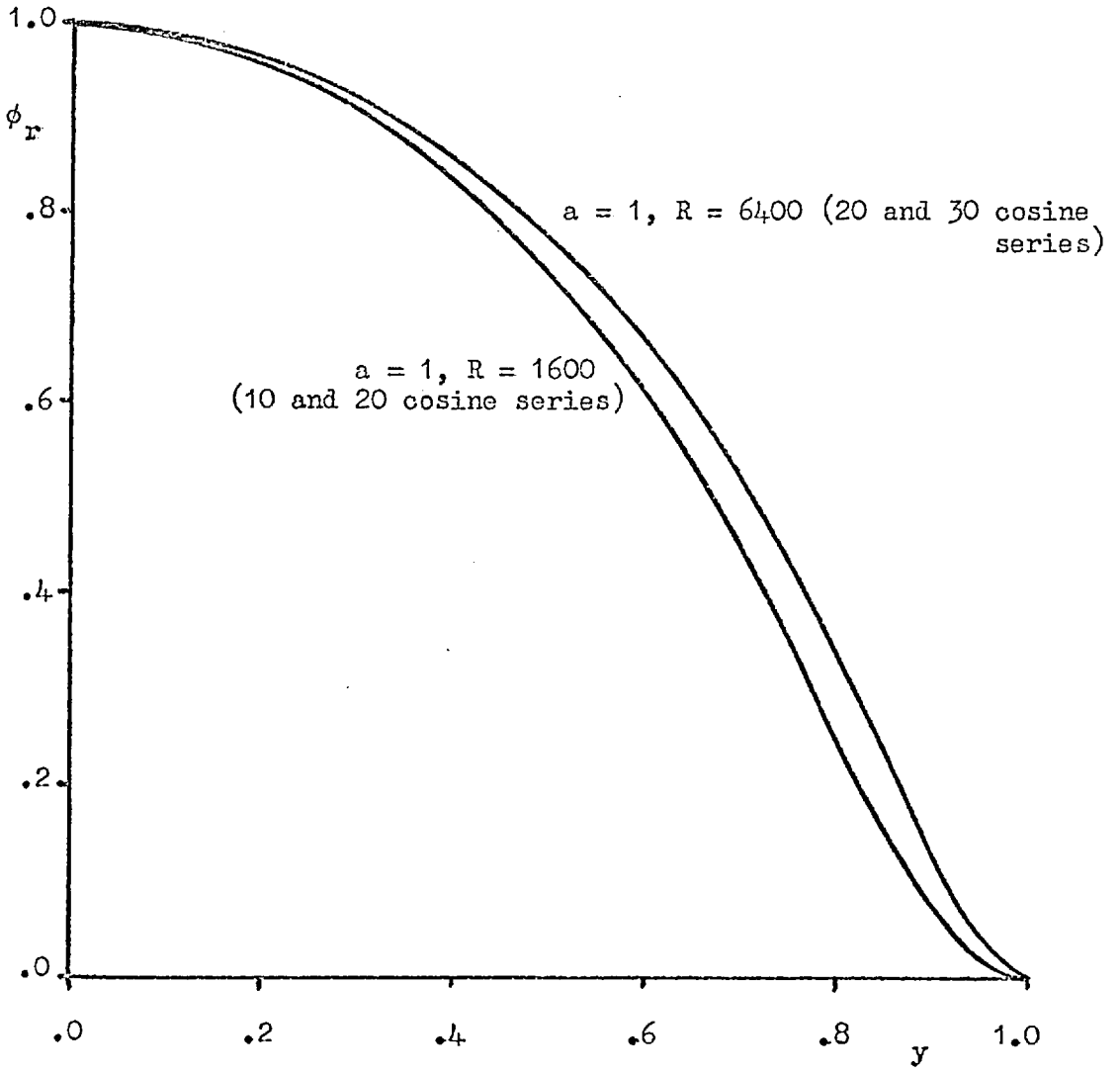

Figure 11. Convergence of the real parts of the rigid wall stream function distributions.

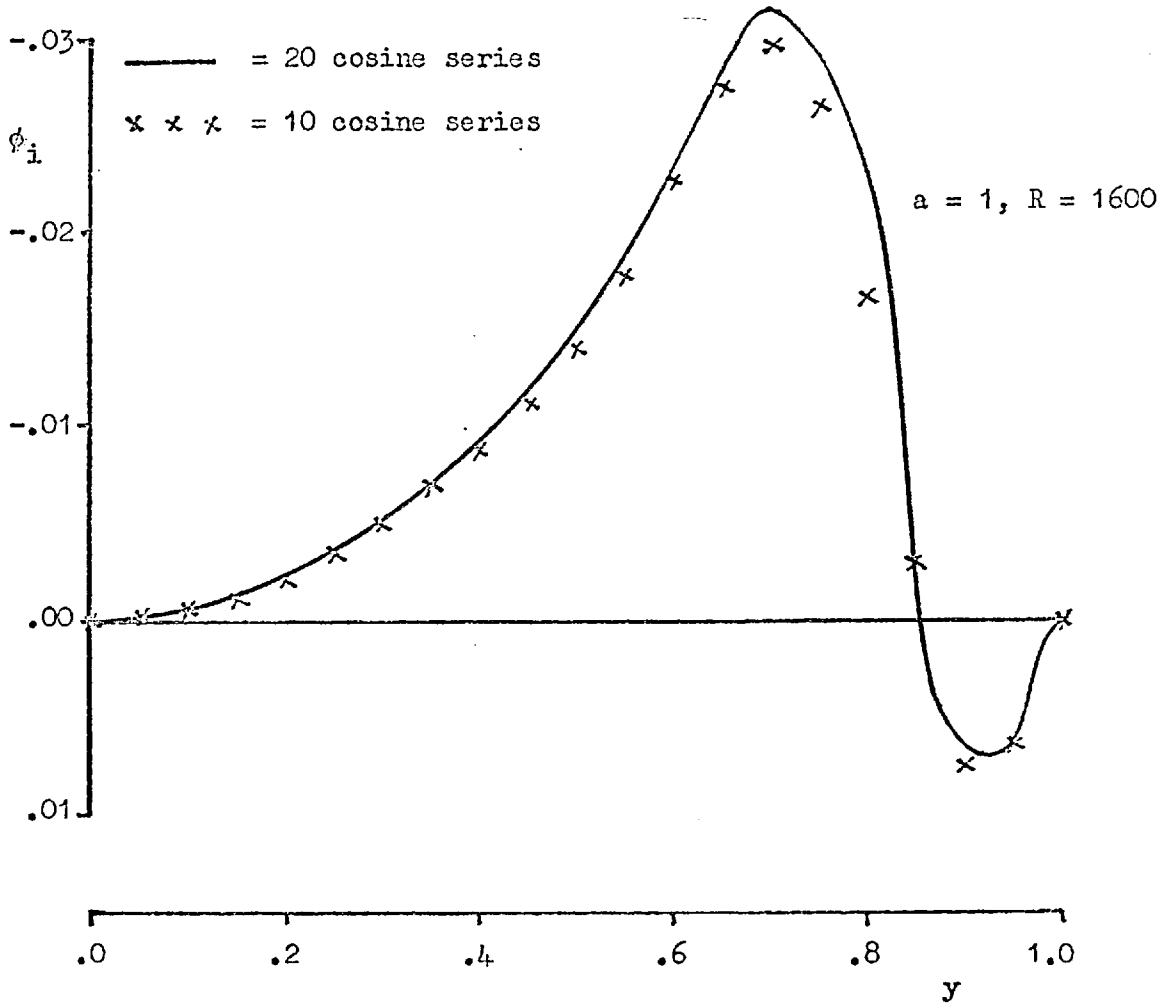

Figure 12. Convergence of the imaginary part of the rigid wall stream function distribution at (a,R) = (1,1600).

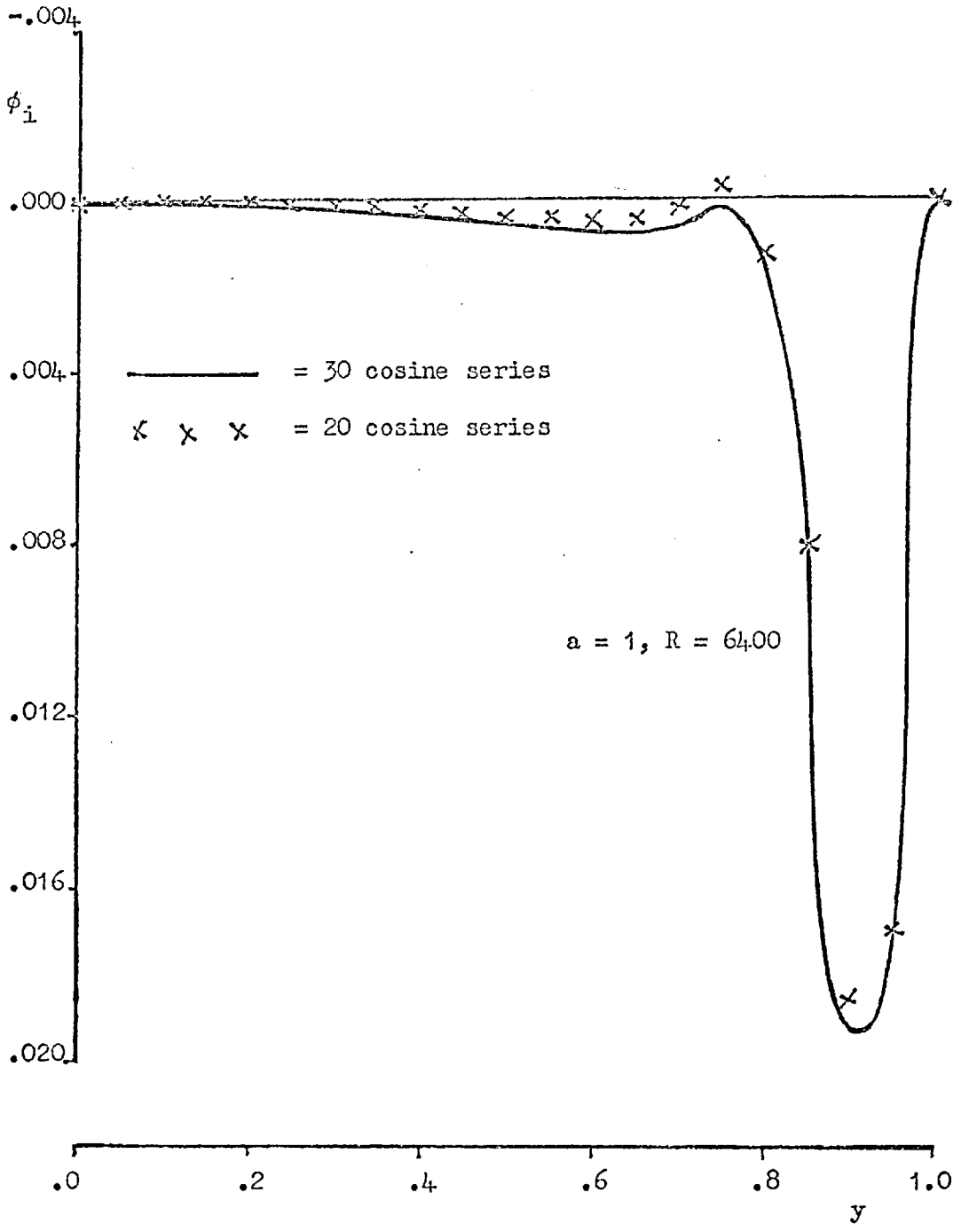

Figure 13. Convergence of the imaginary part of the rigid wall stream function distribution at (a,R) = (1,6400).

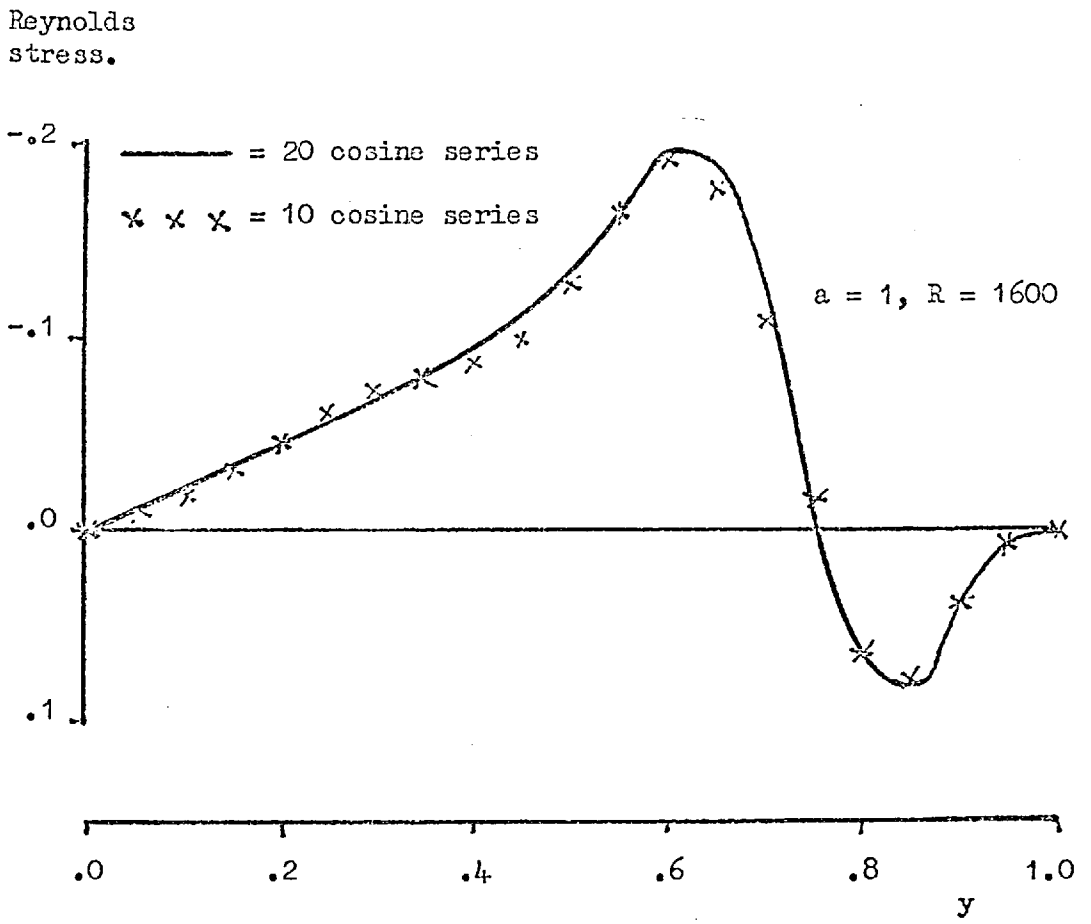

Figure 14. Convergence of the rigid wall Reynolds stress distribution at $(a,R) = (1,1600)$.

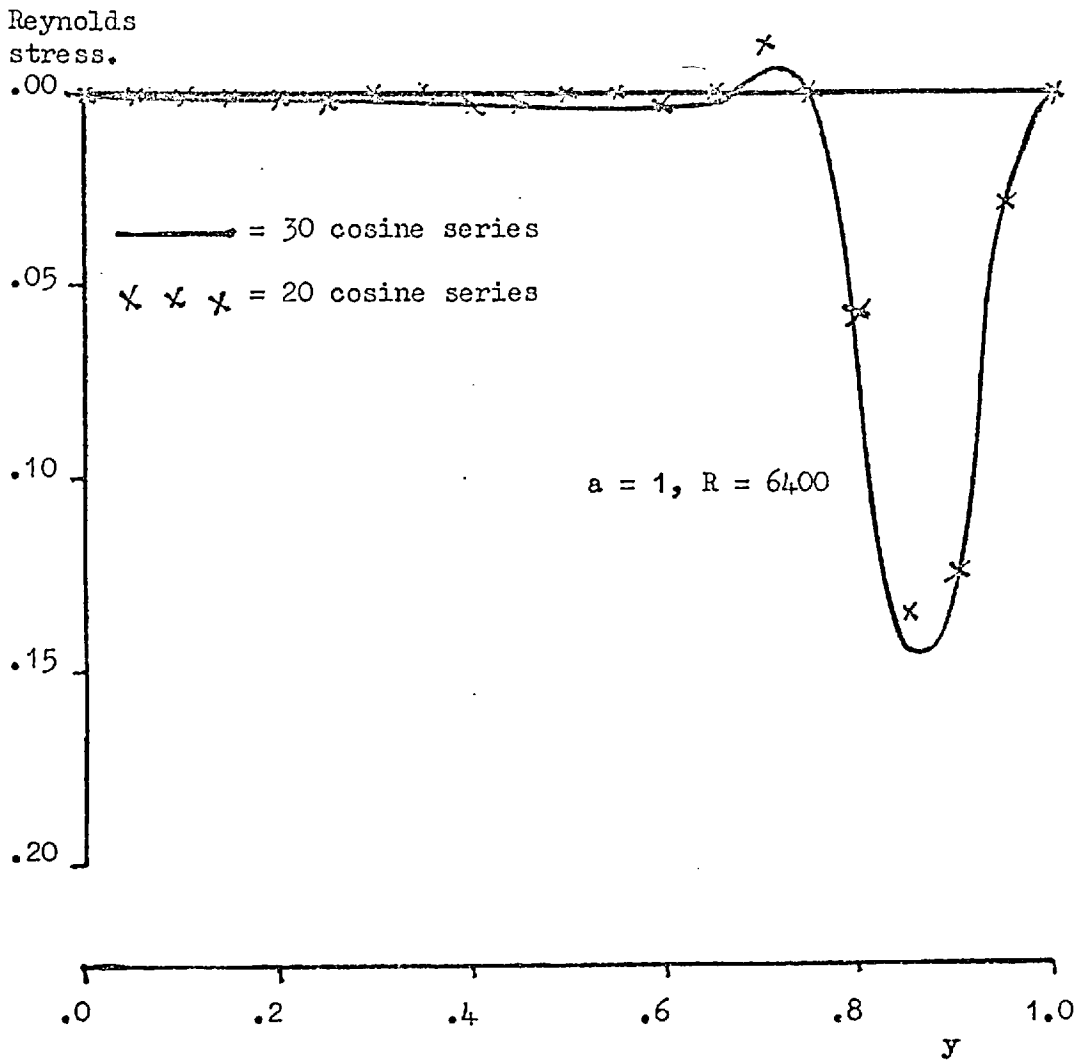

Figure 15. Convergence of the rigid wall Reynolds stress distribution at (a,R) = (1,6400).

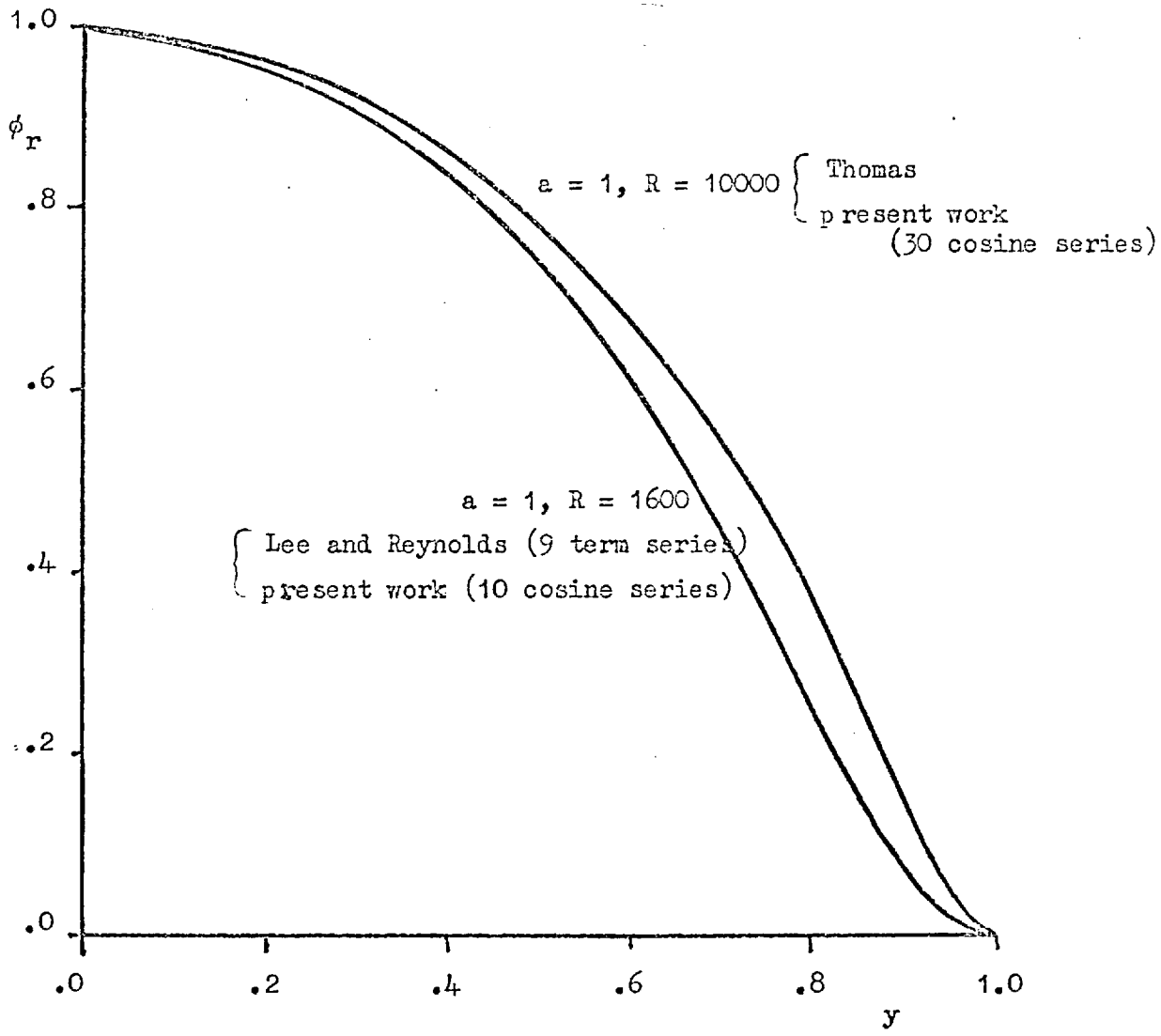

Figure 16. Comparisons of the real parts of the present rigid wall stream function distributions with previous work.

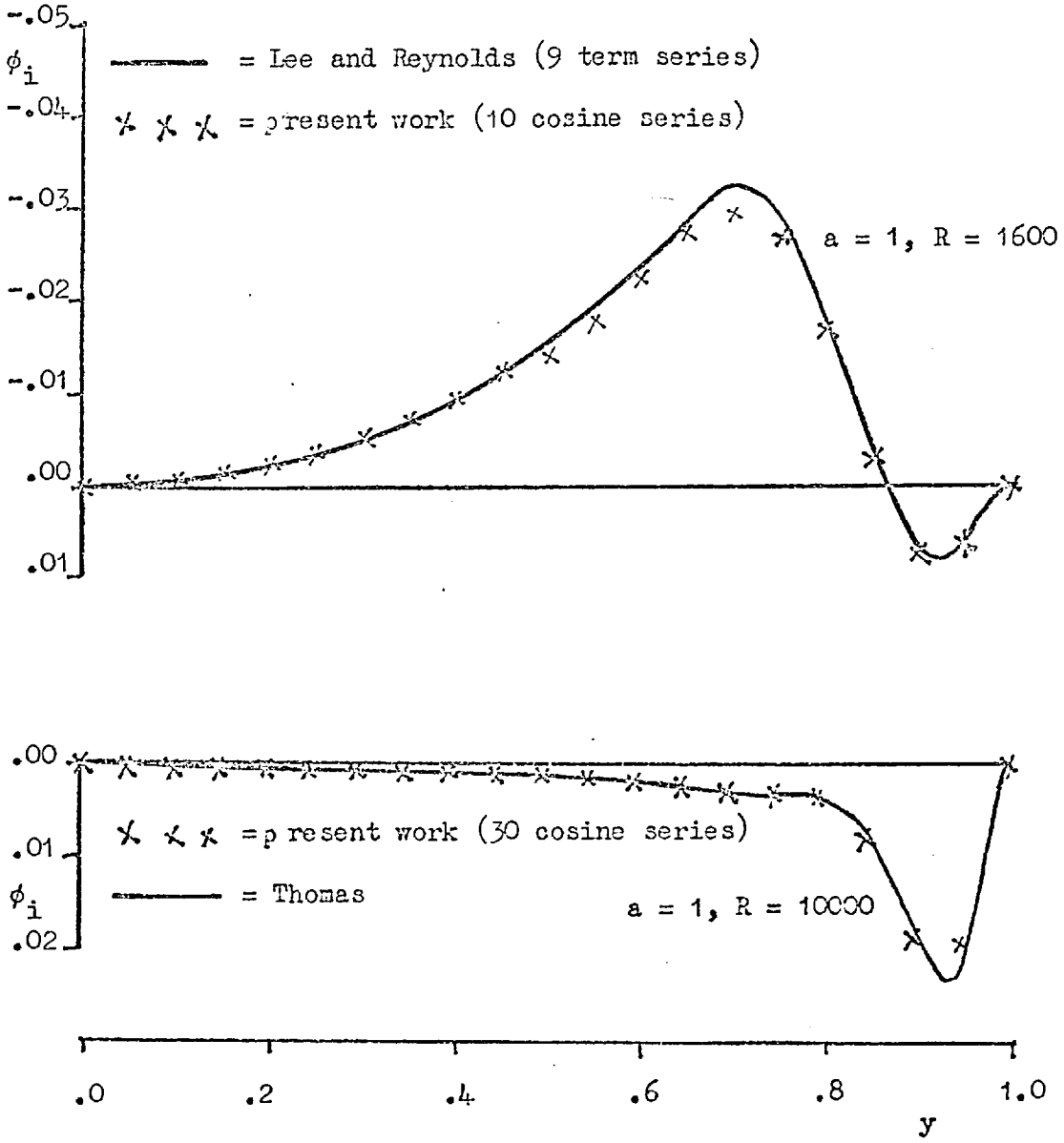

Figure 17. Comparisons of the imaginary parts of the present rigid wall stream function distributions with previous work.

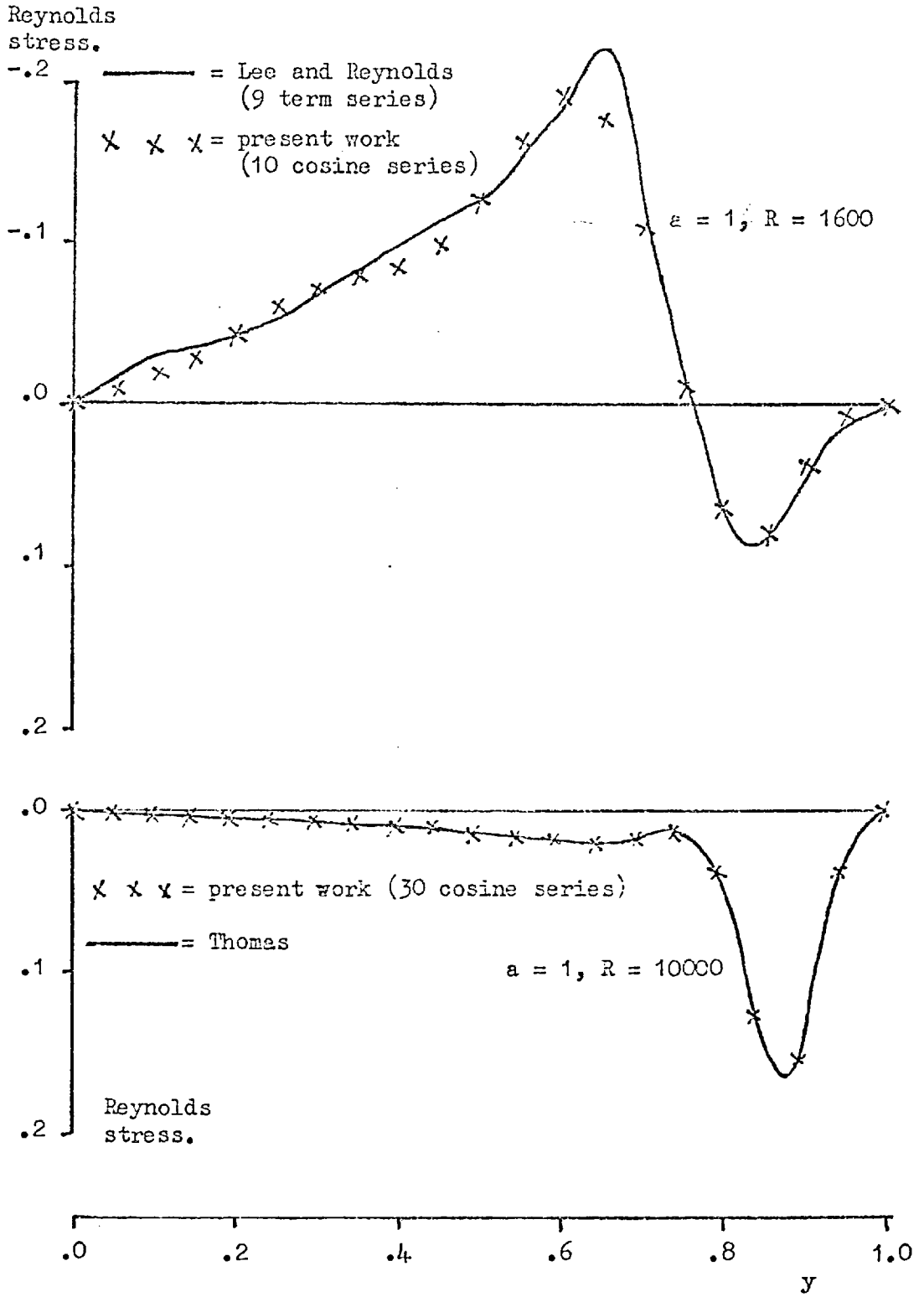

Figure 18. Comparisons of the present rigid wall Reynolds stress distributions with previous work.

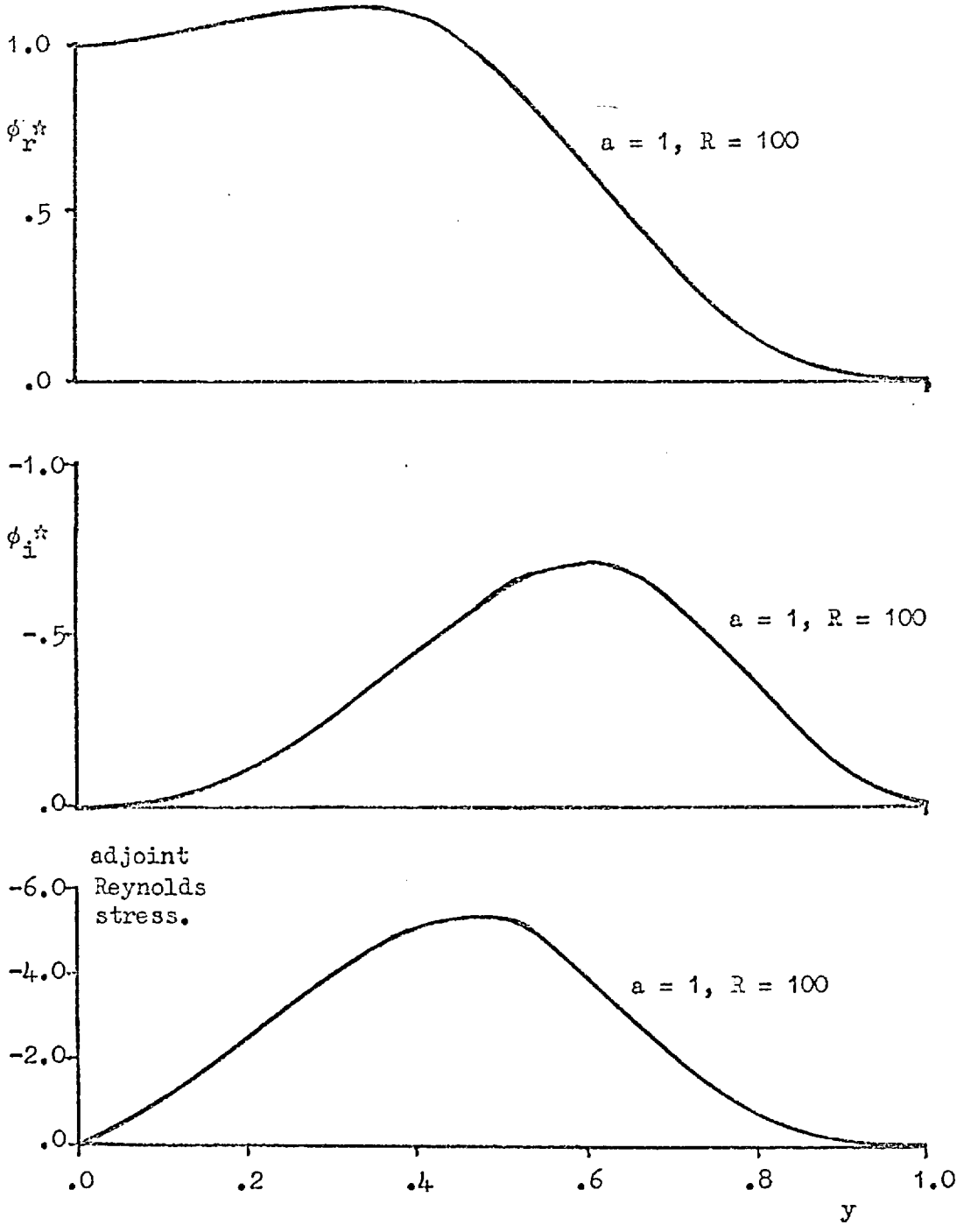

Figure 19. The adjoint rigid wall distributions at (a,R) = (1,100), obtained using a thirty cosine series.

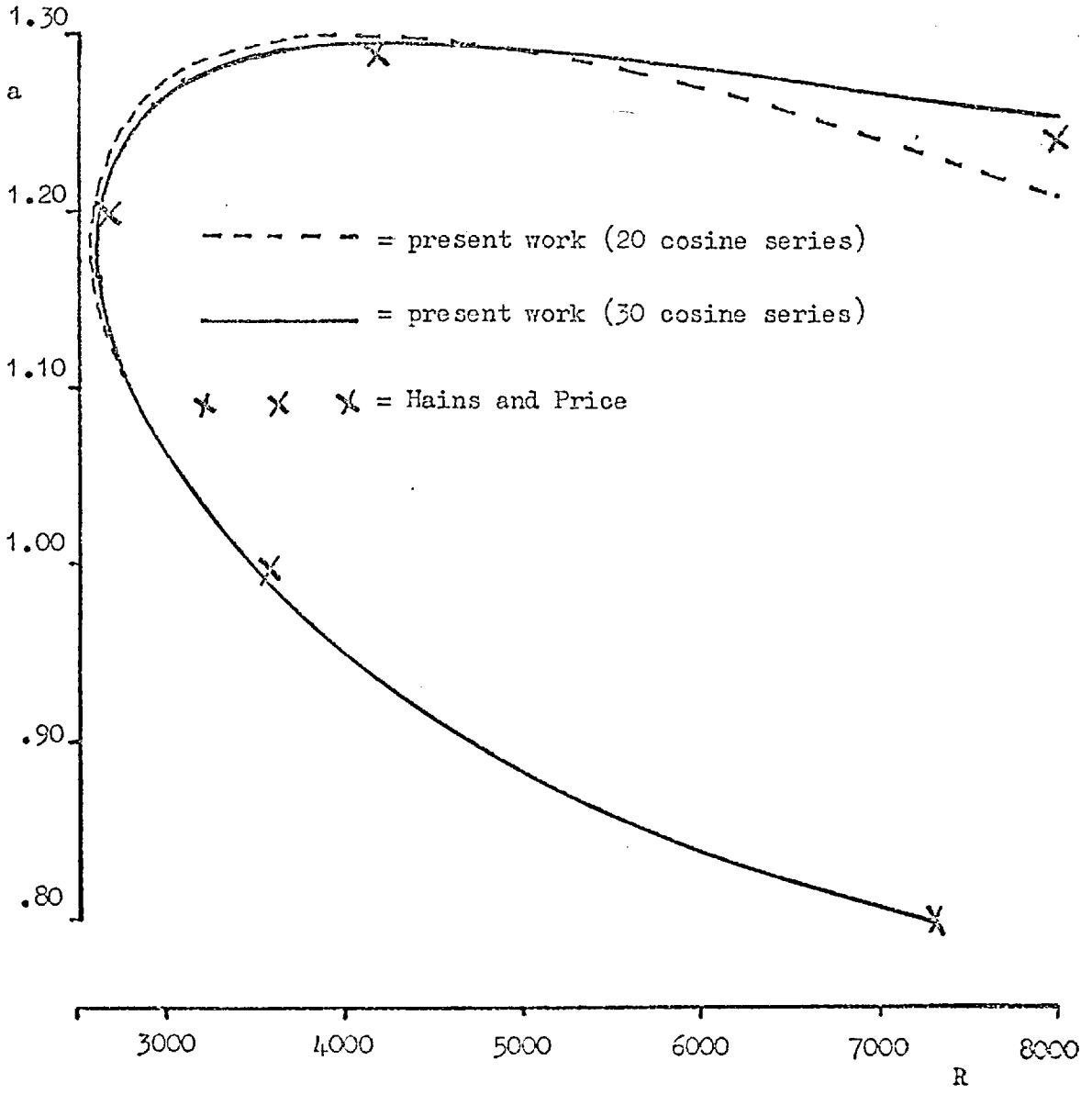

Figure 20. Convergence of the present neutral stability curve and comparison with that of Hains and Price, for values of $E_1^{-1} = E_2^{-1} = -10$.

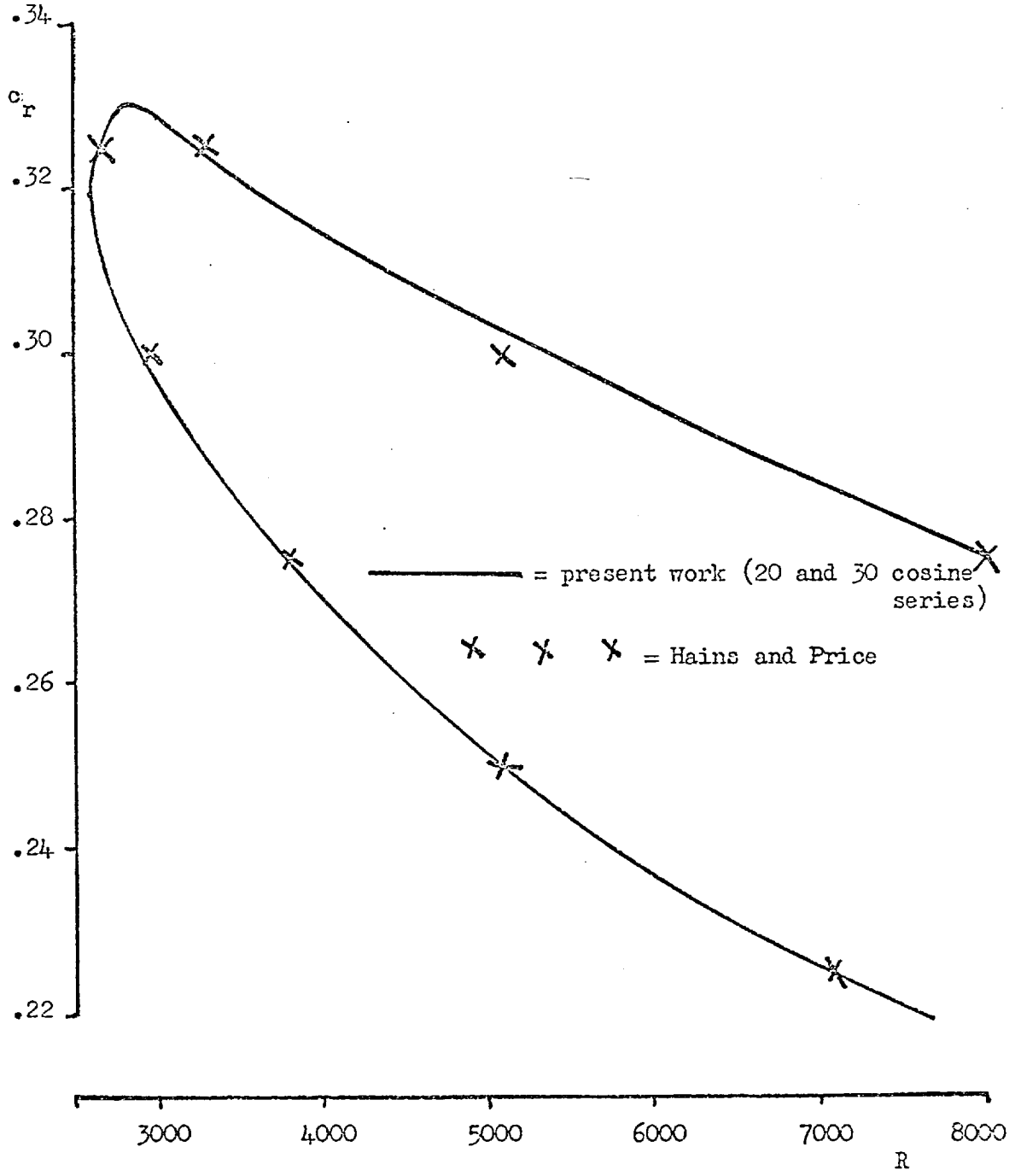

Figure 21. Convergence of the present spatial stability curve and comparison with that of Hains and Price, for values of $E_1^{-1} = E_2^{-1} = -10$.

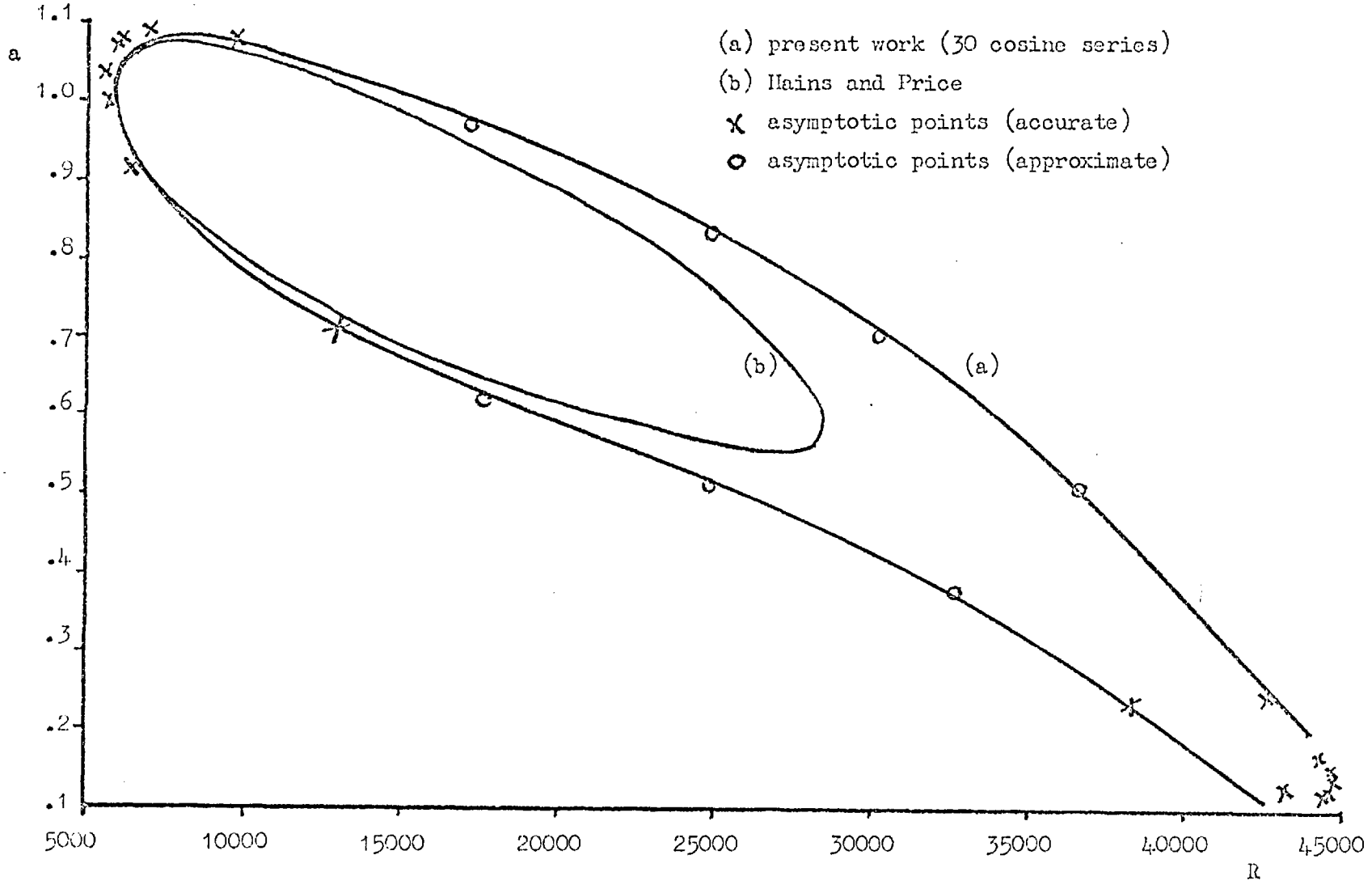

Figure 22. Comparison of neutral stability curves for a membrane with tension only. The value of the tension is $.5 \times 10^9$.

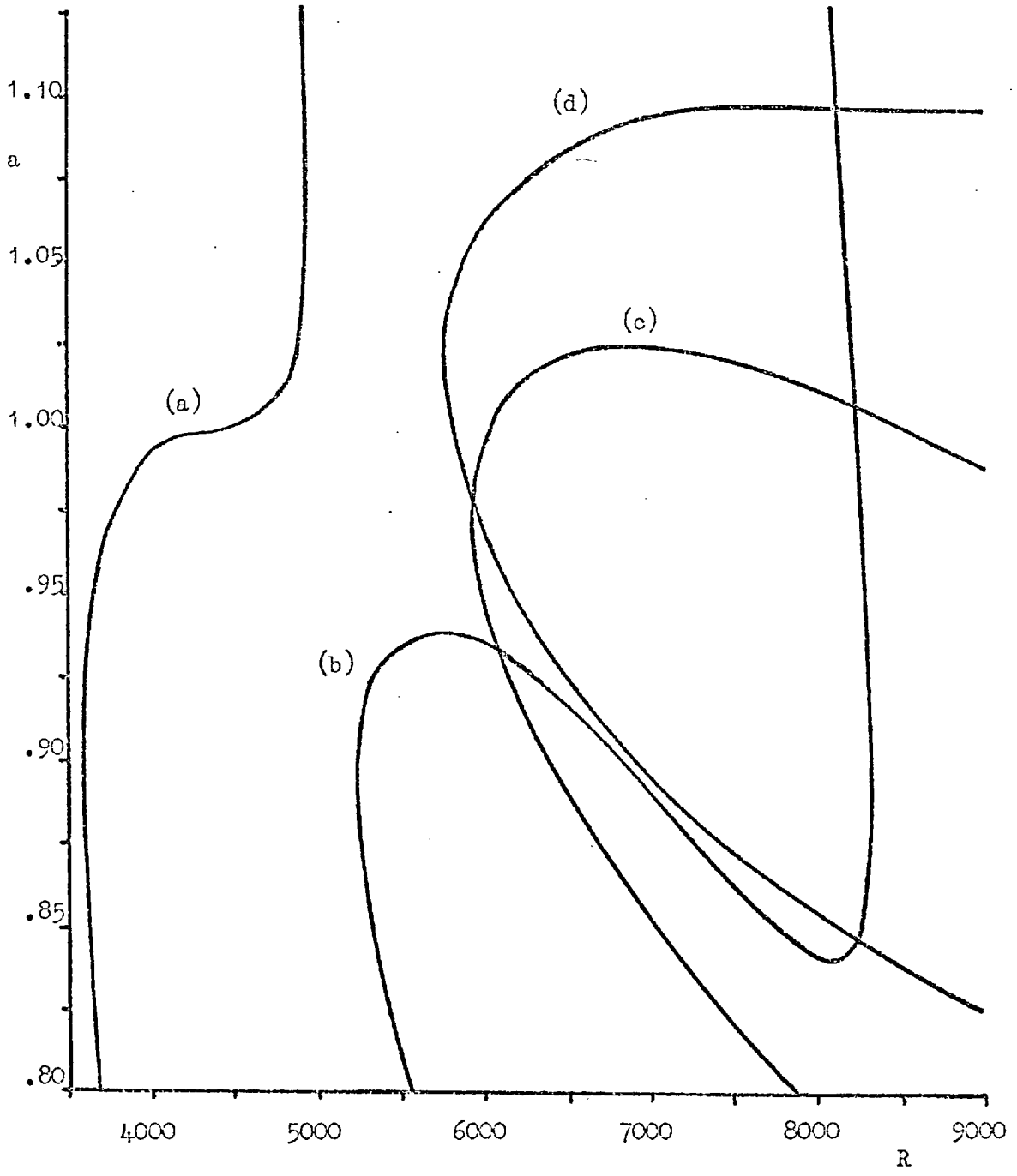

Figure 23. Neutral stability curves calculated for damped membrane walls with (m,D) = (1,1000) and (a) c_o = 3000, (b) c_o = 5000, (c) $c_o = 10^4$ and (d) $c_o = 10^5$, using a thirty cosine series.

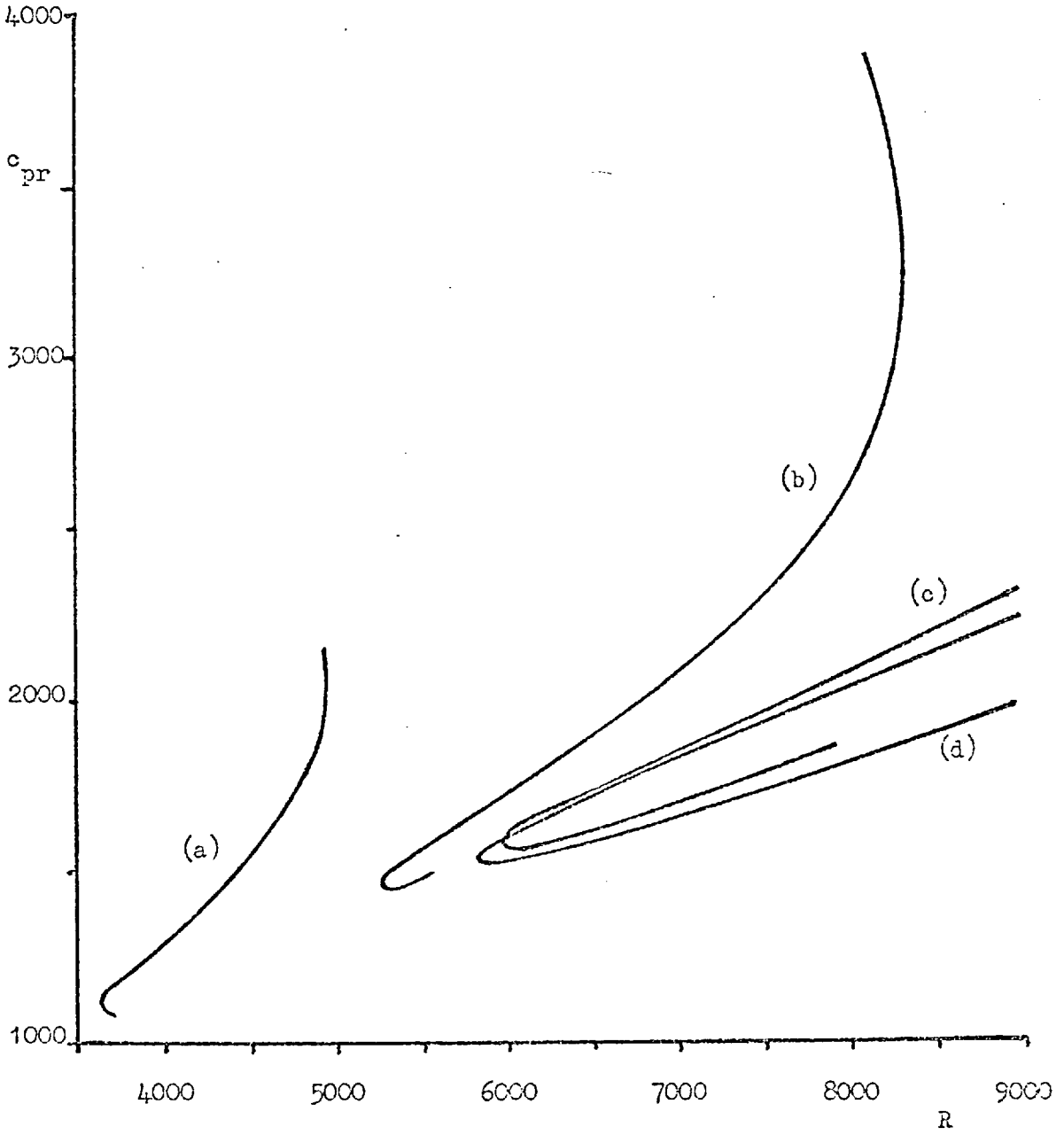

Figure 24. Spatial stability curves calculated for damped membrane walls with (m,D) = (1,1000) and (a) c_o = 3000, (b) c_o = 5000, (c) $c_o = 10^4$ and (d) $c_o = 10^5$, using a thirty cosine series.

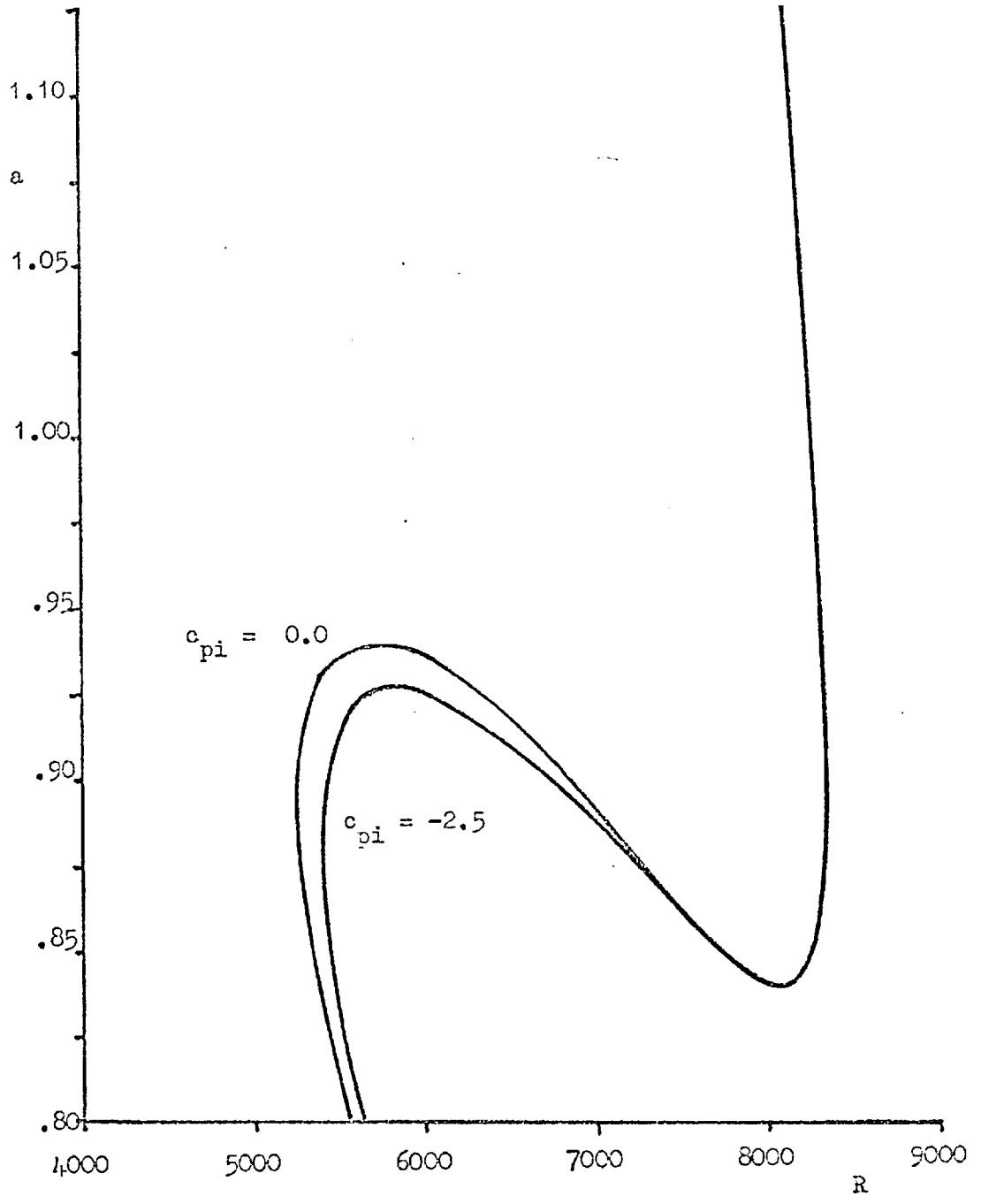

Figure 25. Constant amplification curves calculated for a damped membrane with $(m,D,c_o) = (1,1000,5000)$ using a thirty cosine series.

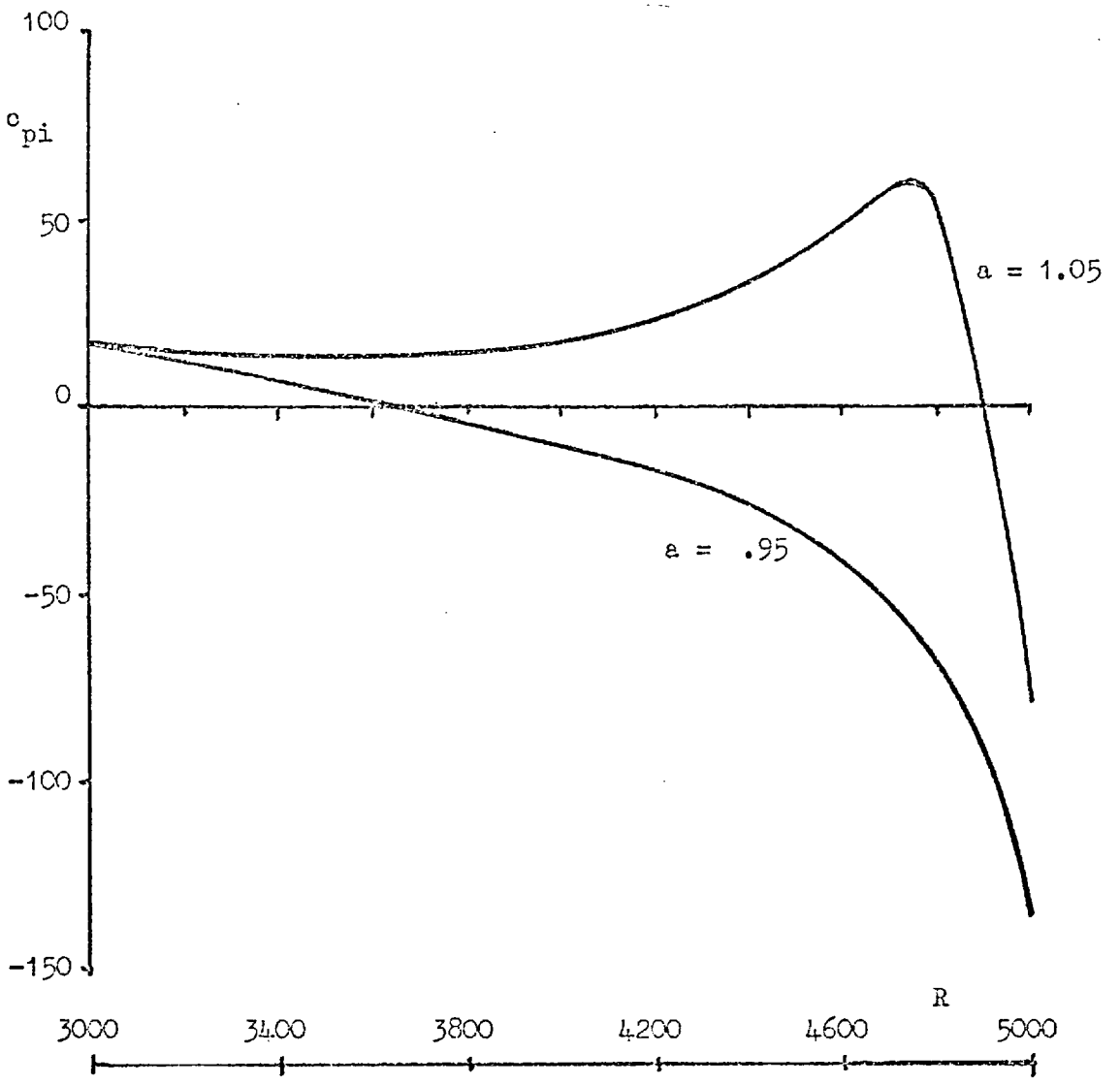

Figure 26. Curves showing the variation of c_{pi} with R at fixed a, calculated for a damped membrane with $(m,D,c_c) = (1,1000,3000)$ using a thirty cosine series.

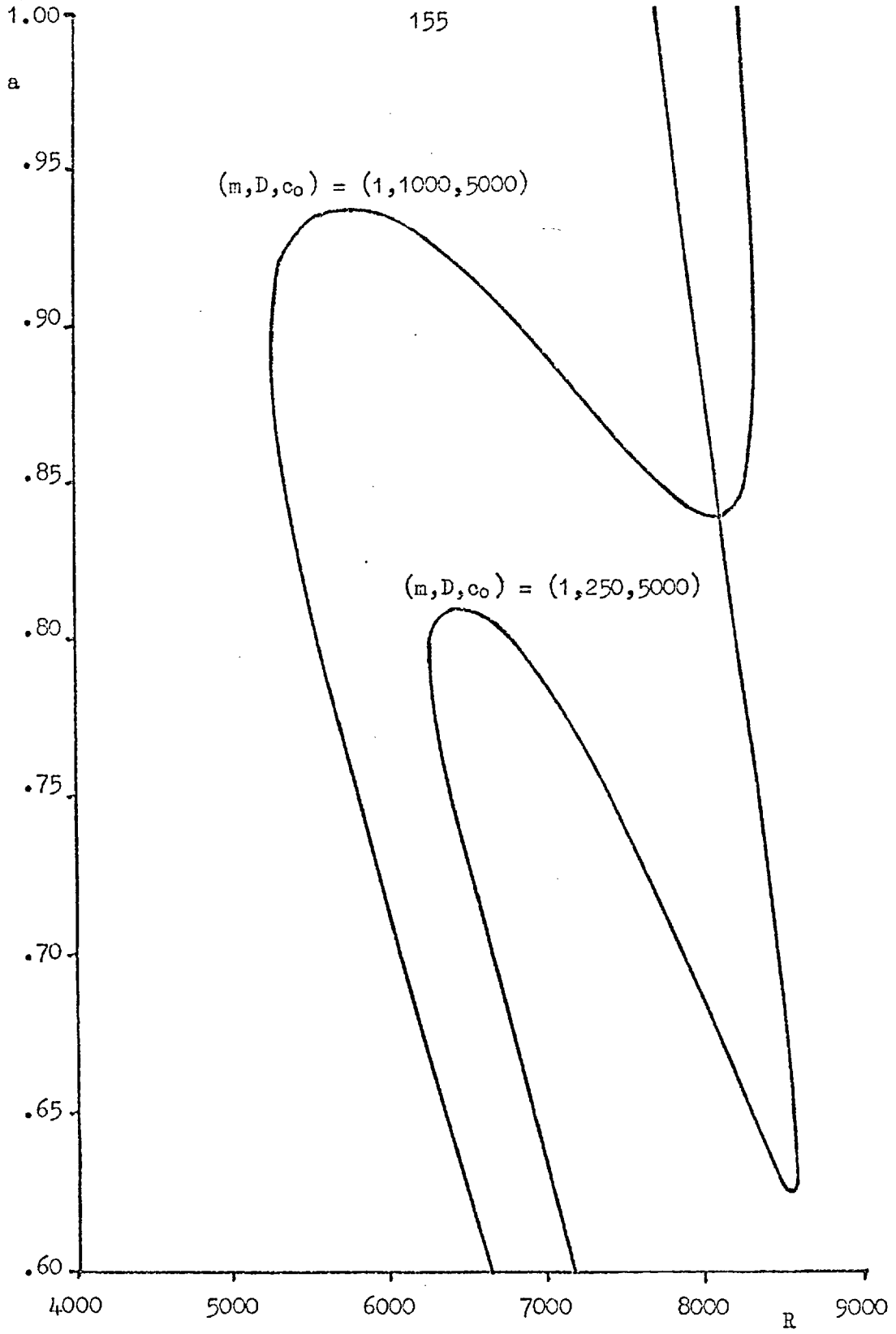

Figure 27. Neutral stability curves calculated for damped membrane walls using a thirty cosine series.

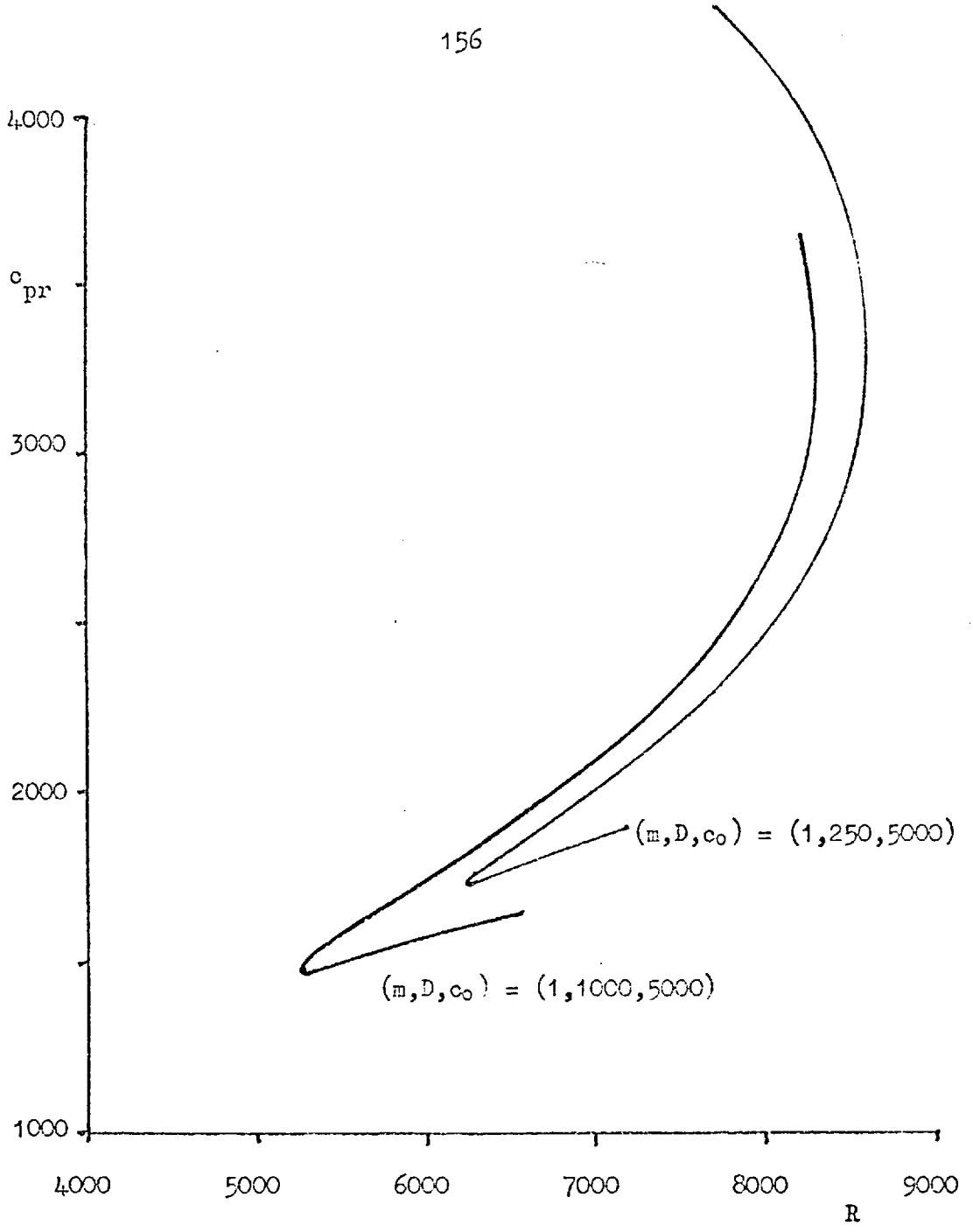

Figure 28. Spatial stability curves calculated for damped membrane walls using a thirty cosine series.

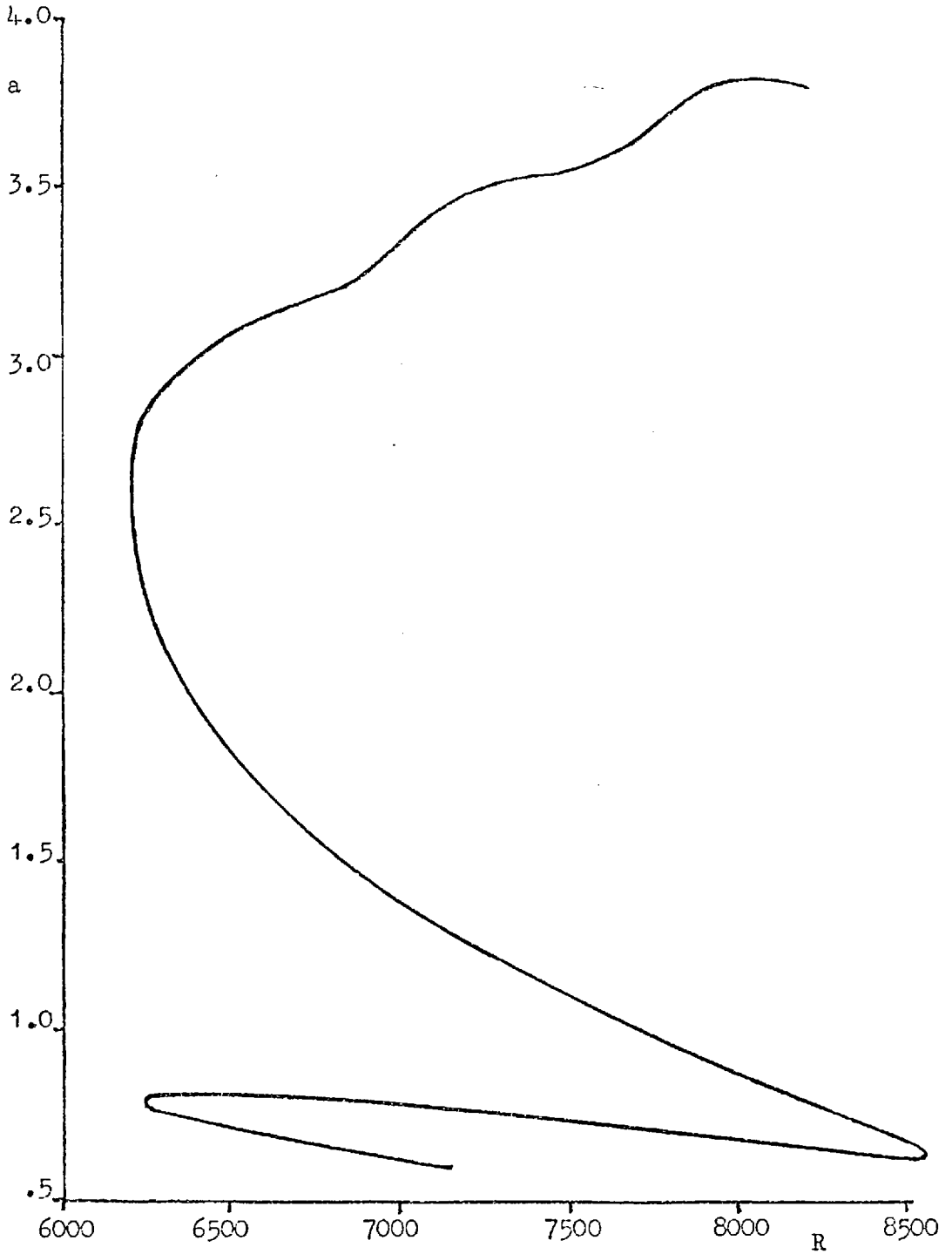

Figure 29. The more complete neutral stability curve calculated for the damped membranes with $(m,D,c_o) = (1,250,5000)$ using a thirty cosine series.

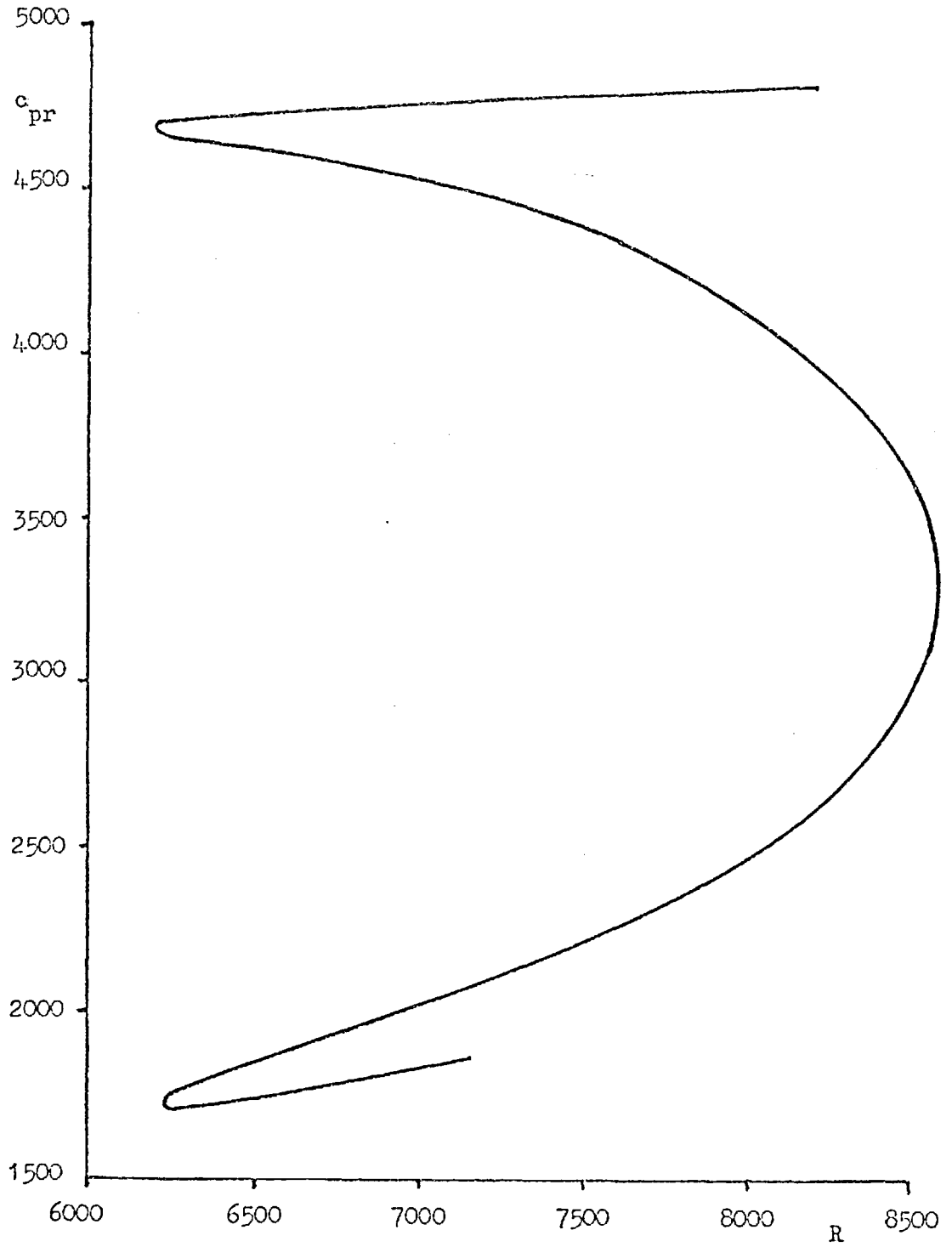

Figure 30. The more complete spatial stability curve calculated for the damped membranes with $(m,D,c_o) = (1,250,5000)$ using a thirty cosine series.

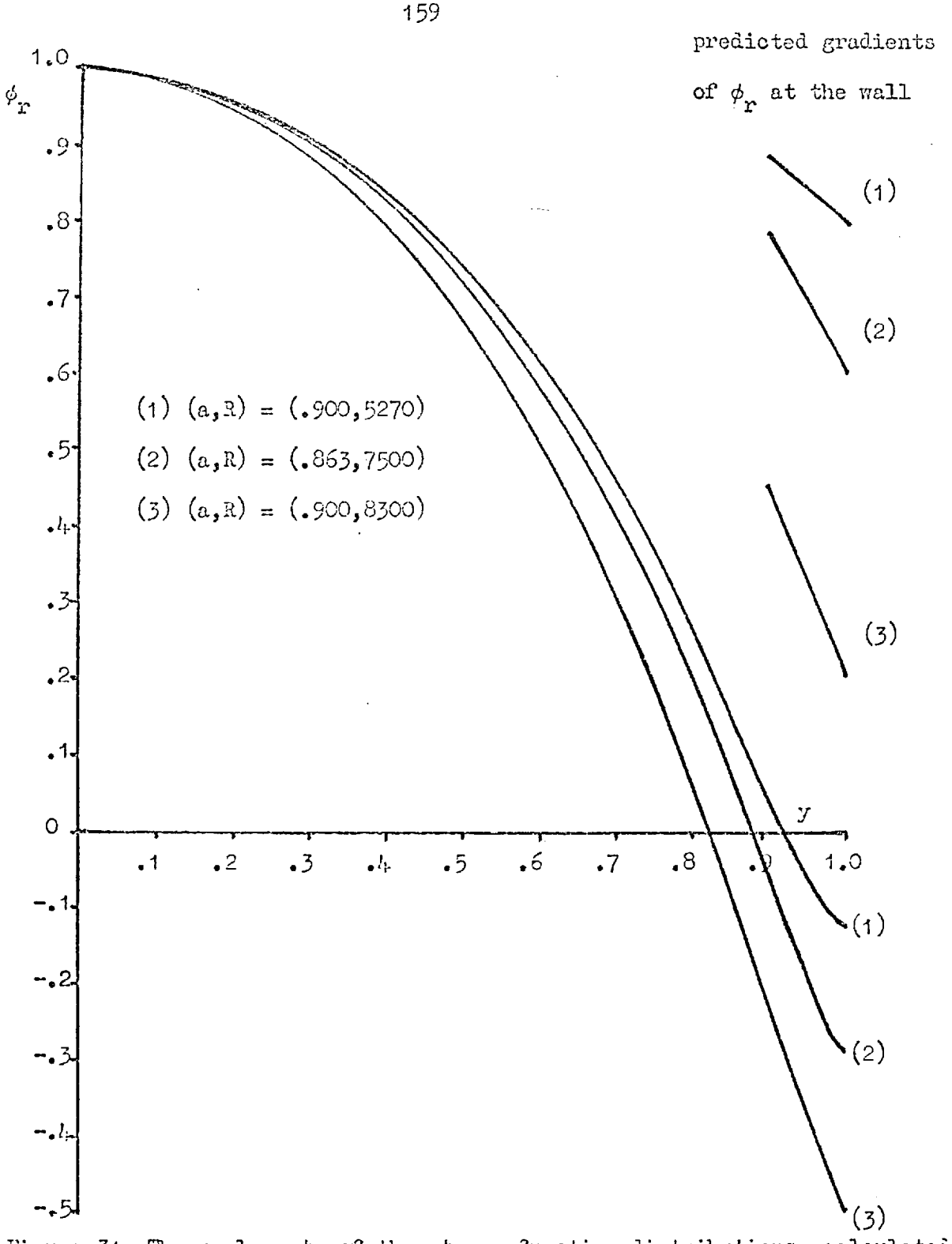

Figure 31. The real parts of the stream function distributions, calculated for damped membranes with $(m,D,c_o) = (1,1000,5000)$ using a thirty cosine series.

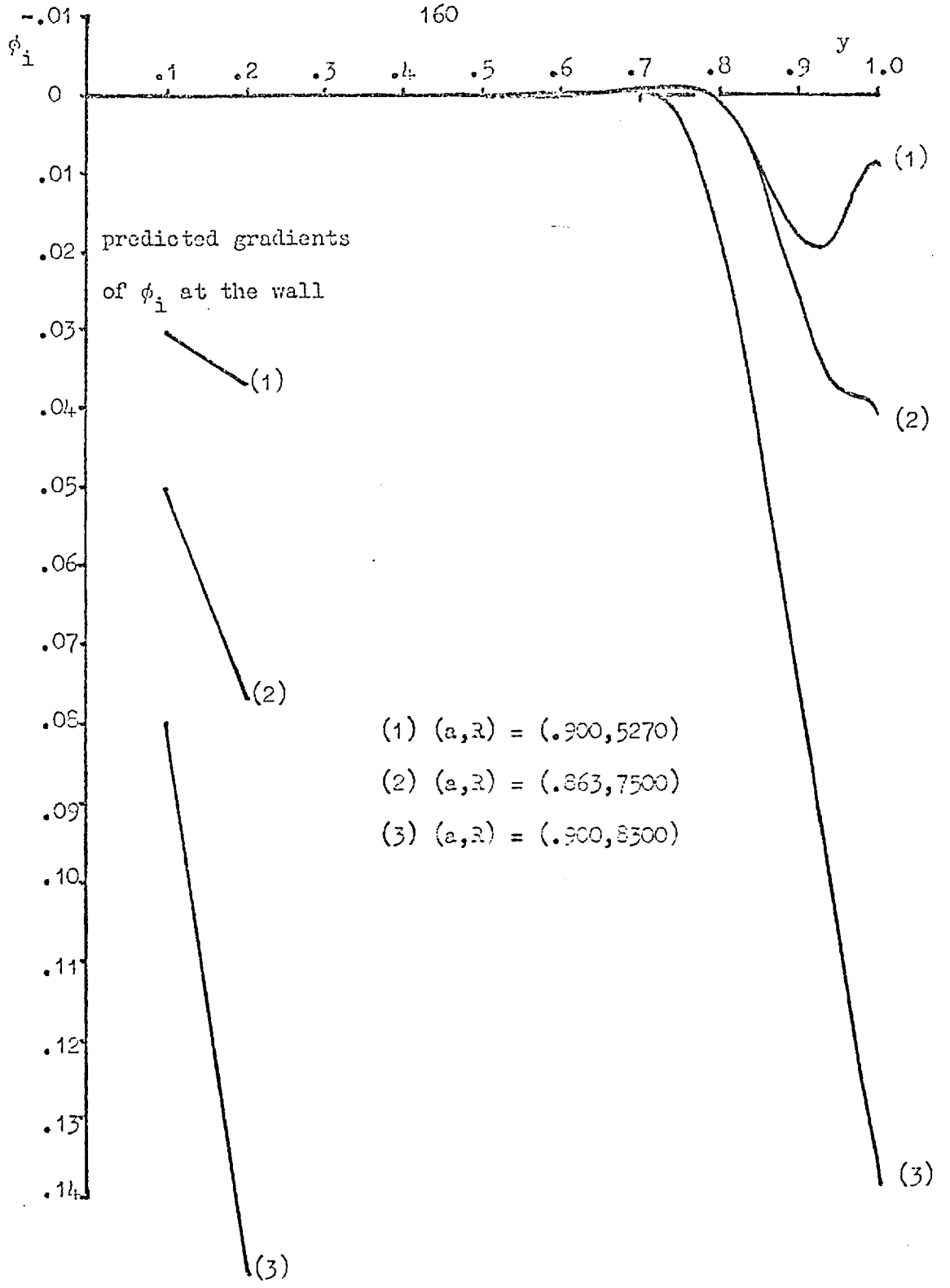

Figure 32. The imaginary parts of the stream function distributions, calculated for damped membranes with $(m,D,c_0) = (1,1000,5000)$ using a thirty cosine series.

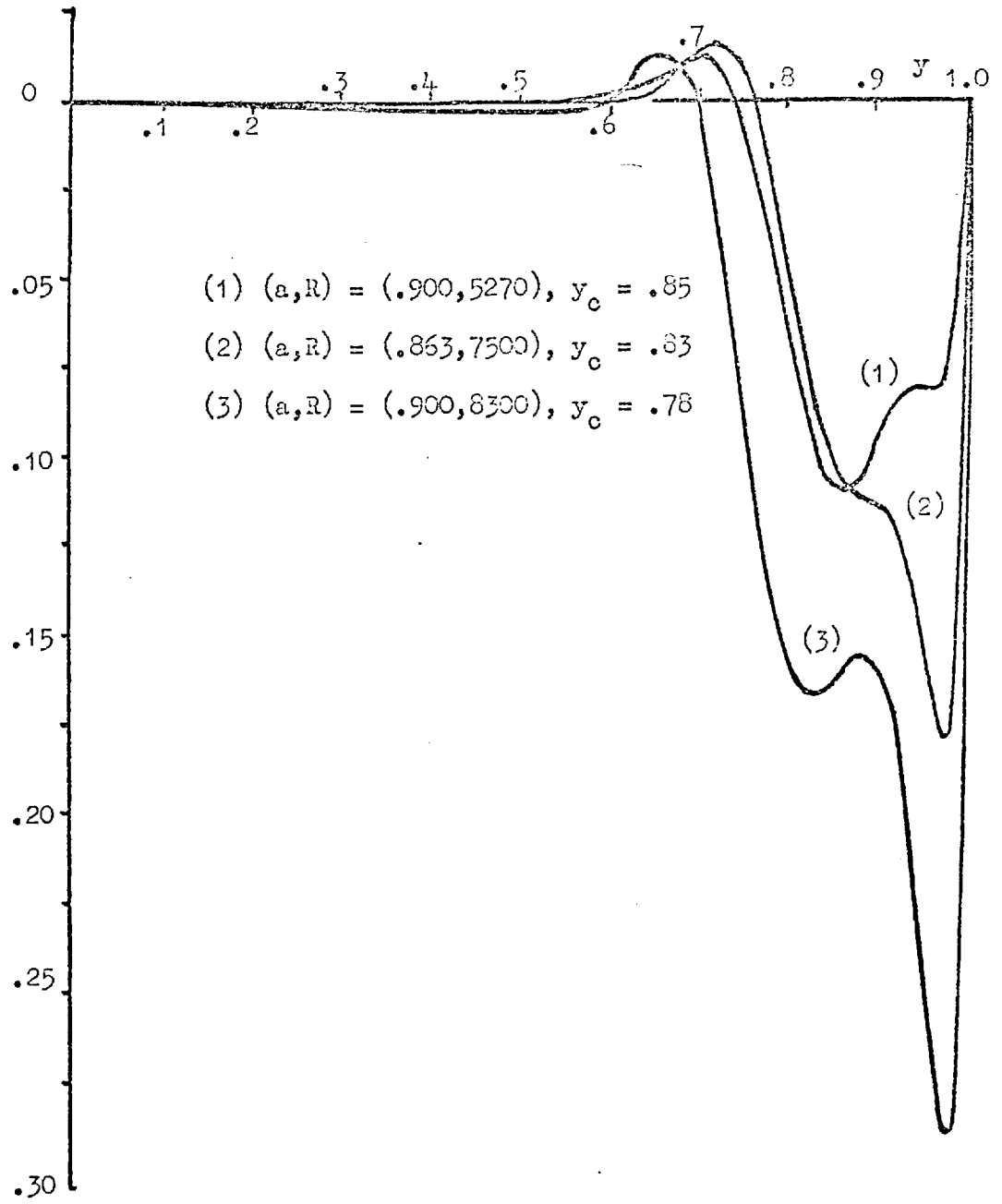

Figure 33. The Reynolds stress distributions, calculated for damped membranes with $(m,D,c_o) = (1,1000,5000)$ using a thirty cosine series.

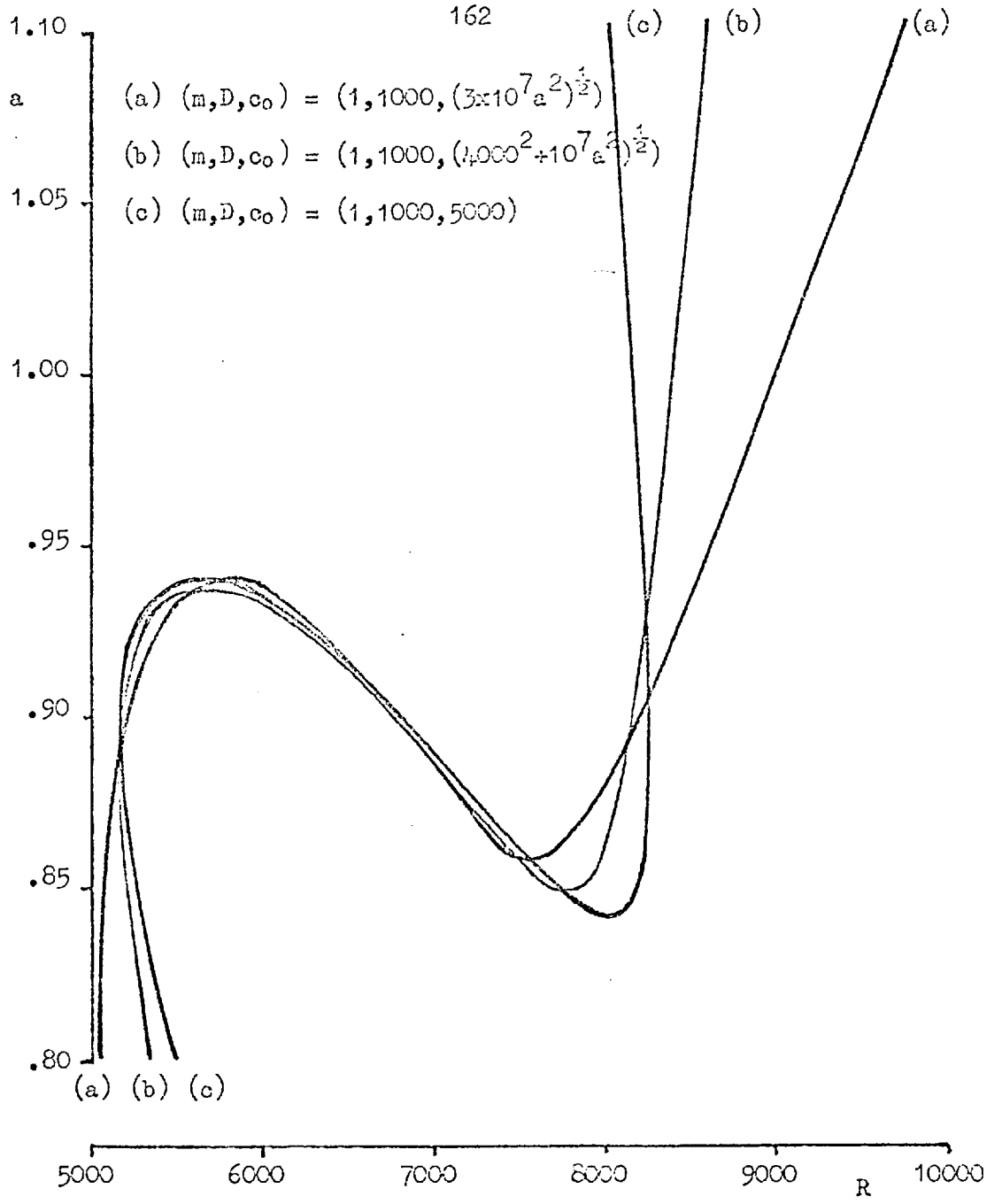

Figure 34. Neutral stability curves for thin plate walls, calculated using a thirty cosine series.

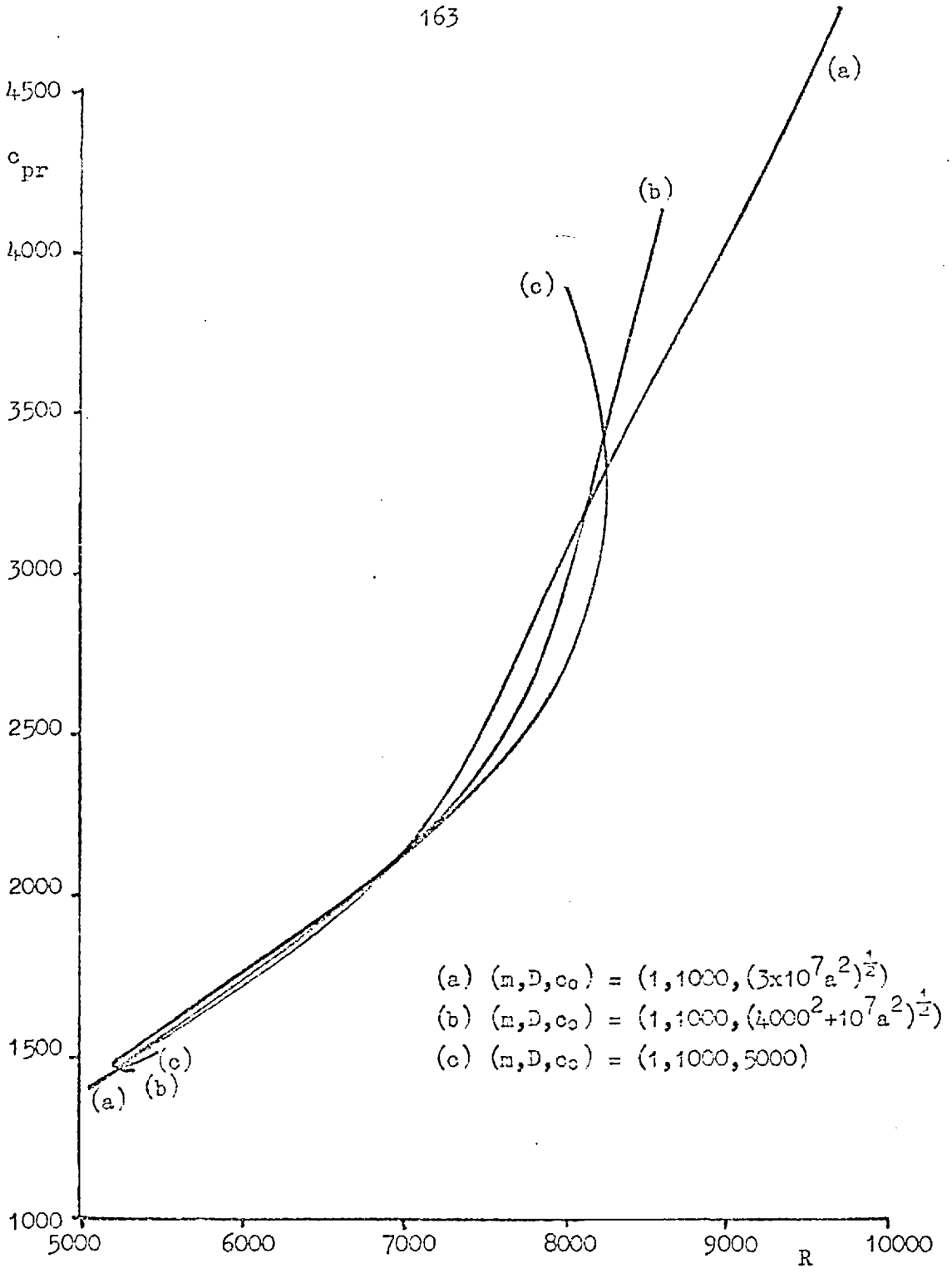

Figure 35. Spatial stability curves for thin plate walls, calculated using a thirty cosine series.

References.

Benjamin, T. B. (1960). Effects of a flexible boundary on hydrodynamic stability. J. Fluid Mech. , 9, 513-532.

Benjamin, T. B. (1963). The threefold classification of unstable disturbances in flexible surfaces bounding inviscid flows. J. Fluid Mech. , 16, 436-450.

Benjamin, T. B. (1964). Fluid flow with flexible boundaries. Proc. of 11th International Congress of Appl. Mech. , Germany, 109-128.

Boggs, F. W. , and Tokita, N. (1962). Theoretical study of compliant coatings to achieve drag reduction on underwater vehicles. U. S. Rubber Co. , Wayne, N. J. , Tech. Rep. .

Dolph, C. L. , and Lewis, D. C. (1958). On the application of infinite systems of ordinary differential equations to perturbations in plane Poiseuille flow. Quart. Appl. Math. , 16, 97-110.

Finlayson, B. A. , and Scriven, L. E. (1966). The method of weighted residuals - a review. Appl. Mech. Rev. , 19, 735-748.

Friedman, B. (1956). Principles and techniques of applied mathematics. Wiley.

Grohne, D. (1954). On the spectrum of natural oscillations of two-dimensional laminar flows. Tech. Memor. Nat. Adv. Comm. Aero. , no. 1417.

Grosch, C. E. , and Salwen, H. (1968). The stability of steady and time-dependent plane Poiseuille flow. J. Fluid Mech. , 34, 177-205

Hains, F. D. (1964). Additional modes of instability for Poiseuille flow over flexible walls. AIAA J. , 2, 1147-1148.

Hains, F. D. (1965). Preliminary results on boundary layer stability on a flexible plate. AIAA J. , 3, 775-776.

Hains, F. D. , and Price, J. F. (1961a). Stability of plane Poiseuille flow between flexible walls. Boeing Scientific Res. Labs. , Flight Sciences Lab. Rep. , no. 37.

Hains, F. D. , and Price, J. F. (1961b). Further remarks on the stability of plane Poiseuille flow between flexible walls. Boeing Scientific Res. Labs. , Flight Sciences Lab. Rep. , no. 53.

Hains, F. D. , and Price, J. F. (1962a). Stability of plane Poiseuille flow between flexible walls. Proc. 4th Nat. Congr. Appl. Mech. , 2, 1263-1268.

Hains, F. D. , and Price, J. F. (1962b). Effect of a flexible wall on the stability of Poiseuille flow. Phys. Fluids, 5, 365.

Heisenberg, W. (1924). "Über Stabilität" und Turbulenz von "Flüssigkeitsströmen". Ann. Phys. , Lpz. , 74, 577-627.

Kaplan, R. E. (1964). The stability of laminar incompressible boundary layers in the presence of compliant boundaries. M. I. T. , Aeroelastic and Structures Res. Lab. , ASRL - TR 116 - 1.

Korotkin, A. I. (1965). Stability of plane Poiseuille flow in the presence of elastic boundaries. P. M. M. , 29, 1122-1127.

Korotkin, A. I. (1966). Stability of the laminar boundary layer in an incompressible fluid on an elastic surface. Izv. Akad. Nauk. SSSR Mekhan. Zhidk. i Gaza, 3, 39-44.

Kramer, M. O. (1957). Boundary layer stabilisation by distributed damping. J. Aero. Sci. , 24, 459.

Kramer, M. O. (1960). Readers' forum. J. Aero/Space Sci. , 27, 68.

Landahl, M. T. (1962). On the stability of a laminar incompressible boundary layer over a flexible surface. J. Fluid Mech. , 13, 609-632.

Landahl, M. T. (1966). A time-shared program system for the solution of the stability problem for parallel flows over rigid or flexible surfaces. M. I. T. , Aeroelastic and Structures Res. Lab., ASRL - TR 116 - 4.

Landahl, M. T. , and Kaplan, R. E. (1965). The effect of compliant walls on boundary layer stability and transition. AGARDograph, 97, 363-394.

Lee, L. H. , and Reynolds, W. C. (1964). A variational method for investigating the stability of parallel flows. Stanford Univ. , Calif. , Mech. Engng. Dept. , Tech. Rep. no. FM - 1.

Lee, L. H. , and Reynolds, W. C. (1967). On the approximate and numerical solution of Orr-Sommerfeld problems. Quart. J. Mech. Appl. Math. , 20, 1-22.

Lin, C. C. (1944). On the stability of two-dimensional parallel flows. Proc. Nat. Acad. Sci. , Wash. , 30, 316-323.

Lin, C. C. (1945). On the stability of two-dimensional parallel flows. Pts. I, II, III. Quart. Appl. Math. , 3, 117-142, 218-234, 277-301.

Lin, C. C. (1955). The theory of hydrodynamic stability. Cambridge University Press.

Linebarger, J. H. (1961). On the stability of a laminar boundary layer over a flexible surface in a compressible fluid. S. M. Thesis, Dept. of Aero. and Astro. , M. I. T. .

Lock, R. C. (1954). Hydrodynamic stability of the flow in the laminar boundary layer between parallel streams. Proc. Cambridge Phil. Soc. , 50, 105-124.

Miles, J.W. (1957). On the generation of surface waves by shear flows. J. Fluid Mech. , 3, 185-204.

Miles, J. W. (1959a). On the generation of surface waves by shear flows. Pt. 2. J. Fluid Mech. , 6, 568-582.

Miles, J.W. (1959b). On the generation of surface waves by shear flows. Pt. 3. Kelvin-Helmholtz instability. J. Fluid Mech. , 6, 583-598.

Miles, J. W. (1962). On the generation of surface waves by shear flows. Pt. 4. J. Fluid Mech. , 13, 433-448.

Nonweiler, T. (1963). Qualitative solution of the stability equation for a boundary layer in contact with various forms of flexible surface. A. R. C. , C. P. 622.

Shen, S. F. (1954). Calculated amplified oscillations in plane Poiseuille and Blasius flows. J. Aeron. Sci. , 21, 62-64.

Squire, H. B. (1933). On the stability of three-dimensional disturbances of viscous flow between parallel walls. Proc. Roy. Soc. , A ~~234~~ 142 ~~189-206~~. 621-628.

Stuart, J. T. (1963). Hydrodynamic stability. In "Laminar Boundary Layers" (L. Rosenhead, ed.). Clarendon Press, Oxford.

Timoshenko, S. P. , and Gere, J. M. (1961). Theory of elastic stability. McGraw-Hill.

Thomas, L. H. (1953). The stability of plane Poiseuille flow. Phys. Rev. , 91, 780-783.